On the use of D–Flow FM & MIKE FLOOD models for the analysis of urban fluvial & pluvial inundation

A study case of Colombo Metropolitan region in Sri Lanka

by

Charikleia E. Sifaki

TU Delft

Deltares
Enabling Delta Life

On the use of MIKE FLOOD & D-Flow FM models for the analysis of urban fluvial & pluvial inundation

A study case of the Colombo Metropolitan region in Sri Lanka

by

Charikleia E. Sifaki

to obtain the degree of Master of Science
at the Delft University of Technology,
to be defended publicly on Thursday August 10, 2017 at 16:00 PM.

Student number: 4420071
Project duration: November 2016 – August 2017

Thesis committee:	Dr. ir. Marie-claire ten Veldhuis,	TU Delft, supervisor
	Dr. ir. Frans van de Ven,	TU Delft/ Deltares
	Prof. dr. Nick van de Giesen	TU Delft
	Dr. Hans Gehrels	Deltares
	Ir. Ruben Dahm	Deltares

An electronic version of this thesis is available at http://repository.tudelft.nl/.

TU Delft Delft University of Technology

Deltares Enabling Delta Life

Abstract

In recent years, urban inundation modelling has been stimulated by technological advancements and an increase in data availability and quality. Diminution of modelling restrictions allowed for detailed methodologies, yet escalated the number of required parameters, leading to higher complexity and predictions' uncertainty issues. In the present study, two state-of-the-art models with distinct numerical discretisation strategies, schematisation and rainfall runoff modules, namely MIKE FLOOD and D-Flow FM are evaluated in urban fluvial and pluvial inundation. The case study of Colombo Metropolitan region (Sri Lanka) is used. Dominant factors interpreting models' differentiations are identified and further analysed. Results suggest that D-Flow FM concept is more realistic and sensitive to overland surface information but require higher detail and computational times compared to MIKE FLOOD methodology. The outcome of this research is anticipated to aid modellers in choosing the most appropriate model principle based on the data availability, desired accuracy and computational time.

Acknowledgements

The current MSc thesis report comprises the final requirement for obtaining my MSc in Water Management at Delft University of Technology as well as the end of a long, challenging but also fruitful and exciting journey started nearly three years ago. At the same time, it marks the beginning of a whole new chapter in my life, where the knowledge and expertise gained throughout my studies will be used to fulfil my ultimate dreams and contribute to the common good.

Yet, this report would have been incomplete, if I did not express my sincere gratitude towards the staff, colleagues, friends and family who constantly encouraged and supported me during this period. First and foremost, I would like to thank my main supervisors Dr. ir. Marie-claire ten Veldhuis and Dr. ir. Frans van de Ven, for giving me the opportunity to carry out the present diploma study. Their constructive guidance and assistance along with their valuable feedback and interesting conversations led to the successful completion of the current work.

At this point, I would also like to thank Dr. Hans Gehrels for his critical comments and continuous support throughout my thesis project as well as Prof. dr. Nick van de Giesen for being part of my assessment committee. I take the opportunity to personally thank Dr. ir. Arthur van Dam and Ir. Ruben Dahm for being my daily supervisors, providing their valuable advice, constructive criticism and extensive discussions around my work. Moreover, I would like to thank all those partners in Deltares and university that contributed with their interest and expertise to this project's fulfilment.

My sincere thanks to Prof. dr. ir. Merle de Kreuk for inspiring and motivating me throughout my studies but especially during difficult times, when I needed words of encouragement. You are an exemplary mentor and a wonderful person!

I would also like to thank Alexandra Prodanescu for being a valuable friend, who encouraged, advised but most importantly, was constantly there for me.

Special thanks should also be attributed to my beloved George. His true love, support and smile were always there to steer me in the right direction and fill my life with colours.

Last but not least, I would like to express my gratitude to my family and parents, Lefteris and Eleni, for devoting their entire lives to assure that their virtues – courage, patience, wisdom, discernment, perspective – were imprinted in mine and Frida's souls, so that our choices will reflect our deepest values and highest hopes; they will reflect love.

Charikleia Sifaki

Delft, August 1st, 2017

Contents

List of abbreviations

AD	Absolute Difference
CV	Control Volume
DEM	Digital Elevation Model
D-Flow FM	D-Flow Flexible Mesh
DSM	Digital Surface Model
ENSO	El Niño-Southern Oscillation
FEM	Finite Element Method
FDM	Finite Difference Method
FVM	Finite Volume Method
GS	Gauging Station
HRU	Hydrological Response Unit
ITCZ	Inter-tropical convergence zone
LiDAR	Light Detection and Ranging
MSL	Mean Sea Level
NAM	Nedbør Afstrømnings Model (in Danish, rainfall runoff model)
NSE	Nash-Sutcliffe Efficiency
OL/OP	Observation Location/Point
PDE	Partial Differential Equation
RE	Relative Error
RMSE	Root Mean Square Error
RR	Rainfall Runoff
SWE	Shallow Water Flow Equation
WL	Water Level
1D	One-dimensional
2D	Two-dimensional

List of equations

List of figures

List of tables

1
Introduction

Considering the rapid population growth and urbanisation rates in conjunction with the climate change impact on precipitation and temperature patterns, the necessity to enhance current tactics in urban planning towards flood resilience is acknowledged. Since vulnerability of urban communities continues to comprise a major hurdle in flood risk management (Mechler & Bouwer, 2014; Visser et al., 2014; Koks et al., 2015), the development of cost-effective strategies has become of paramount importance, predominantly in economically developing countries where financial resources for weather-related disasters barely exist.

The abovementioned incentives along with limitations in spatiotemporal measurements and the need for robust decision-making led to the introduction and development of multiple modelling techniques, utilized as inundation hazard analysis tools (Jha et al., 2012; Salvadore et al., 2015). Over the past century, technological improvements and systematic attempts within the research community resulted in remarkable achievements, including models' implementation for flood risk and damage assessment, real-time flood forecasting and water resources management. As breakthroughs in science and technology constantly reinforce computers' capacity and efficiency, restrictions in urban inundation modelling will gradually be diminished allowing for more detailed, qualitative and sophisticated methodologies and outcomes. Nevertheless, models' complexity entails greater requirements for data quantity and quality as well as a larger number of parameters' involvement escalating the calibration difficulties and subsequently, the predictions' uncertainty. Subsequently, balancing the scope, precision, data requirements, complexity and computational demands is required.

1.1. Research objectives & questions

Considering the presence of abundant urban inundation modelling techniques and software packages along with the necessity to provide fast and precise assessment of flood risk, the current master thesis aimed at investigating whether and how advanced modelling approaches and different schematisation influence the model performance and simulation outcomes. For this purpose, two principally different state-of-the-art software products, namely MIKE FLOOD and D-Flow Flexible Mesh (FM) were reviewed, compared and verified using observation data. Being in a beta testing phase, D-Flow FM was implemented for the first time in urban inundation modelling.

The main objective of this work can be outlined as follows:

To compare and evaluate various methods of 1D/2D representation in analysing urban fluvial and pluvial inundation by means of balancing accuracy, computational time and data requirements, using reality as a reference.

Comprising two physically-based, spatially distributed modelling software packages, both D-Flow FM and MIKE FLOOD simulate inundation in urbanised catchments by implementing the full dynamic wave solution. The scheme in which this solution is based constitutes one of the models' fundamental differences. Specifically, D-Flow FM uses the implicit finite volume method to solve the momentum equations while MIKE FLOOD is based on the implicit finite difference approach. Moreover, principal dissimilarities in the models' rainfall runoff concept, components and spatial discretisation are detected and further analysed.

To assess these modelling techniques, the case study of Colombo Metropolitan region in Sri Lanka using three inundation events were selected. Unique weather patterns occurring in Southeast Asia, increasing urbanization rates in conjunction with communities' high vulnerability level comprised the primary reasons for addressing this area. Information was derived from three historical flood events to further compare and evaluate the accuracy and validity of the estimated magnitude of inundation. The events' severity in conjunction with the data availability constituted the motives for these events' selection.

Taking the preceding conditions into account, the main research objective is further translated into the following research questions:

- Could D-Flow FM sufficiently simulate the inundation events occurred in the case study selected?
- Which are the dominant factors interpreting differences in performance between D-Flow FM and MIKE FLOOD?
    i. Which are the differences between the models in terms of results for a given set of events and how can these differences be interpreted?
    ii. In case of dissimilarities in the models' outcomes, which are the crucial parameters and how important are they?

The hydrodynamic models presented in the current study were among the first attempts to simulate the combination of urban pluvial and fluvial inundation in a large spatial scale (approx. 100 km^2) and with a relatively fine resolution (30m mesh cell size). Comparison of the developed D-Flow FM and MIKE FLOOD models was achieved by ensuring identical input data, initial and boundary conditions. Models were validated against field observation data of three inundation events. Specific gauging locations within the catchment along with distinct model evaluation techniques were selected for models' comparison.

1.2. Research methodology

To achieve the abovementioned research goal and objectives, the current study followed a certain research methodology (Figure 1). Specifically, once the literature review was completed and the dominant concepts around inundation models' comparison were essentially understood, the major steps for a comprehensive D-Flow FM and MIKE FLOOD comparison were developed. Firstly, the required datasets were gathered, processed and implemented as model's input. The following stage included D-Flow FM model's building and simulation processes[1]. Once the results from both D-Flow FM and MIKE FLOOD[2] were attained, a validation was due. A detailed description of this analysis is provided in Chapter 3.

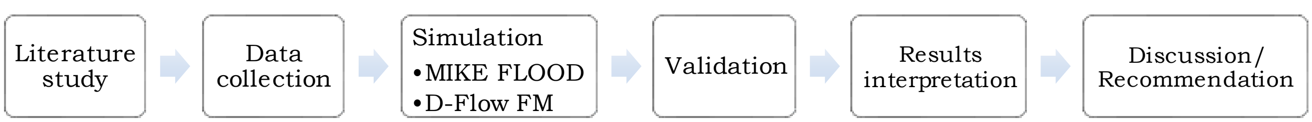

Figure 1. Flow chart of the research methodology followed

The present study is structured as follows: Chapter 2 aims at providing an insight into the main modelling approaches used to represent inundation in urban catchments. In Chapter 3, the study case is introduced, D-Flow FM and MIKE FLOOD along with their differences are presented. Moreover, the models' building process as well as their evaluation are defined and further described. Chapter 4 and 5 demonstrate the modelling results' comprehensive analysis and discussion, respectively while Chapter 6 includes the conclusions and recommendations of the presented work.

---

[1] Due to the software's beta testing phase and limitations, this stage took a fairly long time, as different model versions [i.e. with/without graphical user interface (GUI)] were tested, hydraulic structure types were generated or adjusted etc].

[2] Due to licence limitations, MIKE FLOOD simulations were conducted by the consultants in Sri Lanka. MIKE ZERO was used to process and derive the corresponding results.

2

Urban Inundation Modelling

Review & recent advances

The world is presently undergoing successive waves of migration towards urban and semi-urban zones, particularly in economically developing countries (United Nations, 2014). Yet, the rapidest urbanisation rates are noted in South Asia where within a period of 16 years (2000-2016), the population exceeded 500,000 inhabitants in 40 cities, accounting for the 85% of the world's fastest growing urban agglomerations (United Nations, 2016). In the meantime, urban population is constantly growing, with projections anticipating a further increase of 2.6 billion by 2050, 90% of which is estimated to concentrate in Asia and Africa (United Nations, 2014; UNFPA, 2016).

These trends inevitably influence the contemporary urban environments, resulting in substantial spatial restructuring of land use patterns (Ellis et al., 2013). Deforestation, wetlands' shrinkage, occupation and poorly planned development in floodplains, water resources' manipulation and urban soil sealing depict the magnitude of disruption and degradation. In addition, such modifications significantly disturb the cities' buffering capacity to hazards and further add to their vulnerability (Depietri et al., 2011; Fletcher et al., 2013; Salvadore et al., 2015).

Flooding comprises the most frequent and widespread among all natural disasters (IPCC, 2012; Jha et al., 2012; Guha-Sapir & Wahlstrom, 2015). Stemming primarily from a combination of meteorological and hydrological extremes and further exacerbated by the unique urban structure and characteristics, the occurrence of flood events in urban settlements can encompass serious consequences. Specifically, although more limited in size (land-wise) compared to rural locations, they can pose a key threat to urban development goals, national economies as well as livelihood and stability of the populations affected (Jonkman, 2014). In addition, the alarming increase in urban poverty and slum dwellers across the developing world[3] in conjunction with the poorly planned and managed urban agglomerations constitute factors contributing to the growing flood risk and magnitude of flood-related consequences, reflected in the unprecedented tangible and intangible losses and damages in these areas (Mechler & Bouwer, 2014; Visser et al., 2014; Koks et al., 2015).

Considering all previously mentioned factors as well as the long-term climate change impacts on precipitation and temperature patterns, the necessity to enhance our current tactics in urban planning towards flood resilience is widely acknowledged (IPCC, 2012; Jha et al., 2012). Since vulnerability of urban communities continues to comprise a major hurdle in flood risk management, the development of cost-effective flood risk management strategies has become of paramount importance in numerous metropolitan regions globally and predominantly in economically developing countries where financial resources for weather-related disasters barely exist.

2.1. Modelling in urban catchments

Despite the remarkable technological advancements noted over the last few decades, identifying and evaluating urbanized catchments, the hydrological components and processes involved as well

[3] Despite reporting a decline in the proportion of urban population living in slum households (UN-Habitat, 2012a), UN-Habitat (2016) stated that their absolute number has increased from 791 million in 2000 to 880 million in 2014. In addition, 60% of the latter number represent people living in Asian cities' informal settlements (UN-Habitat, 2016).

as their interrelations and interactions constitutes a fairly challenging procedure. This primarily stems from the unique urban structure and characteristics, dominated by distinctive physical laws and principles (Vojinovic et al., 2011; Fletcher et al., 2013; Salvadore et al., 2015). In addition, the limitation of measurement techniques and spatiotemporal measurements as well as the urgent need for integrated flood risk management strategies and robust decision-making approaches contributed to the development of multiple modelling techniques, utilized as inundation hazard analysis tools (Jha et al., 2012; van Dijk et al., 2014; Salvadore et al., 2015).

As outlined in the historical overview (Appendix A), modelling initiated from empirical relations along with several simplified assumptions and evolved into more advanced and refined representations of reality. In the recent years, numerical methods are widely applied in urban inundation modelling due to their competence to provide comprehensive insight into highly complex dynamics (Popescu, 2014). Lumped conceptual and more recently, physically-based distributed modelling comprise the predominant approaches implemented in urban catchments to describe the various storm water flow components (principally rainfall-runoff, overland and subsurface/sewer flows), processes and interactions (Pina et al., 2016).

2.1.1. One-dimensional modelling approaches

One-dimensional sewer model

Traditionally, the concept of one-dimension (1D) comprised the standardised approach applied in sewer flow models to evaluate urban drainage systems' performance during intense precipitation events. By applying certain simplifying assumptions (i.e. 1D flow and uniform velocity), these parametrically simpler models are characterised by a relatively easy set-up and hydraulic characteristics' representation, high efficiency and low computational time for simulations (Kuiry et al., 2010). Numerous open-source and commercial 1D software products have been developed and are currently available, including SWMM (Huber et al., 1988; Rossman, 2010), XP-SWMM (XP Software, 2013), MIKE MOUSE (DHI Software, 2014) and InfoWorks ICM (Innovyze, 2013). Nevertheless, sole implementation of these models cannot explicitly represent the event's behaviour and magnitude, as their competences are restricted to the sewer network's surcharge volume estimation by means of a depth-volume or area-volume function. The estimated surcharged flow is accumulated upon the model's manholes and released once the system's capacity is made available (Zhong, 1998; Leandro et al., 2009; Rossman, 2010). Moreover, 1D sewer flow model tend to overlook crucial spatial elements of floodplain hydraulics and be facile in the representation of floodplain flows (i.e. assuming no interactions among sub-catchments), resulting in simplified runoff dynamics' outcomes.

One-dimensional surface model

Considering the abovementioned 1D models' limitations in urban inundation simulations, Djordjević et al. (1999) introduced the dual drainage model consisting of two networks, namely the minor (subsurface part, sewer system) and the major (surface part, including the surface flow pathways and retention basins) system (Djordjević et al., 1999; Schmitt et al., 2004). By linking these two networks, an upgrade of the current 1D modelling outcomes using an additional drainage network to compensate for the surface runoff component was targeted. Further adjustments in several data acquisition and linkage parameters reinforced the dual drainage concept and aided in accurately simulating the surcharged flow unit in the surface drainage system (Mark et al., 2004; Leandro et al., 2007; Allitt et al., 2009; Maksimović, et al., 2009). However, taking urban floodplains' large complexity and heterogeneity level (i.e. complex combination of natural and artificial surface cover, processes and flow pathways) into account, the principal assumption of this approach regarding confined inundation flows by the surface drainage network is disproved (Vojinovic & Tutulic, 2009; Kuiry et al., 2010). The model's inability to correctly simulate the situation is highlighted in case flood depth exceeds the assumed conduits' capacity, resulting in indeterminate flow directions and overland flooding (Leandro et al., 2009; Seyoum et al., 2011).

Capturing the relevant characteristics in urban catchments to simulate urban inundation in meaningful scales requires high resolution data (i.e. <5m mesh resolution) and model efficiency (Hunter et al., 2008; Néelz & Pender, 2013). Combining this consideration with 1D sewer flow and 1D/1D models' inability to thoroughly analyse urban flood events, the concept of two-dimensions (2D) has recently been reinstated and further enhanced by the remarkable technological advancements (i.e. powerful computing and Geographic Information System tools, advances in numerical solutions and an increase in data availability).

2.1.2. Two-dimensional modelling approaches

Numerous scientific papers and reports have documented the development and implementation of tailored two-dimensional (2D) overland flow models in various urban inundation cases. Addressing selected features and determinative parameters, the models' performance has been examined over the last two decades. Saint-Venant equations (known also as shallow water flow equations or full dynamic wave solution) and their simplified forms (i.e. kinematic wave solution – acceleration and pressure terms are neglected – and diffusive wave solution – acceleration terms are neglected) comprise the energy and mass conservation laws representing the principles of physical phenomena governing the water behaviour in flood events (Popescu, 2014; Salvadore et al., 2015). The complexity of water flow during inundation events further contributes to the researchers' lack of comprehensive knowledge and understanding in regard to hydrodynamic conditions. Examples of this behaviour include water not in accordance with natural pathways, occurrence of subcritical, supercritical and transcritical flow regimes as well as the difficulty to estimate and describe water head losses around buildings, roads and pavements. Considering these constraints along with their simplicity and low data requirements, Saint-Venant simplified equations are commonly applied (Aronica & Lanza, 2005; Hunter et al., 2008; Fewtrell et al., 2011; Ogden et al., 2011; Almeida et al., 2012). Nevertheless, these equation types tend to simplify the inundation case studies (i.e. assuming solely subcritical flows during inundation events and using respective algorithms) which can lead to unrealistic outcomes and computational instabilities (Djordjević et al., 2004; Vojinovic & Tutulic, 2009).

Advances in resolution topographic data

As mentioned previously, the resolution of topographic data constitutes an additional crucial parameter determining the accuracy level and efficiency of 2D overland models in inundation modelling. Powerful computing tools and high precision of the floodplain topography through Light Detection And Ranging (LiDAR) data resulted in more accurate representations of flow direction and patterns during urban flood events (Fewtrell et al., 2011; Turner et al., 2013; Son et al., 2016). Considering these advancements in conjunction with the competence to introduce urban characteristics (i.e. tarmac roads, kerbs, sidewalks, walls and buildings) through Digital Surface Model (DSM) gave new dimensions to urban inundation modelling and stimulated the switch from irregular sub catchment units (1-10 km^2) used to describe large natural storage sections to fine spatial resolution meshes (mesh elements' range between 10^{-2} and 10^{-3} km^2) (Bates et al., 2010). However, the need for higher spatial resolution and further research into its relation with the urban major system's representation has been constantly highlighted in scientific papers and reports (Mark et al., 2004; Gallegos et al., 2009; Martins et al., 2015).

Numerical discretisation strategies

Numerically solving Saint – Venant partial differential equations by implementing the finite element (FEM) and finite difference methods (FDM) in structured mesh types comprise a standard approach widely used in urban inundation modelling (Cook & Merwade, 2009; Bates et al., 2010; Seyoum et al. 2012; Bellos & Tsakiris, 2015; Gibson, et al., 2016). Nonetheless, the inability to aptly represent complex geometries due to mesh inflexibility in conjunction with computational time restrictions related to the combination of high resolution datasets and fine meshes constitute two major challenges of 2D overland flow models highlighted in the literature (Kuiry et al., 2010; Martins et al., 2015).

On the other hand, finite volume method (FVM) constitutes a favourable alternative to the abovementioned solutions as it can be implemented on arbitrary geometries as well as structured or unstructured meshes (Popescu, 2014). Following its wide implementation in river inundation modelling, FVM is increasingly becoming acknowledged in urban flood studies. Recent applications include Sanders et al. (2008) who succeeded in deriving the porous shallow water flow equations (SWEs) for urban flood modelling while considering constructed dwellings into their approach. By coupling their concept with FVM, urban inundation flows' simulations proved to be considerably faster compared to the classical SWEs (Sanders et al., 2008; Kim et al., 2015). Similarly, having as a purpose to accurately and efficiently simulate overland inundation flow conditions, Martins et al. (2015) developed the Gravity Wave Model (GWM) using a FVM framework. The model was tested in complex conditions and results revealed its superiority over a classical SWE model. Although the research community's preference and suggestions for future investigation are oriented towards FVM and unstructured or flexible meshes, their implementation in urban inundation modelling and their performance evaluation by means of comparing them with different approaches (i.e. FEM or FDM, standard structured mesh) are still very limited.

Discretisation in space and time

Except for the method of solution, space and time discretisation comprise two fundamental steps in numerical modelling. Specifically, structured (rectangular), unstructured (triangular) and flexible constitute the type of meshes implemented for spatial discretisation while implicit and explicit schemes are used for discretisation in time (Popescu, 2014). Flexible meshes comprise the state-of-the-art in model's spatial discretisation with their distinct feature being the implementation of finer resolution around selected perplexing regions and coarser resolution in areas characterised by low spatial variance and interest. The ability to adjust the resolution significantly reduce the computational time and effort needed while enhancing the model's performance.

2.1.3. 1D/2D modelling approaches

Despite the abovementioned 2D overland flow models' limitations, this approach illustrates surface flow routing in two dimensions as well as its topographic characteristics in a more detailed and representative way. Subsequently, coupling 1D computationally efficient sewer flow models with 2D overland flow models can considerably enhance the drainage systems' performance evaluation and thus, comprise a significant improvement in urban inundation modelling (Seyoum et al., 2012). Hsu et al. (2000) attempted to combine the minor and major network using an 1D sewer flow and a 2D-noninertia model. Running these two models in sequence resulted in surcharged flow accumulation atop of manholes along with inundation depths and extents' misrepresentation. To overcome this limitation, two novel coupling techniques, namely coupled 1D/2D and coupled 2D/1D approaches, emerged (Hsu et al., 2002; Chen et al., 2007; Seyoum et al., 2012) and were adopted by various commercial software products, including SOBEK (Deltares, 2017), InfoWorks ICM (Innovyze, 2013) and MIKE URBAN (DHI Software, 2014). In particular, the 1D/2D concept suggests the direct implementation of total precipitation in the drainage network for the sewer flow to be simulated. As this system is interacting bi-directionally with the overland surface, surcharges accounting for inundation will be further simulated using the 2D overland flow model (Chen et al., 2007; Seyoum et al., 2012). On the other hand, Hsu et al. (2002) proposes a more realistic approach by applying the total rainfall in the overland surface while taking into account the wide range of land use types as well as soil infiltration. Time synchronization between models in 1D/2D approaches constituted another serious and well-reported constraint (Hunter et al., 2005; Bates et al., 2010; Seyoum et al., 2012), resolved by Chen et al. (2007) who proposed accurate models' coupling through sufficient linkages to ensure models' communication and interaction. Nevertheless, despite the remarkable progress noted in coupled 1D/2D models, computational, linkage and coupling issues such as momentum exchange simplifications between 1D and 2D model parts, channel flow representation solely as 1D and deviations in water volume exchange between 1D and 2D model parts according to the linkage technique selected continue to prevail hinder models' performance and implementation for quick predictions (Néelz & Pender, 2013; van Dijk et al., 2014).

2.1.4. Comparing modelling techniques

Models' comparison has undubiously been the focal point of interest in the scientific society. Over the years, numerous modelling approaches have been contrasted based on their mathematical background and configurations, spatiotemporal discretization and numerical schemes for distinct purposes. Pina et al. (2016) used InfoWorks ICM software to display a comparison between semi- and fully distributed models, by testing two case studies with certain features and introducing novel concepts in their modelling. Modelling outcomes were compared with the respective drainage system's water depths, flows and photographic records while design storm events and statistical analysis were also applied for further evaluation. They concluded that choosing a model should be based on the purpose of modelling in conjunction with the data availability and quality. In case the latter requirement is fulfilled, fully distributed models comprise a more realistic solution. Acknowledging the importance of understanding the model features' importance along with their role in code efficiency regarding flood risk management in urban areas, Hunter et al. (2008) and Néelz & Pender (2013) evaluated a wide range of software packages. Specifically, selecting both academic, noncommercial and commercial 2D hydraulic models with distinctive characteristics (as to their numerical approach, spatiotemporal discretization and parallelization technique), they aimed at analysing and comparing the models' performance in urban inundation simulations using a certain case study. Both studies concluded that the models tested could sufficiently estimate water depth, velocity and flood extent – critical parameters in flood risk management. Yet, differences noted among modelling outcomes underline the importance of choosing specific crucial parameters in the preliminary assumptions or models' code as well as the need to address uncertainty.

As demonstrated in the state-of-the-art methods' review presented in the current chapter, remarkable advancements have been noted in urban inundation modelling over the past century. Nevertheless, despite their vast utility as flood hazard analysis tools aiding in understanding, evaluation and anticipation of the inundation's repercussions on the environment and society, their extensive potential for future improvements and applications was acknowledged. This potential is further reinforced by taking the remote sensing data collection methods' rapid development and availability into consideration in conjunction with the continuous research progress in the discretisation of fluid flow domain. In addition, considering the advantages of coupling different modelling approaches (i.e. 1D/1D and 1D/2D modelling techniques), such methods are likely to continue and prevail in future modelling, with future software packages involving a greater number of related physical processes in their simulations. Nevertheless, the selection, development and application of a model should be case-specific and oriented towards fulfilling the objectives set. Subsequently, a balance among the scope, precision, data requirements, complexity and computational demands is required.

3
Materials & Methods

3.1. Study site – Colombo Metropolitan & Kolonnawa catchments

Similarly to the rest of the Southeast Asian countries, climate in Sri Lanka is principally influenced by the South Asian Monsoon, the North Indian Ocean Tropical Cyclones and natural climate fluctuations, including the El Niño-Southern Oscillation (ENSO). Located in the humid tropics, the country experiences large seasonal precipitation variations across three main climatic zones, namely the Dry Zone in its northeast part, the Wet Zone in its southwest region and the Intermediate Zone encompassing Sri Lanka's central hills. Subjected to the South Asian monsoon system, the Wet Zone is characterised by a short dry season between January and February as well as uniform precipitation patterns – generating over 4500mm mean annual rainfall – in the rest of the year (Burt & Weerasinghe, 2014). Due to the inter-tropical convergence zone (ITCZ) migration, the country's southwest coastline is particularly vulnerable to tropical cyclones, depressions and thunderstorms. In addition, the inter-annual climate variations in Sri Lanka are further influenced by both the ENSO – reinforcing dry and warm conditions during El Niño periods – and climate change – resulting in wet regions becoming wetter and dry regions becoming drier (Marambe, et al., 2014; World Bank & CIAT, 2015).

Located in the Wet Zone, Colombo Metropolitan region constitutes the commercial and financial core of Sri Lanka as well as the selected case study. The region is relatively flat and predominantly urban (commercial and residential zones), with a unique urban wetland network and an extensive canal system (Figure 2). Kelani River and Diyawannawa Oya's channel network comprise Colombo Metropolitan region's major water resources. Specifically, the former flows along the region's north boundary towards the Indian Ocean driven by seasonal flow patterns while the latter traverses Colombo city – where it is used as a storm water drainage system – and connects to both Kelani River and the Indian Ocean through St. Sebastian north canal outfall and a tunnel system, respectively. Based on bathymetric data (SLLDC), 80% of these channels' bed levels are approximately 1m below the mean seal level (MSL) and subsequently, their flow is driven by hydraulic gradient. The existing micro drainage and sewer network are not considered in the current study. The project area is further split into two divisions, namely Colombo Metropolitan and Kolonnawa catchments (Figure 2).

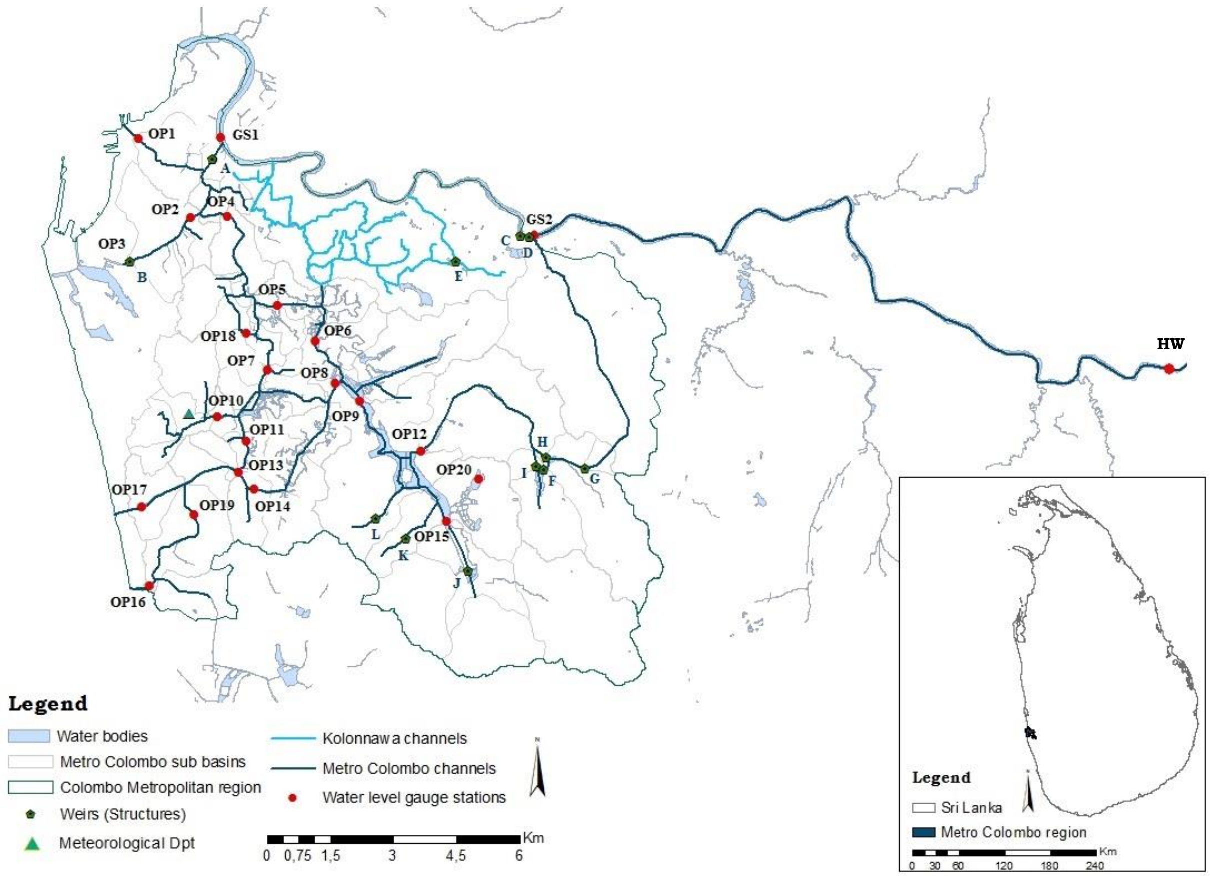

Figure 2. Overview of Colombo Metropolitan region[4]

Despite its growing economy, the project area is particularly vulnerable to urban flooding with its consequences hampering the country's potential for further development. In the recent years, Colombo Metropolitan region has experienced several flood events which affected hundreds of citizens and properties.

3.2. Data availability

The ability to reproduce the conditions and inundation patterns observed in Colombo Metropolitan and Kolonnawa catchments primarily depended on data availability and accuracy. The type and sources of data, methods of their collection and implementation as well as their accuracy were presented in Table 1. Data limitations with respect to continuous water level (WL) and discharge measurements in both catchments were acknowledged.

[4] The name, location and short description of both water level gauge stations and hydraulic structures present in the study site are provided in Tables 4 and 5 (Appendix B).

Table 1. Overview of datasets applied in the hydrodynamic models

Type	Description	Application	Source
Input dataset			
Topography	Digital Elevation model (DEM) obtained from LiDAR survey with 1m horizontal and 0.15 - 0.20m vertical accuracy	30m DEM (resampled from the 1m DEM) was used for 2D model mesh bathymetry	SLLRDC
Land-use	Land use data as reported in the period between 2012 and 2015 consisted of the following categories: buildings, public buildings, roads, forests, farms, marshes and other areas	Based on land use categories, surface roughness was specified	LUPPD
Ground-survey	Cross sections and structures' features were based on LHI [Kelani River (2003), Metro Colombo canals (2012)] and SLLRDC surveys (Kolonnawa canals (2012)]	Used to build the 1D model. Cross sections' bottom points used for 1D model bathymetry	SLLRDC
Stream gauge observations	Tidal measurements at Colombo port (1 location) and discharge measurements (1 location) along Kelani River.	River discharge and tidal measurements were used as model input (boundary conditions)	Sri Lanka Ports Authority, SLLRDC and Irrigation Department
Climate	Rainfall (15min measurements in 1 location) and evaporation	Model input	Department of Meteorology
Evaluation dataset			
Stream gauge observations	Water level point measurements in 8 (0510), 7 (1110) and 12 (0516) locations of Colombo Metropolitan catchment. Water level time series in the 2 Kelani River gauging stations for 0510, 1110 and 0516 events. Water levels in 25 (0516) locations obtained from field survey in Kolonnawa catchment	Used to compare with D-Flow FM and MIKE FLOOD outcomes and evaluate their performance	SLLRDC and Deltares

WL point measurements and time series were manually collected from gauge stations located in Metro Colombo region (Figure 2). Staff gauges with an upper limit of 7.65m (25ft), 3.65m (12ft) and 2.00m were used to estimate the WL observed in Ambatale (Kelani River, GS2), Nagalagama Street (Kelani River, GS1) and catchment's channels, respectively (Figure 22). Moreover, approximations were carried out in channels under inundation conditions in where WLs exceeded 2.00m. Measurement errors were subsequently introduced and a standard deviation of 0.10m in all field observations was accepted. This assumption was in compliance with previous reports addressing Colombo Metropolitan region (COWI, 2013; Deltares, 2016) and no further analysis of the field measurements' accuracy was conducted. Moreover, discharge in Hanwella station (HW, the most upstream catchment's point) was estimated using yearly established rating curves.

Rainfall time series (15min data) were obtained from the Department of Meteorology, located within Metro Colombo catchment (Figure 2). A pluviograph and a bucket (for daily control) were utilised for these recordings (Figure 23). These measurements were implemented in both MIKE FLOOD (MIKE 11 NAM rainfall runoff model's input) and D-Flow FM (spatial rainfall on the grid) models.

3.3. MIKE FLOOD & D-Flow FM set-up

Hydrodynamic models comprise mathematical models aiming at reproducing the water flow dynamics by solving equations formulated by physics' principles. The two hydrodynamic software tools implemented in the present study are briefly described in the following subchapters. Primarily due to data limitations, models were not calibrated but validated based on the abovementioned WL datasets. The methodology applied for their validation is presented in the sub section 3.5 while further analysed and discussed in Chapters 4 and 5, respectively.

3.3.1. MIKE FLOOD model

MIKE FLOOD comprises a physically-based, spatially distributed flood modelling software package. Developed by the Danish Hydraulic Institute (DHI) group, it dynamically combines two separate software tools, namely MIKE 11 (1D) and MIKE 21 (2D) (DHI, 2010). To describe the mass and momentum conservation, MIKE 11 applies the full dynamic wave solution, which is based on an implicit finite difference scheme[5] introduced by Abbott and Ionescu (1967). In addition, MIKE 21 solves the full, time-dependent, nonlinear conservation laws for continuity and momentum by means of implementing the implicit finite difference methods' variables into each cell of a rectangular mesh. MIKE FLOOD couples MIKE 11 and MIKE 21 through a number of linkage types including the standard, lateral, structure, urban and zero flow links. An extensive description of the MIKE FLOOD software -including details about the software components, theoretical scientific background and references- is given in its user and reference manuals (DHI, 2010).

3.3.2. D-Flow FM model

D-Flow Flexible Mesh (FM) constitutes the latest, hydrodynamic software system developed by Deltares for multiple applications, including that of rainfall-runoff in urban environments. Likewise MIKE FLOOD, D-Flow FM comprises a physically-based, spatially distributed modelling package which uses the full dynamic wave solution to guarantee mass and momentum conservation, yet, in an utterly different scheme, namely implicit finite volume method[6]. Significant modelling flexibility and high efficiency are provided by means of a staggered unstructured mesh with the ability to be orthogonalized and refined (or coarsened) at specific locations. Additionally, several meshes (1D/2D/3D) can be merged into a single mesh. Characteristics such as points' partly wetting-and-drying allow for a more gradual inundation and drying process, making D-Flow FM suitable for inundation computations. A detailed description of the software components, its theoretical baseline and references is provided in D-Flow FM user and reference manuals (Deltares, 2017).

3.3.3. 2D Floodplain flow

Floodplain roughness comprises one of the key elements controlling the flood propagation, with its values being highly dependent on the vegetation cover type. In the current case, Manning's "n" roughness map was developed based on recently updated land use categories obtained by the Land Use Policy Planning Department (LUPPD) and reviewed using literature studies with similar project features. The coefficients varied from 0.035 $\frac{s}{m^{1/3}}$ to 0.055 $\frac{s}{m^{1/3}}$.

Aiming at decreasing MIKE FLOOD model runtime in acceptable levels while maintaining sufficient spatial resolution, several important aspects were addressed. Specifically, the initial DEM was modified by excluding elevation data above 3.5m+msl, as these regions were not expected to flood. Kelani River and channel networks were also excluded from the DEM. Yet, marshy areas with an elevation lower than 10m+msl were considered in the model schematisation to represent the full flood storage during extreme inundation conditions. Additionally, to balance the inundation hazard

---

[5] This method uses the differential equations describing the physical phenomena governing water behaviour and solves the system of equations by specifying values of the unknown variable function in the computational domain's distinct nodes (Popescu, 2014). The implicit scheme indicates that the entire domain needs to be solved prior to proceeding to the next time step.

[6] In this method, the computational domain is discretised into control volumes (CV) in where the respective differential equations are implemented. Values of the unknown variable function and their derivatives are approximated and problem solution is achieved by solving the system of equations derived from assembling the obtained equations over a CV (Popescu, 2014).

accuracy, model runtime and 1D/2D efficient coupling, a 30m grid cell resolution was chosen after several test model simulations.

The above described DEM was also applied in D-Flow FM, to allow direct comparison with MIKE FLOOD. However, by considering the different models' principle in estimating rainfall-runoff as well as the importance of including the entire surface area, topographic and roughness features, the additional D-Flow FM simulation was carried out using the initial DEM with a 30m grid cell resolution.

3.3.4. Rainfall runoff (RR) concept

The 1D river and channel network was developed based on a digital elevation model (DEM). Cross sections were schematised based on previous surveys (LHI and SLLRD).

NAM deterministic, lumped, conceptual modelling and a hydrological response unit (HRU) technique were applied to estimate the MIKE 11 surface runoff in Colombo Metropolitan and Kolonnawa catchments, respectively. Specifically, the former catchment was divided into 51 sub-catchments, modelled using certain parameters (i.e. elevation zones, maximum water content in surface and root zone storages, time constants for interflow and routing overland flow, runoff coefficient and time of concentration), calibrated and validated based on observed river and channel WLs of this region[7]. In addition, due to the lack of WL and discharge data in Kolonnawa catchment, a unit hydrograph method using the SCS-CN technique was applied to derive the MIKE 11 input. Water bodies (i.e. lakes) present in the study area were included in MIKE 1D network. In addition, hydrological processes evaporation and infiltration were considered while building MIKE 11's RR component.

Comprising a fully distributed and physically-based model, D-Flow FM replicated the rainfall-runoff process by implementing a different approach. Specifically, rainfall was directly applied on the 2D mesh, the water movement and direction was primarily driven by features including the topography, roughness and thickness of water layers on the surface while runoff was generated at each mesh node. Once water reached the 1D network, it automatically entered the system. Yet, limitations with respect to the current D-Flow FM version did not allow for hydrological processes' application (i.e. evaporation, interception and infiltration), leading to a less representative water balance.

3.3.5. Coupling 1D & 2D flows

Taking advantage of both 1D and 2D methods' benefits, 1D/2D coupling mechanisms were implemented in both MIKE FLOOD and D-Flow FM models to ensure sufficient similarity between physical and model behaviour as well as accurate flow simulation through hydraulic structures and complex urban terrain.

Considering the region's distinctive features, the coupling methodology followed in MIKE FLOOD differentiated according to the unit addressed. Specifically, due to the large mean cross section width of Kelani River (~100m), its cross sections' majority was represented by multiple grid cells. Subsequently, lateral links comprised the most suitable linking option, as they considered non-sequential banks as banks of the cross section and interpolated to create artificial levees on each side of the river. On the other hand, the mean cross section width of the channel network was less than 30m and thus, the lateral link option (centre line) with solely one coupling considered the appropriate choice.

In D-Flow FM, smooth and realistic water flow representation was highly dependent on 1D and 2D networks' bathymetry in conjunction with precise coupling. By taking the site's distinctive characteristics into consideration, two types of 1D/2D internal net links were implemented, namely lateral and embedded linkages. Similarly to MIKE FLOOD, the former type was applied to couple Kelani River's banks – represented solely in 1D network – with the 2D floodplain. The 1D/2D

[7] A detailed description of the MIKE 11 NAM rainfall runoff model built and used in the current case study is presented in Appendix B.

embedded linkages were implemented in all Metro Colombo and Kolonnawa channels. Correct 1D and 2D bathymetries comprised essential elements as they aided in diminishing double counting of water at these parts of the model.

3.3.6. Structures

Weirs, culverts and control structures comprised the three structure types present in the project area. Specifically, Colombo Metropolitan catchment consisted of 57 structures, namely 7 weirs, 49 culverts and 2 control structures while in Kolonnawa catchment, 72 culverts existed. According to the software used, distinct structure tools were applied for their model representation while their identification characteristics (i.e. geometrical type, length and coordinates) were obtained from previous surveys conducted by LHI and SLLRD.

In MIKE 11, weirs were implemented in the model by using the 'broad crested weir' type and a detailed structure description (i.e. location, attributes, geometry, Q/h relation). Control structures were separately introduced and described in the model while their control definition was based on WLs. Culverts' cross-section shape (i.e. standard rectangular, standard circular or irregular), main characteristics (i.e. location, length, upstream/ downstream invert levels, number of parallel culverts etc.) and flow conditions were specified for each of the 121 culverts included in this study.

D-Flow FM limited options with respect to structure types and their attributes hindered weirs, culverts and control structures' application in the model. In particular, weirs were introduced as gates and their location, sill level and width were specified. Culverts' attributes (i.e. coordinates, bed level and diameter) were defined and implemented as part of the 1D network. Due to beta testing issues, control structures were not implemented in the current model's version. To compensate for this shortcoming, the model was interrupted by the user and local 1D bathymetric values were manually increased to the desired level[8].

3.3.7. Roughness coefficient

The bed roughness was described using the Manning roughness coefficient "n" which typically varies between 0.01 $\frac{s}{m^{1/3}}$ (smooth surface) and 0.10 $\frac{s}{m^{1/3}}$ (densely vegetated surface). In this case, the 1D network consisted of natural earth channels covered by vegetation and subsequently, an initial global value of 0.04 $\frac{s}{m^{1/3}}$ was set.

In MIKE 11, Manning's "n" values were locally refined, based on distinct channel conditions and characteristics. They ranged between 0.02 $\frac{s}{m^{1/3}}$ and 0.05 $\frac{s}{m^{1/3}}$. On the other hand, a surface roughness map containing values for both 1D and 2D networks was implemented in D-Flow FM. A uniform value of 0.04 $\frac{s}{m^{1/3}}$ was also set for 1D/2D links.

3.3.8. Boundary & initial conditions

The boundary conditions for the river and channel networks of Colombo Metropolitan and Kolonnawa catchments were decided based on data availability. Specifically, the river hydrograph at Hanwella gauge station comprised the upstream 1D model boundary while at downstream, tide gauge data at Colombo Port gauge station were used to represent WLs at four locations, namely the sea outfalls of Kelani River, Mutwall tunnel, Wellawatta and Dehiwala channels[9]. Considering a range of water depth measurements carried out in previous years (2000-2016) along with the study site's bathymetric data, the initial water depth for Kelani River, Kolonnawa and Colombo channel network was set at 0.4m in both models.

---

8 This solution was event-specific. WLs were cautiously inspected at certain OLs and specific threshold WLs were reached prior to D-Flow FM's interruption.

9 Due to Colombo port's close distance with the four catchment's outfalls, the port's tidal record was assumed to be representative of the sea level fluctuations occurring in the abovementioned outlets.

3.4. Model analysis

D-Flow FM and MIKE FLOOD models were analysed based on three historical inundation events, for each of which WL records (point measurements and time-series at specific locations) were available. The events' description and available field observations are summarised in Table 2 and Table 8, respectively. For each event, solely the time frame corresponding to the main rainfall event was simulated and analysed.

Table 2. Summary of historical inundation events in Colombo Metropolitan catchments

Event ID*	Event type	Duration	Total rainfall depth (mm)	Maximum rainfall (mm/h)
0510	Major	13 – 21/05/10	616	≤ 56
1110	Major	10 – 11/11/10	440	123
0516	Dangerous	15 – 16/05/16	329.5	45

* Note: The event ID is derived based on the event's month/year (mmyy) of occurrence and used as a reference in the current study.

3.5. Evaluation of models' results

Graphical and statistical model evaluation techniques were applied to assess D-Flow FM and MIKE FLOOD models against field observation data. Due to lack of continuous measurements in most of the WL gauging stations, distinct evaluation techniques were implemented according to the nature and availability of data. Specifically, in part 2.6.1, WL graphs, the Absolute (AD) and Relative Difference (RD) indicators were applied for models' performance comparison with field point measurements. In part 2.6.2, three quantitative statistics were implemented in comparing both the models' performance with time series derived from WL gauging stations in Kelani River as well as D-Flow FM and MIKE FLOOD models. The results are presented in Chapter 3.

3.5.1. Evaluation of Metro Colombo channels (point observations)

Graphical methods comprised valuable assessment tools as they provide a visual comparison between simulated and field observation data along with an initial overview of the model performance. Due to data limitations, graphs illustrating WLs at certain gauging locations within the Colombo Metropolitan catchment were selected for the comparison (Table 3). Gauge records' availability in conjunction with their spatial distribution constituted the primary reasons for these sites' selection. For each of these locations, both D-FLOW FM and MIKE FLOOD simulated results (time series) were plotted against the respective field observation data (point observations). Absolute (AD) and relative differences (RD) were computed at the point observations available. Despite the restricted number of field measurements for these 3 events, lack of peak observations was also noted in the observation locations' (OLs') majority. Subsequently, mean RDs were estimated to further understand and evaluate the variability of those deviations while maps were generated for visualisation purposes. In addition, RDs were combined with the corresponding calculated ADs to provide a better view to the values of differences. Positive RD values revealed an underestimation by the simulated results while negative RD values indicated an overestimation.

$$RD = (H_{obs} - H_{sim})/H_{obs} \quad (1)$$

where H_{obs} comprised the observed WL at a specific site and time while H_{sim} described the respective simulated WL at this location and time.

3.5.2. Evaluation of Kelani River gauging stations (time series)

Nagalagamaa and Ambatale comprised the only gauging station locations where WL time series were available. Evaluation of these datasets in conjunction with an additional comparison between MIKE FLOOD and D-Flow FM model outcomes was conducted based on the abovementioned evaluation techniques[10] along with three quantitative statistics, namely Pearson's coefficient of determination (R^2), Nash – Sutcliffe efficiency (NSE) and root mean square error (RMSE).

Specifically, to identify the relation between predicted and measured data in conjunction with its strength, Pearson's coefficient of determination was selected. R^2 varies between 0 and 1, with values closer to 1 indicating less error variance.

$$R^2 = \left[\frac{n\cdot(\sum_{i=1}^{n} x_i y_i) - (\sum_{i=1}^{n} x_i)\cdot(\sum_{i=1}^{n} y_i)}{\sqrt{n\cdot[\sum_{i=1}^{n}(x_i{}^2)] - (\sum_{i=1}^{n} x_i)^2}\sqrt{n\cdot[\sum_{i=1}^{n}(y_i{}^2)] - (\sum_{i=1}^{n} y_i)^2}}\right]^2 \quad (2)$$

where n comprises the total number of observations, x_i is the the i[th] field observation and y_i is the i[th] simulated value.

In addition, aiming at providing a relative model assessment, NSE technique was chosen as it 'determines the relative magnitude of the residual variance compared to the field observation data variance' (Nash and Sutcliffe, 1970).

$$NSE = 1 - \left[\frac{\sum_{i=1}^{n}(Y_i^{obs} - Y_i^{sim})^2}{\sum_{i=1}^{n}(Y_i^{obs} - Y_i^{mean})^2}\right] \quad (3)$$

where n comprises the total number of observations, Y_i^{obs} is the i[th] field observation, Y_i^{sim} is the i[th] simulated value and Y_i^{mean} is the mean WL derived from the field observation data. NSE reflects the degree to which the simulated versus measured data match the 1:1 line (regression line with a slope equal to 1).

Moreover, RMSE technique comprises one of the most commonly implemented error index statistics and was selected to obtain a quantitative estimation of the deviation between the measured and predicted WL datasets available.

$$RMSE = \sqrt{\frac{\sum_{i=1}^{n}(Y_i^{obs} - Y_i^{sim})^2}{n}} \quad (4)$$

where n comprises the total number of observations, Y_i^{obs} is the i[th] field observation and Y_i^{sim} is the i[th] simulated WL value. By also taking the field observation's magnitude and standard deviation into consideration, the lower the RMSE, the greater the model simulation performance.

10 For Kelani River gauging stations (time series available), ADs and RDs in WL peaks were also calculated.

4
Results

4.1. Simulation of water level

WL measurements comprised the only observations available in the present case study area for the 3 inundation events. Subsequently, the models' comparison and assessment were based on this reference at event – specific observation locations.

4.1.1. May 2010 (0510) event

For 0510 event, field WL point observations were plotted against the corresponding simulated MIKE FLOOD and D-Flow FM models' time-series at 10 OLs [Appendix C, May 2010 (0510)]. Focusing on the models' performance (Figure 3), underestimations were observed in all but two locations (OP16 & OP20), with the largest being marked in the most downstream points, namely OP14 (>30%), OP16 (>25%) and OP17 (up to 56%). Low estimated Pearson's R^2 and NSE along with high RMSE values (Table 3) were noted in both Ambatale (GS2) and Nagalagama (GS1) gauging stations during this event. Progressively increasing deviations were inspected further downstream in Heen Ela – Mahawatta connection (OP7), Torrington channel (OP10), Heen Ela (OP11) and Kirulapoana channel (OP13) where WLs were underestimated by more than 24%, 26%, 28% and 27%, respectively.

a. Upstream observation locations

Gauging stations in Kelani River

Ambatale gauging station (GS2, Figure 25) comprised the most upstream OL in the current study case. As indicated in the respective graph (Figure 25), measured WLs were oscillating between 1m+msl and 1.5m+msl in the event's first 4 days (May 13th – 16th). An abrupt rise was noted in May 17th (c. 04:00) where WLs increased by more than 3m in a time span shorter than 16h. This change was followed by constant WL fluctuations ranging between 4m+msl and 4.5m+msl for the rest of this event (May 17th – 22nd).

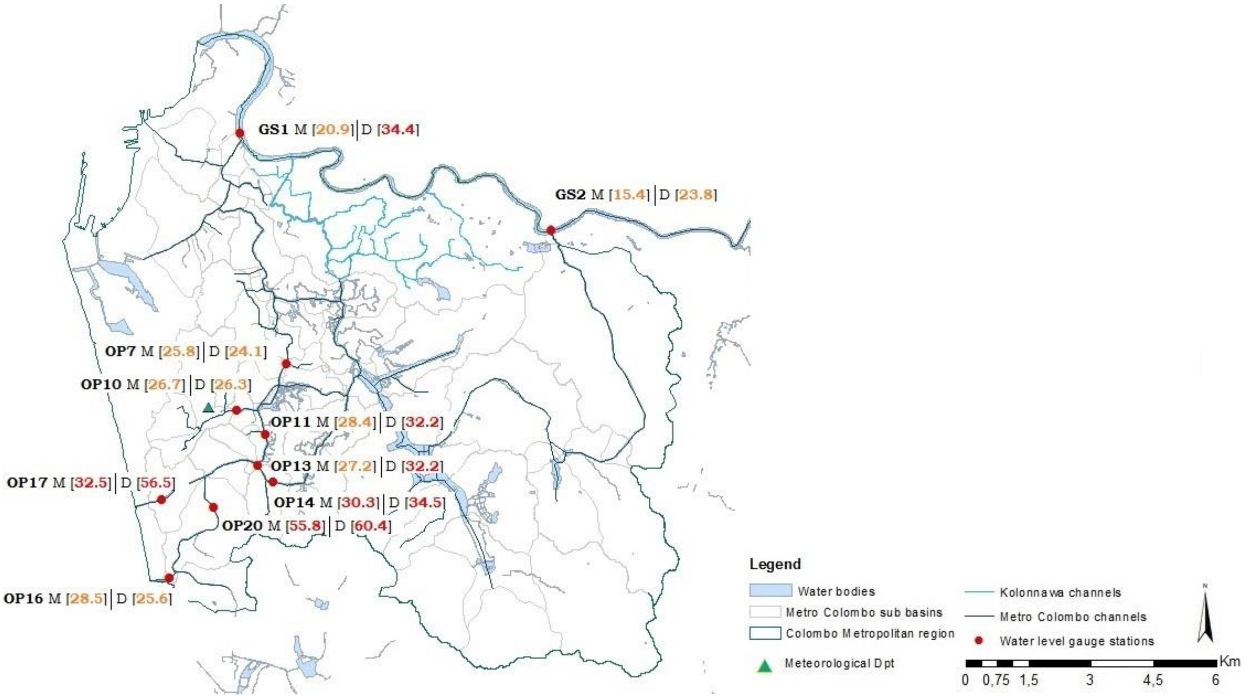

Figure 3. Mean MIKE FLOOD and D-Flow FM RDs (%) in the study site's observation locations (0510)

By taking the above described observed WL behaviour into consideration and comparing it with MIKE FLOOD and D-Flow FM outcome, differences with respect to the overall simulated behaviour of WLs' fluctuations in conjunction with the event's WL peak detection and specification were noticed. More specifically, both models -primarily MIKE FLOOD- responded to the short but intense rainfall occurring on May 13th (c. 00:15 – 02:45) and May 14th (c. 07:15 – 15:00), with simulated WLs rising above 1.8m+msl while deviating by more than 80% (overestimation, MIKE FLOOD, AD ≅ 0.82m) and 55% (overestimation, D-Flow FM, AD ≅ 0.70m) from the respective real observations. From May 17th onwards, both models followed a similar pattern, with their simulated WLs rising gradually but slowly. As shown in Figure 25, MIKE FLOOD and D-Flow FM's simulated WL rise was not in accordance with the abrupt measured one, taking approximately 2 days to reach peak WLs – compared to the 16h in reality – while underestimating by more than 15% (underestimation, MIKE FLOOD, AD ≅ 0.73m) and 24% (underestimation, D-Flow FM, AD ≅ 1.12m) the event's WL peak. This discrepancy was also demonstrated in the high RMSE values (MIKE FLOOD: 0.90 & D-Flow FM: 1.08) for GS2 (Table 3).

Table 3. MIKE FLOOD and D-Flow FM performance indicators[a] for water levels in Kelani gauging sites

Gauging station ID	0510			1110			0516		
	R^2	NSE	RMSE	R^2	NSE	RMSE	R^2	NSE	RMSE
MIKE									
GS1	0.77	0.20	0.38	0.58	-0.39	0.24	0.93	0.75	0.21
GS2	0.79	0.69	0.90	0.20	0.14	0.54	0.98	0.94	0.25
D-Flow FM									
GS1	0.72	-0.25	0.48	0.69	0.64	0.24	0.94	0.94	0.15
GS2	0.73	0.55	1.08	0.46	0.37	0.46	0.98	0.98	0.19

[a] Performance ratings of the statistics selected (R^2, NSE, RMSE) were based on Henriksen et al. (2008) and Moriasi et al. (2007). Specifically, $R^2 \geq 0.85$ very good, $0.85 \geq R^2 \geq 0.65$ good, $0.65 \geq R^2 \geq 0.50$ satisfactory and $R^2 \leq 0.50$ unsatisfactory; NSE ≥ 0.75 very good, 0.75 ≥ NSE ≥ 0.65 good, 0.65≥ NSE ≥ 0.50 satisfactory and NSE ≤ 0.50 unsatisfactory; RMSE ≤ 0.10 very good, 0.10 ≥ RMSE ≥ 0.20 good, 0.20 ≥ RMSE ≥ 0.30 satisfactory and RMSE ≥ 0.30 unsatisfactory[11].

[11] The RMSE values were based on the abovementioned literature but adjusted for the current case's results.

In addition, similar WL patterns were noted further downstream, in Nagalagama street gauging station (GS1). Focusing on the period prior to the abrupt WL rise (May 13th – 17th), both MIKE FLOOD and D-Flow FM showed an almost identical behaviour (Figure 26), with their fluctuations being influenced by the tidal signal. Even though both simulated and observed WLs displayed a comparable overall pattern, the models underestimated by more than 30% the respective real observations. Similar to the case of GS2, both models did not succeed in temporally detecting and determining the event's WL peak, resulting in a 33h time shifting along with underestimations of 21% (MIKE FLOOD) and 34% (D-Flow FM) – as indicated in Figure 26. The above described models' performance was also depicted in the very low NSE values at GS1, reflecting the disparity of simulated and observed values.

b. Downstream observation locations

OLs in Metro Colombo channels

As shown in Figure 26 – Figure 30 (Appendix C), D-Flow FM simulated accurately the WL peaks in the event's first 5 days (May 13th – 17th), with its values deviating less than 9% (OP7 & OP10) and 15% (OP11, OP13 & OP14) compared to the respective observed peaks. However, from May 17th onwards, the model underestimated the observed WL fluctuations by more than 26% (AD ≥ 0.45m) in each of the abovementioned locations. Focusing on the first half of 0510 event and the same observation points [Figure 26 – Figure 30 (Appendix C)], MIKE FLOOD showed a constant underestimation of the event's WL fluctuations – including its peaks, with each of the simulated values deviating by more than 29% compared to real observations (Figure 3). Nevertheless, in the event's second half, deviations between simulated data and field measurements were diminished. Specifically, the model's values deviated by less than 15% (0.12m ≤ AD ≤ 0.28m) compared to real observations.

OLs close to the catchment's outfalls (Indian Ocean)

Wellawatta (OP17) and Dehiwala (OP16 & OP20) channels constituted the catchment's most downstream points, located close to the Indian ocean. Primarily due to their location, the tidal signal in conjunction with its impact on the overall behaviour of WL fluctuations were apparent [Figure 31 – Figure 33 (Appendix C)]. Focusing on OP17 and solely taking the available real observations into consideration, oscillations between 0.8m+msl and 1.2m+msl were noted throughout the event. However, as indicated in Figure 4, MIKE FLOOD and D-Flow FM models' performance diverged from the field measurements resulting in WL differences of up to 0.7m (underestimation, RD≅67%) and 1m (underestimation, RD≅100%), respectively. Despite the event's general underestimation by both models at this point, MIKE FLOOD simulations were closer to the WL rise observed due to high intensity rainfall.

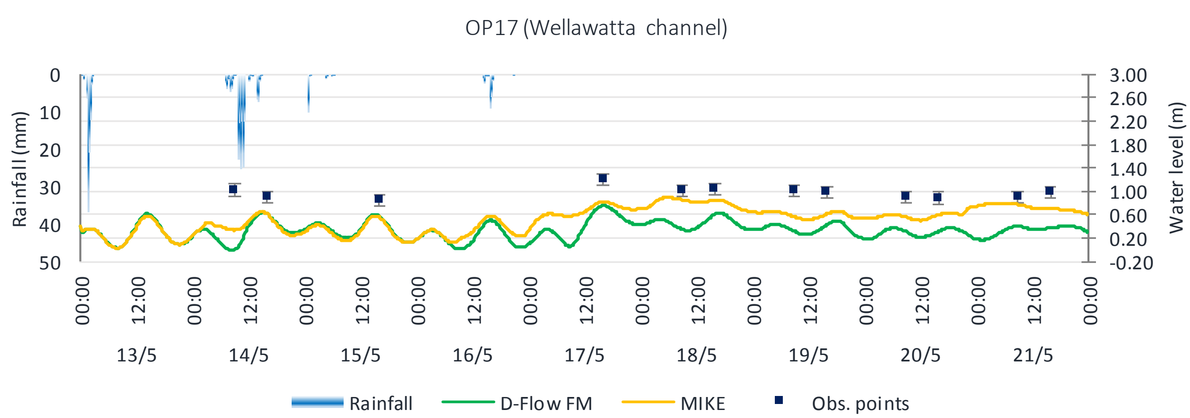

Figure 4. Simulated WL fluctuations against field observations in OP17 (0510)

On the other hand, field measurements in the two Dehiwala OLs (OP16 & OP20) showed that tide comprised the dominant factor influencing WL fluctuations more compared to the 0510 inundation event. Although the tidal signal was pronounced in both MIKE FLOOD and D-Flow FM outcome, their WL patterns were also affected by the high intensity rainfall, leading in WL rises and over 60% WL overestimations (Figure 3). Despite this trend, D-Flow FM simulated values were closer to the respective observed water fluctuations – as shown in Figure 31 and Figure 33, with deviations not exceeding 26% (OP16) and 30% (OP20) in the points' majority.

4.1.2. November 2010 (1110) event

For November 2010 event (1110), the results obtained from MIKE FLOOD were less consistent with the D-Flow FM simulations' outcome and real observation data – in terms of overall behaviour of WL fluctuations in conjunction with event's WL peak temporal detection and determination. Considering all observation points, MIKE FLOOD appeared to underestimate the event by 30% compared to D-Flow FM – the underestimation percentage of which oscillated around 16%. However, a consonance between the models was noted on the deviations' order of magnitude in distinct locations. Specifically, GS1 and OP7 displayed the smallest divergences in both models while similar behaviour and deviations were also depicted in GS2. The largest divergences in both MIKE and D-Flow FM were observed in the most downstream points (OP11, OP16 & OP17).

a. Upstream observation locations

Gauging stations in Kelani River

As indicated in Figure 35, the WLs as well as their overall oscillations recorded in Ambatale gauging station (GS2) during the 1110 event demonstrated divergences from the corresponding MIKE FLOOD and D-Flow FM simulations. Observed water fluctuations were ranging from 1m+msl to 1.5m+msl prior to the event, with a sudden increase noted in November 10th (c. 18:00). During this time span, WLs rose more than 1.9m in less than 18h and gradually returned to their initial levels – after 1.5d. By comparing the above described measured data with the corresponding models' predicted values, little association was noted – also reflected on their calculated R^2 and NSE performance indicators (Table 3). Specifically, prior to the event's initiation, no correlation between the models' simulations and real observations was observed. MIKE FLOOD and D-Flow FM performance convergence was marked immediately after the rainfall started (November 10th, c.10.30). Their convergence was also combined with the models' instantaneous response to rainfall, resulting in a 7h time shifting and an underestimation [MIKE FLOOD: AD≅0.49m (18%) & D-Flow FM: AD≅0.34m (13%)] of the event's WL peak.

Tide-driven water fluctuations were observed in GS1, with WLs ranging between 0.20m and 0.85m prior to the 1110 event. Despite showing a comparable overall pattern, both models' simulations underestimated by more than 30% the respective field measurements at this period. Additional differences were noted in the WL behaviour shortly after the rainfall event's start, with simulated values diverging both from real observations and themselves. Moreover, neither MIKE FLOOD nor D-Flow FM matched the event's WL peak and corresponding oscillations, resulting in deviations of up to 13% and 1.5%, respectively. The above described models' performance was also depicted in the low R^2 and NSE values at GS1, reflecting the disparity of simulated and observed values (Table 3).

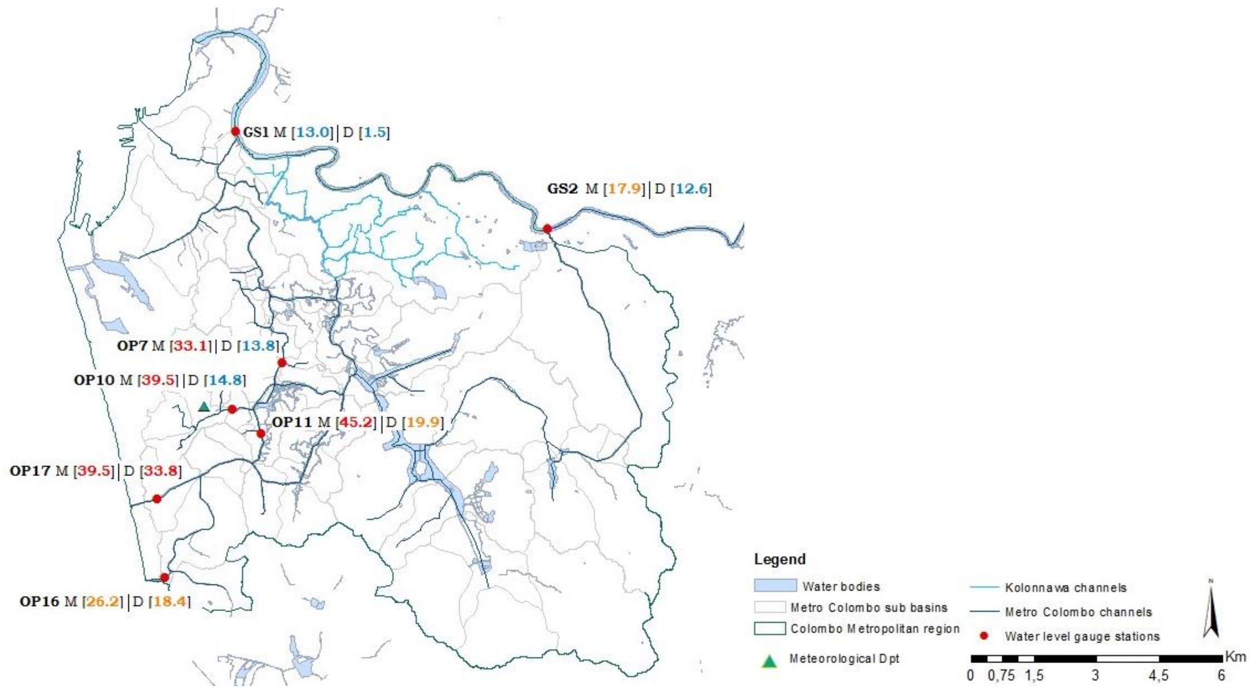

Figure 5. Mean MIKE FLOOD and D-Flow FM RDs (%) in the study site's observation locations (1110)

b. Downstream observation channels

OLs in Metro Colombo channels

During this event, the WL fluctuations in Metro Colombo channels (OP7, OP10 & OP11) displayed similar patterns, as demonstrated by the limited field measurements available. This similarity between the indicated channels' behaviour was also noted in both D-Flow FM and MIKE FLOOD simulated WLs. However, once the models' outcome was plotted against real observations, divergences between models and reality as well as models themselves were observed [Figure 36 – Figure 38, (Appendix C)]. In general, simulated WL behaviour in D-Flow FM at these locations represented more accurately the reality, including the inundation event's peak. Deviations were small prior (RD<5%, with AD<0.02m) but also during the rainfall event (RD<5%, with AD<0.1m). The largest WL differences were noted on the event's attenuation (from November 12th onwards) where D-Flow FM underestimated by more than 5% (OP7) and 14% (OP10) the respective observed WL measurements. In Heen Ela (Kirimandala – Mawatha bridge, OP11), observed data were not available after November 10th and subsequently, comparison and evaluation of the models' outcome using reality as a reference was not possible.

Prior to the inundation event's start, MIKE FLOOD simulated WL fluctuations were proportionated to the respective field measurements and D-Flow FM outcome, with small deviations ranging from less than 0.01m (underestimation, RD<2%) to 0.09m (underestimation, RD≤ 24%) in all Metro Colombo channels (OP7, OP10, OP11, OP16 & OP17). However, since the beginning of the 1110 event, the above described MIKE FLOOD pattern significantly mutated and abrupt WL rises were noted [Figure 36 – Figure 38, (Appendix C)]. By taking Torrington channel OL (Figure 6) as an example, this divergence – in terms of overall behaviour, temporal detection and determination – between MIKE FLOOD simulated WLs and reality was shown. More specifically, although real observations depicted an at least 5.5h response time – which was also demonstrated in D-Flow FM results, MIKE FLOOD simulated WLs showed an immediate response to rainfall which also resulted in a shifted WL peak in OP10. Additionally, from November 11th onwards, WLs deviated by more than 22% (underestimation, AD ≅ 0.5m) and up to 37% (underestimation, AD ≅ 0.7m), for the same location. Similar performance was noted for OP7 (Figure 36) and OP11 (Figure 38) with respect to this event.

OLs close to the catchment's outfalls (Indian Ocean)

As mentioned previously, due to their locations (Figure 2), Nagalagama street (GS1), Wellawatta (OP17) and Dehiwala (OP16) WLs were significantly influenced by the tidal signal. Focusing on the latter two OLs and considering their overall behaviour during 1110 event (Figure 39 & Figure 40), a general agreement between the observed and simulated values was observed, with deviations not exceeding 20% (AD ≅ 0.1m) for both models. Focusing on the OP16, both MIKE FLOOD and D-Flow FM matched most of the field observations during and after the inundation event, with estimated ADs being less than 0.1m (RD<15%). Nevertheless, underestimations of up to 55.2% (MIKE FLOOD, AD ≅ 0.61m) and 61.7% (D-Flow FM, AD ≅ 0.74m) were observed in OP17, after the rainfall event's start.

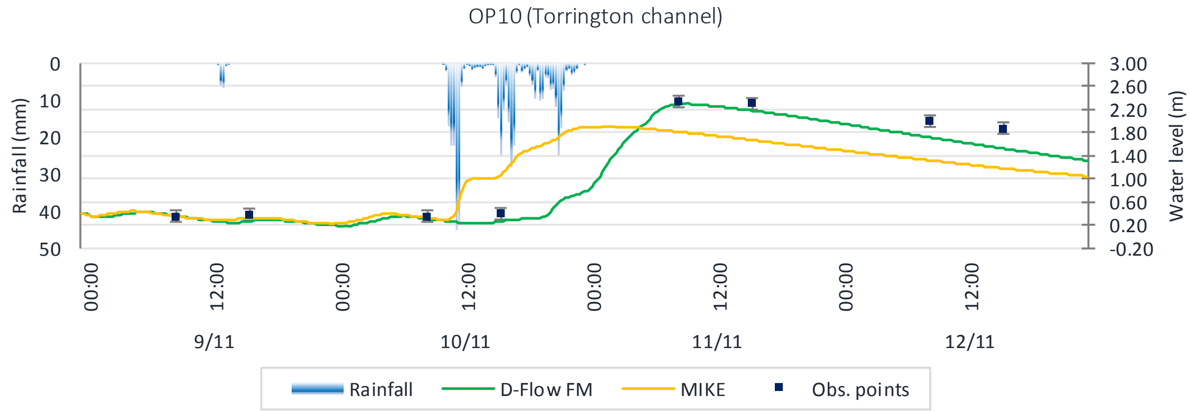

Figure 6. Simulated WL fluctuations against field observations in OP10 (1110)

4.1.3. May 2016 (0516) event

Aiming at assessing MIKE FLOOD and D-Flow FM models' performance regarding May 2016 event (0516), the ADs and RDs between observed and simulated data at specific locations were computed and evaluated. As illustrated in Figure 7, both models showed similar patterns. Specifically, fluctuating WLs were adequately represented in upstream OLs, as also indicated by the performance indicators in Ambatale (GS2) and Nagalagama (GS1) stations (Table 3). Gradually increasing deviations were noted further downstream in Metro Colombo channels. Both models underestimated the event's WLs by approximately 10% and 4% in OP7 and OP9, respectively while this trend became clearer in OP11 (downstream of OP7) where MIKE FLOOD and D-Flow FM underestimated the peak by 12% and 14%, respectively. In addition, simulated WLs in locations close to the Indian Ocean deviated by more than 20% (underestimation in OP17 and overestimation in OP16) compared to real observations while a similar behaviour was observed in points near the Parliament lake (underestimations of up to 10% in OP12 and 40% in OP15).

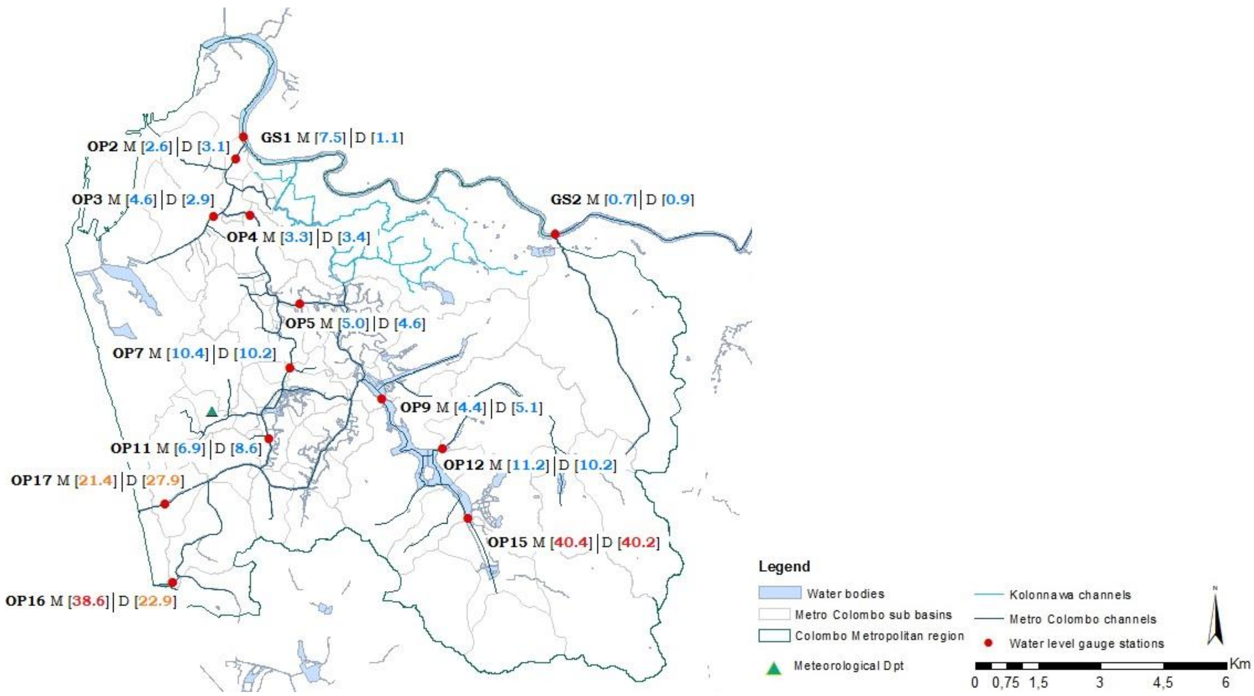

Figure 7. Mean MIKE FLOOD and D-Flow FM RDs (%) in the study site's observation locations (0516)

a. Upstream observation locations

Gauging stations in Kelani River

Prior to 0516 event, WLs in Ambatale (GS2) and Nagalagama (GS1) gauging stations were fluctuating around 2m+msl and 0.7m+msl, respectively. After almost 6 hours of rainfall, an abrupt WL rise (c. 3m in less than 24h) was observed in GS2 while approximately 2 hours later, this increase was also noted in GS1 (c.1m WL rise). From May 16th (c.9:30) onwards, consistent WL oscillations at 5.9m+msl (GS2) and 2.1m+msl (GS1) were observed.

As stated previously, both MIKE FLOOD and D-Flow FM reproduced the above described behaviour of WLs, showing small deviations from the observed time series in both gauging stations. The similarity of observed and simulated data in combination with the overall models' performance were also depicted in the respective calculated indicators, with R^2 and NSE values exceeding 0.93 and 0.94[12], respectively and RMSE values being lower than 0.25 for both models and stations (Table 3).

b. Downstream observation locations

In spite of having a greater number of OLs in Metro Colombo channels, the number of field measurements available for the 0516 event were very limited [Table 8 & Figure 43 – Figure 53, (Appendix C)]. Likewise previous inundation events (0510 & 1110), WL fluctuations in the majority of Metro Colombo channels showed a similar pattern [Figure 43 – Figure 53, (Appendix C)], as indicated by the general agreement of both models' performance at these locations (OP2, OP3, OP4, OP5, OP7, OP9, OP11, OP12 & OP15). This performance was in accordance with the limited real observations available in OP2, OP3, OP4 and OP5, with deviations ranging at 3% (underestimation, AD ≤ 0.05m) but not exceeding 6% (underestimation, AD ≤ 0.09m).

OLs in Metro Colombo channels

In general terms, WLs derived from D-Flow FM simulations were in accordance with the respective MIKE FLOOD ones for the greatest part of this event, excluding its start and attenuation, as indicated in Figure 43 –Figure 50, (Appendix C). Specifically, similarly to 1110 event, MIKE FLOOD showed a higher level of sensitivity to rainfall, with simulated WLs rising almost immediately after the event's

[12] NSE values exceeded 0.94 for both GS1 and GS2 in D-Flow FM as well as GS2 in MIKE FLOOD. MIKE FLOOD's respective value for GS1 was calculated at 0.75 (rated as 'very good').

start and gradually but slowly returning to their initial condition. Despite the models' general agreement, increasing divergences were observed further downstream in Metro Colombo channels (OP7, OP9 & OP11). Specifically, by taking the limited field measurements into consideration, absolute WL differences varying from 0.2m (underestimation, OP7 & OP9) to 0.25m (underestimation, OP11) close to the event's peak were observed. As indicated in Figure 47 – Figure 49 (Appendix C), these divergences progressively diminished from May 17th onwards (lower rainfall intensities), with deviations ranging from 2% (underestimation, AD ≅ 0.04m) to 8% (underestimation, AD ≅ 0.1m).

The observation points 9, 12 and 15 were located adjacent to Kimbulawala and Parliament lakes in Colombo Metropolitan region, with OP9 being the most upstream and OP15 the most downstream point. As shown in the respective graphs [Figure 8,Figure 49 – Figure 50, (Appendix C)], the simulated WL fluctuations in this region followed similar to the rest of Metro Colombo channels' patterns, yet, both models' performance demonstrated deviations from the field observations available. In particular, small divergences were noted in OP9 and OP12 (upstream locations), where simulated values from both models underestimated by 4.5% (OP9, AD ≅ 0.09m) and 10.5% (OP12, AD ≅ 0.09m) the respective measured ones. Their largest differences in both locations were detected close to the event's peak (May 16th). On the other hand, both D-Flow FM and MIKE FLOOD did not capture the observed behaviour of WLs at Kimbulawala road bridge (Figure 8). As indicated by Figure 8, the WLs simulated by both models at this location followed the same pattern as the rest of Metro Colombo channels. Subsequently, OP15's simulated levels ranged from 0.4m+msl to 1.5m+msl with peak values estimated at 1.92m+msl (D-Flow FM) and 1.85m+msl (MIKE FLOOD). However, by taking the available field measurements into consideration and comparing with the respective models' outcome, absolute WL differences of 1m to 1.2m – close to the event's peak – were observed. This discrepancy was addressed and further interpreted in sub section 5.4.

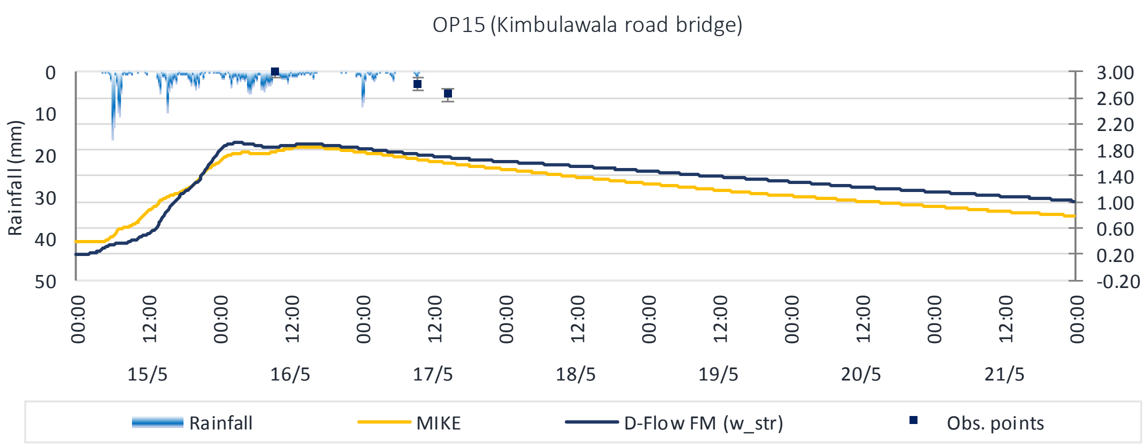

Figure 8. Simulated WL fluctuations against field observations in OP15 (0516)

OLs close to the catchment's outfalls (Indian Ocean)

Considering the field observations available for Wellawatta (OP17) and Dehiwala (OP16) channels, their WL oscillations during the 0516 event were estimated at approximately 0.47m+msl and 1.13m+msl, respectively. Despite the limited number of field measurements, the disparities between the overall observed and simulated behaviour of WL fluctuations were noted (Figure 52 & Figure 53). Specifically, for OP17, MIKE FLOOD and D-Flow FM displayed similar patterns – their deviations were smaller than 3.5% or 0.03m throughout 0516 event – yet both models underestimated by more than 0.24m and 0.32m, respectively the corresponding real observations. Focusing on OP16, the MIKE FLOOD and D-Flow FM performance diverged from the field measurements resulting in WL differences of up to 0.18m (overestimation, RD≅39%) and 0.10m (overestimation, RD≅23%), respectively. In spite of the event's general overestimation at this point, D-Flow FM simulations were closer to the WLs observed.

4.2. Simulation of inundation extent

Inundation extent mapping comprised the second aspect on which MIKE FLOOD and D-Flow FM performance was evaluated. Flood data limitations (i.e. lack of flood marks and satellite images of flood extent) with respect to the 3 events selected did not allow for additional analysis and assessment of the models' outcome. Figure 9 displayed a comprehensive view of the maximum predicted water depth and extent, as simulated by the models, during the 2010 and 2016 events. Distinct colour groups were generated to represent the various simulated inundation depths.

Viewed from a general perspective, the D-Flow FM simulated water volume captured along with its distribution within the catchment deviated from MIKE FLOOD corresponding results, regardless of the event selected. Yet, focusing on specific regions and events, these divergences were even more apparent. Examples included D-Flow FM inundation depth underestimations in Kolonnawa catchment and part of Kelani River's floodplain – region surrounding Ambatale GS (GS2) – during the 0516 event as well as its water depth and extent overestimation in the region close to the Parliament and Kimbulawala lakes in the 1110 event – compared to MIKE FLOOD respective performance.

Addressing the former case, MIKE FLOOD simulated water depths of 2m to 3m in the largest part of Kolonnawa floodplain, with specific locations – very close to Kelani River – surpassing 3.5m (max. value simulated at 3.8m). On the other hand, D-Flow FM results demonstrated a larger inundation extent but shallower waters, with mean and maximum values estimated at 1m and 2m, respectively. On the same wavelength, MIKE FLOOD showed a severe flooding in the upper part of Kelani River floodplain close to GS2 but also near the wetlands located downstream of this point. Specifically, despite its simulated inundation extent being restricted within areas close to the river and channels, the corresponding predicted depths rose up to 4.9m. Similar to the previous case, D-Flow FM demonstrated lower water depths (max. simulated values at 2.1m) but the distribution of water volume within these regions was broader.

Focusing on the 1110 event (Figure 9), the flooding magnitude depicted by MIKE FLOOD differed significantly from the respective D-Flow FM results. As indicated by Figure 9, the former model detected inundation in specific study site's districts, including wetland areas northwest and around Parliament lake, with inundation depths not exceeding 1.7m. In addition, water depths ranging from 0.02m to 1m were also depicted within Kolonnawa region. On the other hand, D-Flow FM demonstrated severe flooding in both Colombo Metropolitan and Kolonnawa catchments. According to Figure 9, during this event, both the Parliament and Kimbulawala lakes surpassed their buffering capacities, inundating surrounding areas, including the island where the Parliament building is located. Simulated water depths at these locations ranged from 2m to 3m. Moreover, Kelani River floodplain was also flooded, with mean and maximum water depths oscillating at approximately 1m ad 2.5m, respectively. Apart from the higher water depths, the volume of water retained as well as its extent within the catchment were overestimated by D-Flow FM compared to MIKE FLOOD performance.

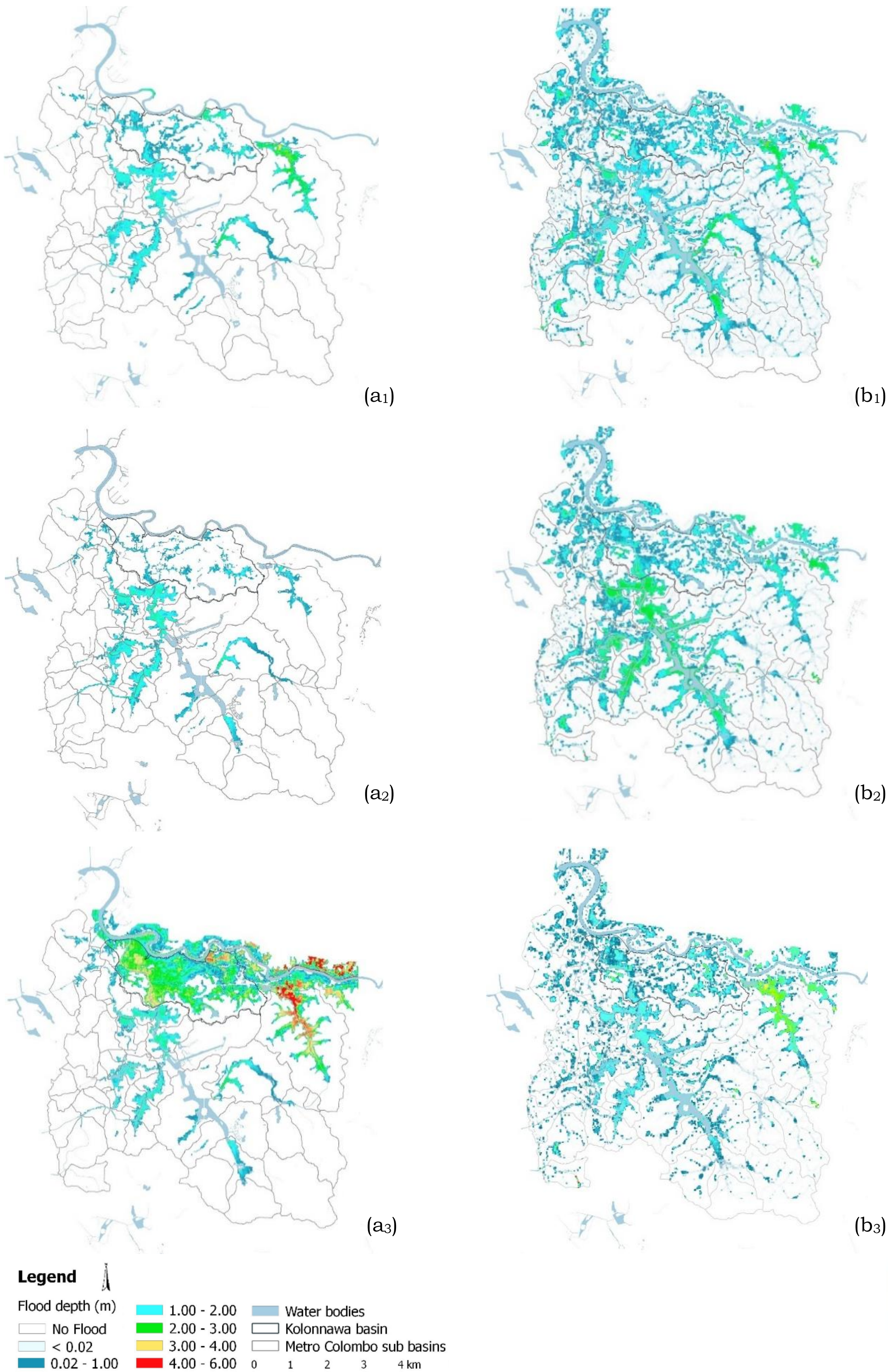

Figure 9. MIKE FLOOD (a) & D-Flow FM (b) inundation extent maps for 0510(1), 1110(2) & 0516(3) events

4.3. Computational time

The elapsed time taken by MIKE FLOOD to simulate the 2010 and 2016 events differed from the respective time used by D-Flow FM model. As indicated in Table 4, small models' divergences were noted in short duration events (i.e. 1110 event), yet, these were increased as the simulation time span became longer (i.e. 0510 and 0516 events). Two indicators, namely the number of grid cells and time steps[13] were additionally displayed to provide a comprehensive understanding of the models' computational time. As demonstrated in Table 4, despite MIKE FLOOD's greater number in both time steps (3 times higher) and grid cells (46.000 cells more), its performance with respect to computational time was equivalent to D-Flow FM. However, when addressing computational times, the different models' RR concept and components should be considered. In addition, when referring to D-Flow FM's performance, methodological constrains (i.e. no optimisation) should be taken into consideration.

Table 4. Models' elapsed time taken for the simulations of 0510, 1110 and 0516 events

Software product	Event ID								
	0510 (13-22/05/10)			1110 (9-13/11/10)			0516 (15-22/05/16)		
	Elapsed time	Grid cells	Time steps	Elapsed time	Grid cells	Time steps	Elapsed time	Grid cells	Time steps
MIKE FLOOD	3h 05min	197,870	155,520	1h 25min	197,870	69,120	2h 45min	197,870	120,960
D-FLOW FM	3h 20min	152,021	47,127	1h 20min	152,021	20,809	3h 30min	152,021	48,960

Specifications of the computers' systems used to run MIKE FLOOD and D-Flow FM models are provided in the table below (Table 5).

Table 5. Computer systems' information

System	Software product	
	MIKE FLOOD	D-FLOW FM
Processor	Intel ® Core ™ i7-6700 CPU @3.40GHz	Intel ® Core ™ i7-4700MQ CPU @3.40GHz
Installed memory	8.00GB	8.00GB
System type	64-bit Operating System, x64-based processor	64-bit Operating System, x64-based processor

[13] The "time step" has two functions, including the provision of i. regular consistent update intervals for a physics simulation and ii. as many steps as necessary for accurate real world physics.

5
Discussion

As mentioned in Chapter 3, MIKE FLOOD and D-Flow FM implement the full dynamic wave solution to simulate inundation in urbanised catchments. Their principle differences laid on the scheme in which this solution is based in combination with the distinct rainfall-runoff and coupled 1D/2D modelling concepts applied. Subsequently, similar overall behavioural patterns were anticipated between the two models with divergences stemming primarily from the above described aspects. Additional deviations due to the D-Flow FM beta testing phase in urban inundation modelling (i.e. lack of standard types of hydraulic structures as well as key hydrological processes' concepts including infiltration, interception and evaporation) were expected.

These considerations were practically demonstrated in Chapter 4, where MIKE FLOOD and D-Flow FM performance – with respect to 0510, 1110 and 0516 events – was presented and further descripted. As reflected in the results, models diverged from real observations and themselves in multiple locations and to different extents. In the current chapter, these dissimilarities were further addressed and interpreted.

5.1. Models' response to rainfall

5.1.1. Analysis of representative cases

As pinpointed in Chapter 4, temporal differences were noted in MIKE FLOOD and D-Flow FM response to the rainfall events' start. This behaviour resulted in WL divergences between models and reality as well as models themselves in multiple study site's OLs. Selected representative examples including OP17 (Figure 4) along with OP10 (Figure 6) for 0510 and 1110 events, respectively were further interpreted below[14].

Wellawatta OL (OP17, 0510 event)

In the descriptive analysis conducted (Chapter 4), both models' constant WLs' underestimation in conjunction with the apparent tidal signal and its impact on the WL fluctuations at this point were highlighted. Considering the nearly identical models' WL behaviour prior to the event (first 24h of simulation), their continuous WL misestimations (0.3-0.5m) during the event along with the OP17's location in the catchment, the tidal time series (input data) implemented as downstream boundary conditions as well as the models' RR components were framed to cause these deviations. For correctness reasoning purposes, the most downstream point – where real observations were available – was further investigated. However, MIKE FLOOD and D-flow FM simulated WL time series in OP16 (Figure 10) fitted most field observations, with deviations not exceeding 0.11m (AD with RD ≤ 25.5%).

[14] OP16 (0510 event) as well as OP7 and OP11 (1110 event) displayed similar to OP17 and OP10 patterns, respectively.

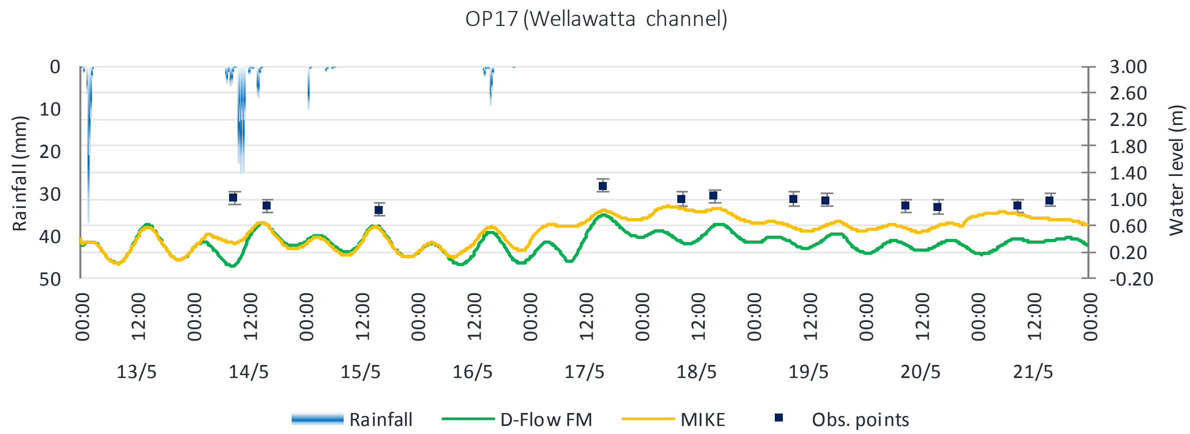

Figure 10. Simulated WL fluctuations against field observations in OP17 (0510)

Subsequently, the differences noted in OP17 were not caused by incorrect system boundaries and input data but mostly due to the applied RR components and thus, no further testing on the models' sensitivity to altered tidal time series was conducted. Yet, D-Flow FM model was additionally tested in sub section 5.3 to identify potential reasons explaining the significantly low simulated WLs.

Torrington OL (OP10, 1110 event)

The limited number of field measurements available in OP10 for 1110 event hampered the understanding of WL oscillations' behaviour during this event and subsequently, the assessment of D-Flow FM and MIKE FLOOD performance using real observations as a reference. Despite data limitations, Figure 6 demonstrated MIKE FLOOD's divergence – in terms of overall WL behaviour, temporal detection and determination of abrupt WL rise due to the event – compared to real observations and D-Flow FM performance. Like OP17, MIKE FLOOD RR elements were presumed to generate this temporal deviation, resulting in a shifted (earlier) WL peak. Incorrect initial conditions and/or input values were excluded as models' simulated WLs prior to 1110 event matched well with the respective field observations – illustrated in Figure 6 (first 3 observation points). In addition, the WL point measured in November 10^{th} at 16:00 (OP10, WL=0.40m) comprised a value with high weight as it aided in assessing the WL fluctuations at this moment in time and demonstrated that MIKE FLOOD responded significantly faster to the rainfall event.

5.1.2. Models' RR component

To investigate the causes of these rapid WL rises detected in MIKE FLOOD, NAM technique – applied to estimate the MIKE 11 surface runoff in Colombo Metropolitan region – was considered. The fundamental hypothesis behind this behaviour encompassed NAM predicted runoff being directly introduced into the 1D MIKE system, resulting in a primary runoff wave overestimation and an initial delay omission. To substantiate this concept, the lateral time series derived from NAM model and implemented as discharge boundaries to the 1D MIKE system were examined. An example of this analysis is demonstrated below for OP10 (Figure 11).

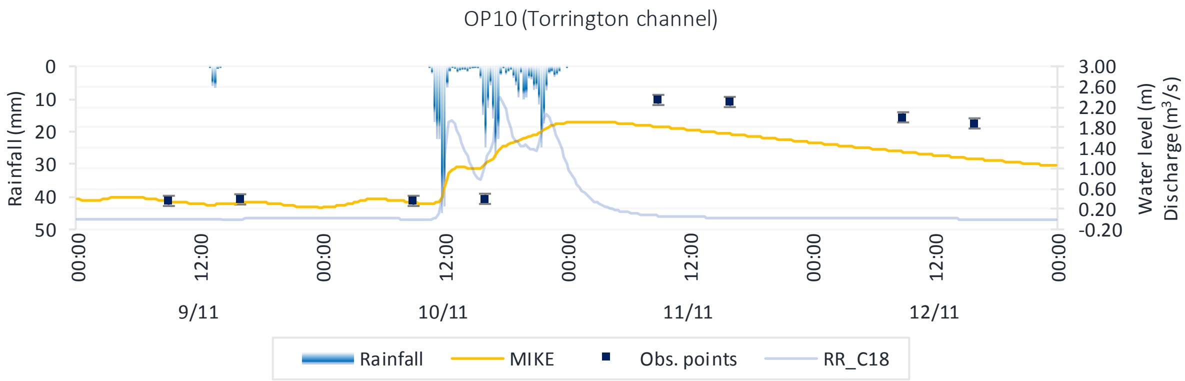

Figure 11. Discharge forcing data for C_18 against MIKE FLOOD WL time series

Figure 11 illustrated the RR discharge estimated by NAM model for C_18 Metro Colombo sub catchment, in where OP10 was located. As confirmed by the graph, the abrupt rise depicted in MIKE FLOOD WLs stemmed primarily from the high discharge prescribed by NAM and applied in the 1D MIKE system right at the start of the event. Subsequently, the selected MIKE 11 NAM parameters comprised the cause of these differences and required further investigation.

Focusing on the same location (OP10) but considering D-Flow FM model, the overall behaviour of WL oscillations derived displayed a distinct pattern, matching most of the field observations (Figure 6). This divergence could be attributed to the model's type (fully distributed), resulting in a different RR process – rainfall was directly applied on the 2D mesh, the water movement and direction were driven by the topography, roughness and thickness of water layers on the surface while runoff was generated at each mesh node. In the current case study, the accurate bathymetry and roughness values constituted key elements aiding in a satisfactory WLs' representation in the 1D channels' network. Specifically, the former determined the water volume distribution over the catchment and channels – thus, the respective estimated WLs in the 1D network – whereas the latter regulated the runoff wave's time behaviour, leading at the event's WL peak temporal detection.

Nonetheless, considering that part of the runoff processes – namely initial and infiltration losses – were not implemented in D-Flow FM model, its simulated WLs were anticipated to be higher compared to the respective observed values. Yet, the low simulated runoff volumes could be attributed to local surface depressions. This assumption was confirmed by Pina et al. (2016) who concluded that fully distributed models could 'inaccurately retain runoff volumes on the overland surface due to surface depressions' (Pina, et al., 2016).

5.2. Kelani River GSs: Deviations among 2010 & 0516 events

Focusing on the current study site's most upstream locations, Kelani River gauging stations (GS1 & GS2) were addressed and the models' performance at these points was further observed and analysed for the events selected.

As illustrated in Figure 12, MIKE FLOOD and D-Flow FM reproduced well the river's WLs and its oscillations in the 0516 event but displayed an unsatisfactory performance in both 2010 events (0510 & 1110). Incorrect system boundaries and input data, initialization phase issues, alterations in the 1D bathymetry and/or inaccurate hydraulic structures' representation (i.e. dimensions and crest levels) could constitute possible reasons explaining the depicted outcome. Considering that the ground survey conducted to determine the 1D cross sections in Kelani River took place in 2003 (Table 1) in combination with the fact that they were implemented in both 2010 and 2016 events, the argument of non-representative cross sections' application was rejected, as in that case, the models' performance in 0516 event would have also been disturbed. On the same wavelength, although incorrectly implemented weirs' dimensions and crest levels at GS2 could have possibly contributed to the insufficient replication of WL rises during these events (0510 & 1110), yet, such discrepancy would have also been reflected on the behaviour of WL fluctuations in the 0516 event.

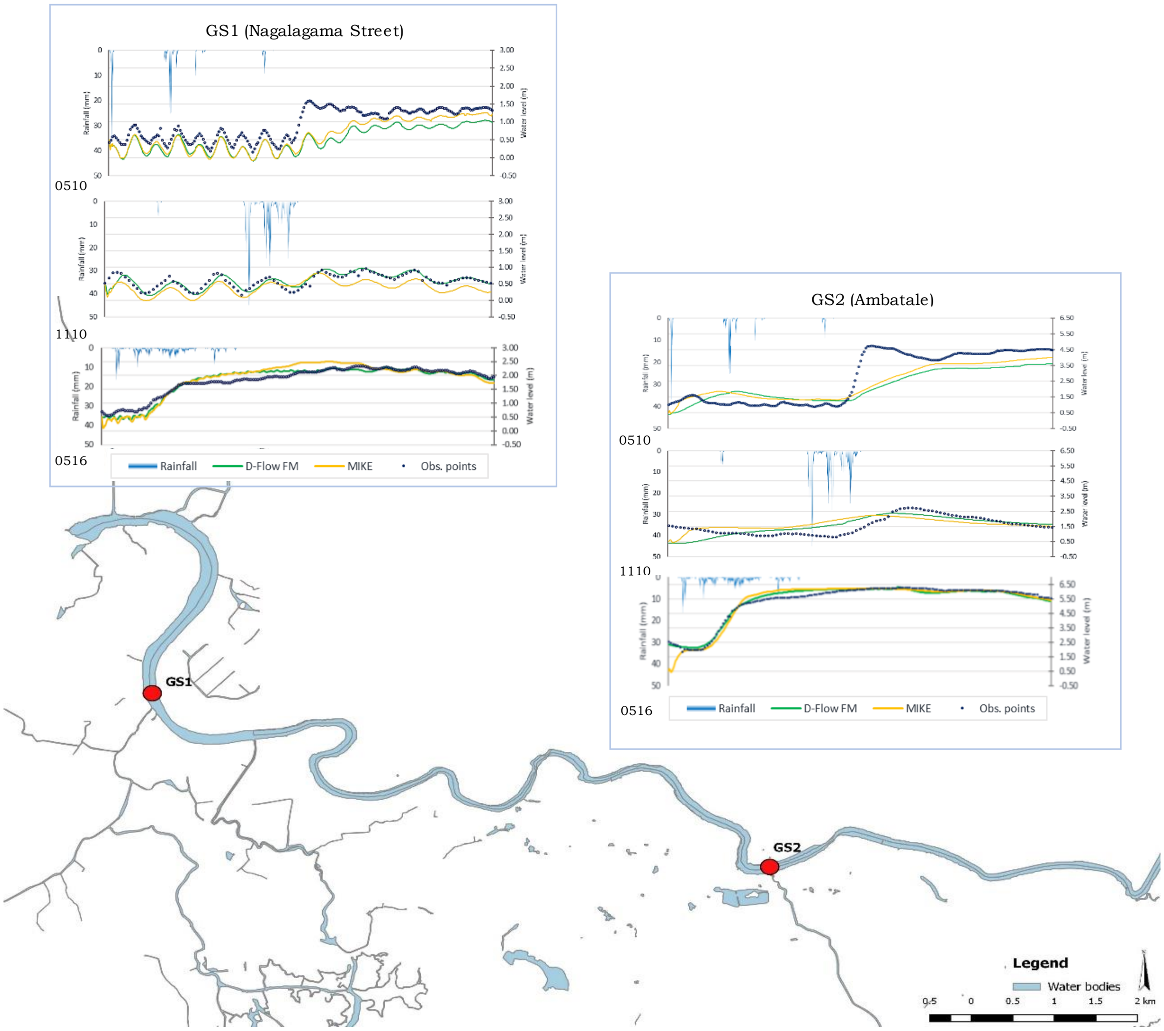

Figure 12. Divergences among 2010 & 0516 events in Kelani River GSs

Nagalagama street, GS1

On the other hand, nearly identical MIKE FLOOD and D-Flow FM WLs in GS1 – prior to 0510 and 1110 rainfall events, their constant WL underestimations compared to measured observations at this gauging station in conjunction with the GS1's location in the catchment, reinforced the concept which pointed out incorrect input data (tidal time series) as the principal motive of these divergences. This consideration was further boosted by acknowledging that the tidal WLs implemented in the study site's 4 downstream boundaries (Kelani River, Mutwal tunnel, Wellawatta and Dehiwala outfalls) comprised tidal time series measured in Metro Colombo port gauging station (by assuming that divergences due to the different boundary sites' position would have been minor). Moreover, the level of water observed in GS1 was further influenced by the magnitude of WL oscillations noted in GS2 (explained further in "*GSs' interrelation & impact on Metro Colombo WL oscillations*", below).

Ambatale, GS2

By comparing the GS2's observed time series illustrated in (Figure 25) and (Figure 42) for 0510 and 0516 events, respectively, an association between their WL responses was noted. Specifically, despite their differences in shape, the observations had the same order of magnitude, with absolute jumps of approximately 4m being observed in both events. Subsequently, equivalent models' performance was anticipated for 0510 rainfall event. Nevertheless, both MIKE FLOOD and D-Flow FM underestimated the respective WLs, as indicated in Figure 25. Considering GS2 – Hanwella distance (HW, Figure 2) as the principal cause of this discrepancy was rejected, due to three reasons, including: i. observed and simulated WLs' matched well in 0516 event at GS2, ii. in general, distance determines the flood wave's time behaviour (mainly responsible for delays) and iii. the absolute jump observed was primarily determined by the water arriving at this point (no inundation/water loss observed upstream in this time span). Considering the latter reason along with the significantly lower simulated WLs (Figure 25), the discharge time series at Hanwella upstream boundary were suspected. For correctness reasoning purposes, the 0510 and 0516 events' discharge timeseries implemented as boundary conditions at HW were plotted (Figure 13) to further examine their order of magnitude. As indicated in the graph below, remarkably low discharges (values differed by three orders of magnitude) were applied in 0510 event, explaining the notable deviations in GS2 but also in GS1. Peak discharges above 1000m³/s – compared to 550m³/s currently applied – would have considered more realistic for the event addressed.

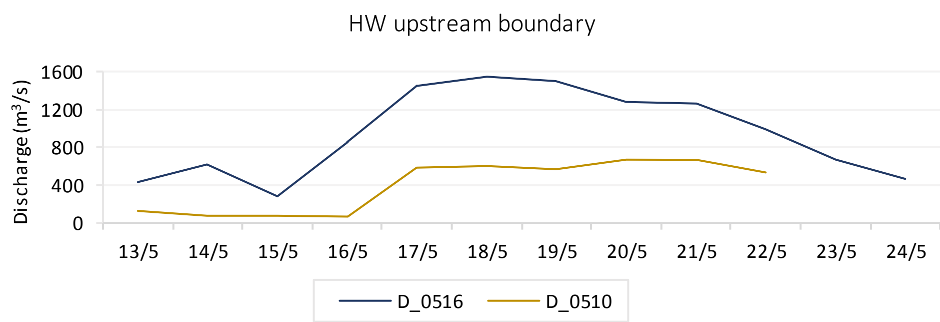

Figure 13. Discharge time series applied in HW upstream boundary for 0510 and 0516 events

GSs' interrelation & impact on Metro Colombo WL oscillations

The system boundary and input data's role and importance were investigated by shifting the catchment's most upstream boundary from Hanwella (HW) to GS2[15] and replacing the proven incorrect discharge time series (applied in HW) with WL time series measured at GS2. Figure 14 demonstrated the improvement noted due to accurate input – reflected on D-Flow FM simulated WLs (D-Flow FM_WL) – at both Kelani River GSs.

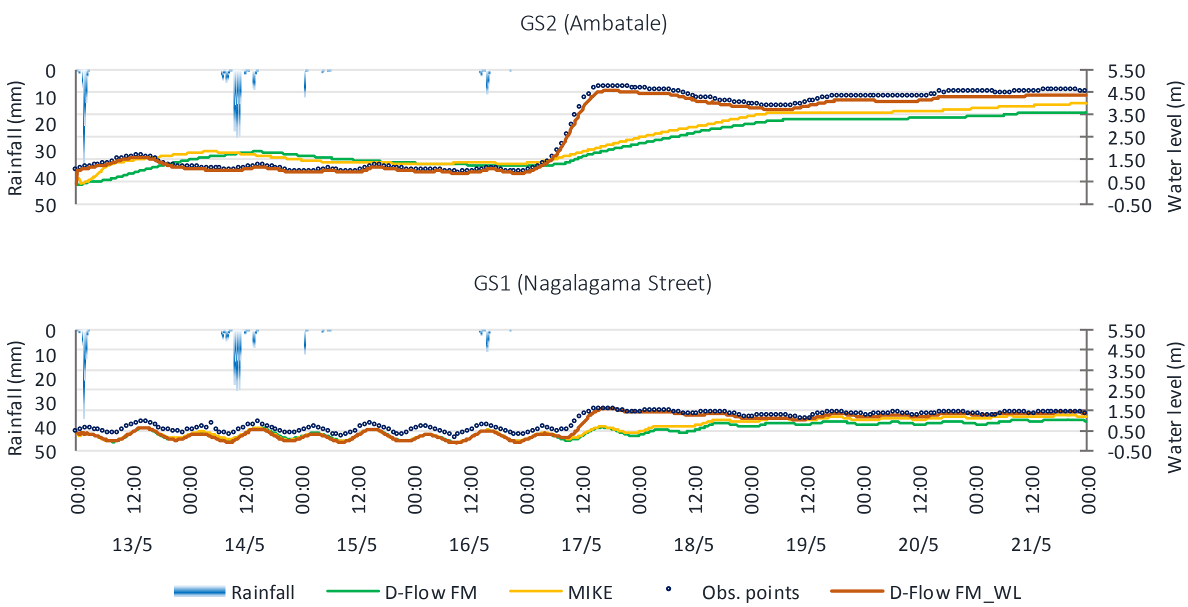

Figure 14. Impact of system boundary and input data on GSs' simulated WLs for 0510 event

15 The boundary was placed right upstream of GS2.

In particular, precise reproduction of WL oscillations observed in Ambatale (Figure 14, GS2, brown line) resulted in 1m difference – in the event's WL peak – between previous models' simulations (Figure 14, yellow & green lines) and anew predicted values (Figure 14, brown line) in Nagalagama street (GS1), with the latter performing in general agreement with the corresponding observed data ($R^2 = 0.98, NSE = 0.72$ & $RMSE = 0.23$). Moreover, by correctly simulating the wave's water volume and time behaviour at GS1, the respective water volume and fluctuations predicted further downstream in Metro Colombo channels were also influenced (Figure 15). Specifically, RD_{mean} between observed and predicted WL values were diminished by 11% ($AD_{mean} \cong 0.3m$) resulting in an overall model's performance improvement of 20%.

The same procedure was followed for 1110 event to investigate the causes in inspected deviations. Like 0510 event, the input data's role and significance along with their impact on the overall WLs' behaviour were additionally highlighted. Moreover, D-Flow FM simulations in GS1 (green & brown lines) demonstrated similarities both with real observations and themselves, resulting in a well reproduced overall behaviour of WL oscillations in the catchment's channels. By comparing these two cases (previous & anew D-Flow FM simulations at GS1 & Metro Colombo channels), the importance of GS1 correct wave's water volume and time behaviour determination was again outlined, demonstrating the GS2 influence on GS1 fluctuations.

In addition, by taking the anew D-Flow FM simulations at GS2 (Figure 14, brown line) into consideration and comparing it with the respective field measurements, the initialization phase issues' hypothesis – suspected for the differences between observed and simulated values demonstrated at GS2 prior to the event – was excluded, since – as indicated in the graph below – the model was capable of instantly capturing the water fluctuations at this point.

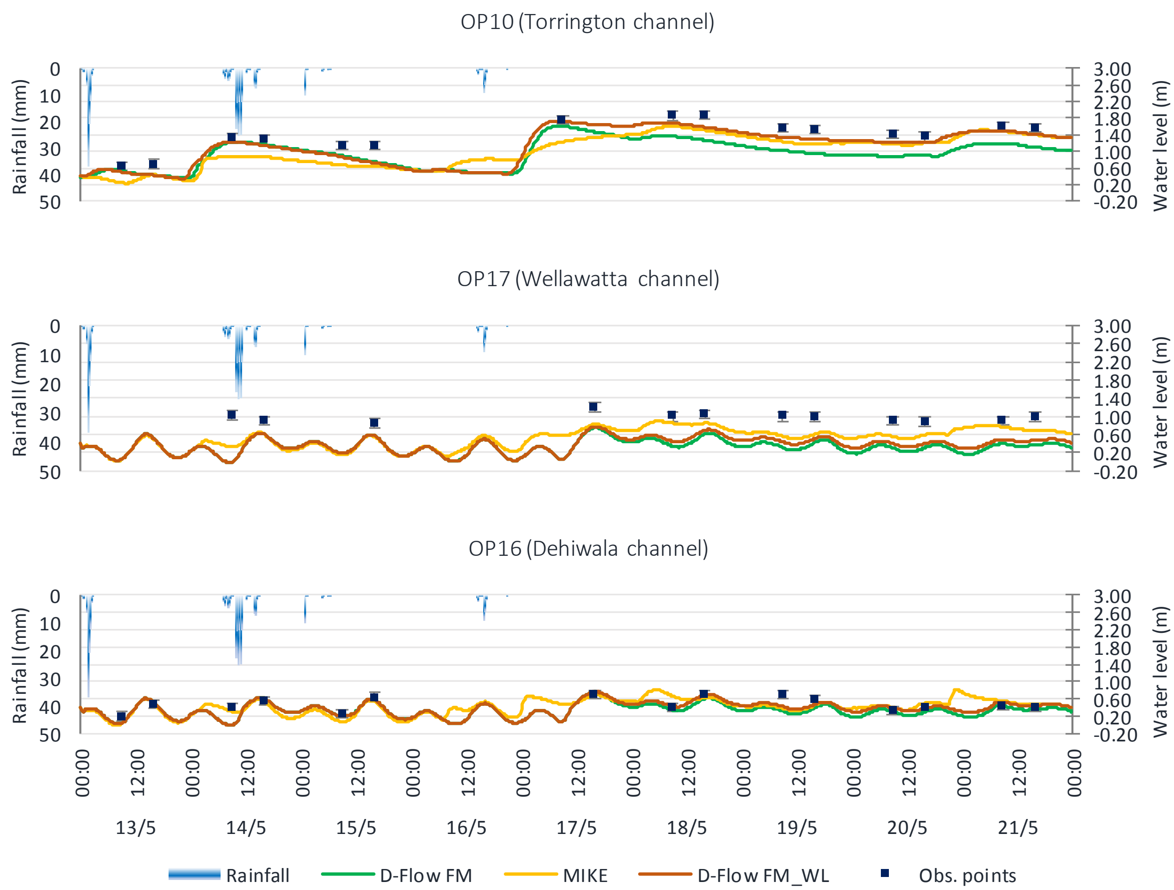

Figure 15. Impact of system boundary and input data on Metro Colombo channels for 0510 event

5.3. OP16 & OP17: Simulated & observed WL divergences

As mentioned previously, Wellawatta (OP17) and Dehiwala (OP16 & OP20) channels constituted the catchment's most downstream points, located close to the Indian ocean. Primarily due to their location, the tidal signal was apparent and reflected on these points' observed water fluctuations, typically occurring below 0.40m.

Wellawatta OL (OP17)

Implementing MIKE FLOOD and D-Flow FM models to reproduce the above described WL oscillations during 2010 and 2016 events and evaluating their performance based on available field measurements demonstrated significant deviations. Considering the OP17, both models misestimated the high WLs observed during the selected rainfall events, despite showing a good fit prior to their start (i.e. first 33h, Figure 40). To check the validity of input data applied, adjacent observation points located downstream of OP17 (i.e. OP16) were further investigated. Nevertheless, a good correlation between the models' simulated values and the respective field observations in OP16 was demonstrated and subsequently, the concept framing incorrect input data to cause this discrepancy was excluded. On the other hand, considering that notable divergences – between models and reality as well as models themselves – were observed soon after the rainfall event started, the models' rainfall-runoff elements were suspected. Additionally, focusing particularly on Figure 40 and Figure 53, MIKE FLOOD's tendency to respond immediately after the event's start was anew highlighted.

In addition, the OP17 region's distinct features were detected and specified. Using web mapping services, bridges along with dense vegetation upstream of the OP17 were identified (Figure 23, d). MIKE FLOOD implemented 'energy losses' to cope with such structural components, yet, D-Flow FM beta testing phase's limitations did not allow for bridges' representative description. Subsequently, the divergences noted between MIKE FLOOD and D-Flow FM simulated values could possibly be explained by D-Flow FM lack of this standard hydraulic structure type. To crosscheck this hypothesis, two alterations were separately implemented and further tested during 0510 event, namely i. local roughness values' modification[16] and ii. hydraulic structure (i.e. gate to represent the bridge) incorporation at this point of the 1D network. By addressing the first alteration, a range of roughness values were tested (i.e. 20, 25, 30 and 40[17] $m^{1/2}/s$), with the coefficients of 25 $m^{1/2}/s$ comprising the most representative one (Figure 16).

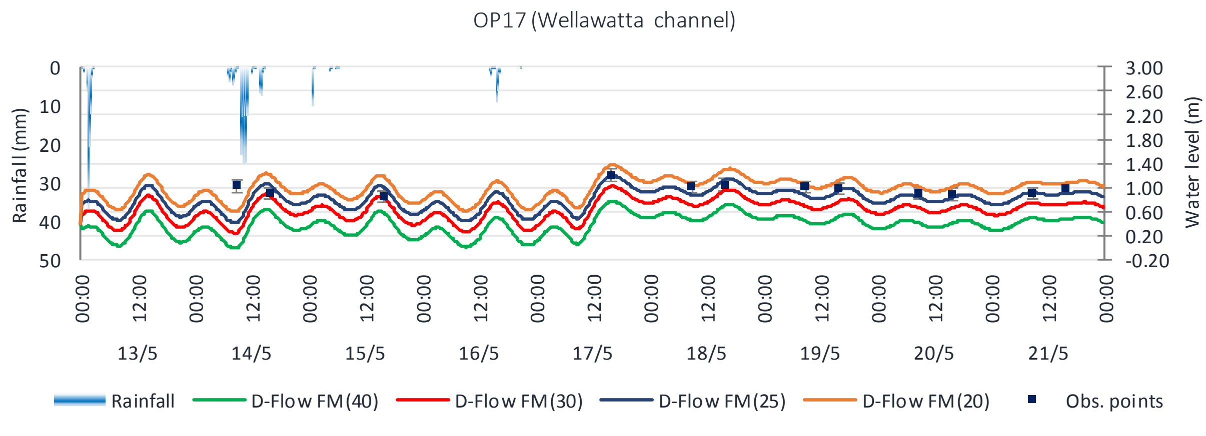

Figure 16. OP17: D-Flow FM simulations using different roughness values

Moreover, Figure 17 depicted D-Flow FM performance once the gate upstream of the OP17 was introduced [D-Flow FM (40)]. By implementing a combination of the abovementioned alterations (gate and 30 $m^{1/2}/s$ as a roughness coefficient value), the deviations between observed and simulated values were diminished (Figure 17, Gate_30).

---

[16] The fact that surface roughness also comprised a form of 'energy loss' was acknowledged.

[17] The roughness value 40 $m^{1/2}/s$ comprised the initial used in all events' simulations.

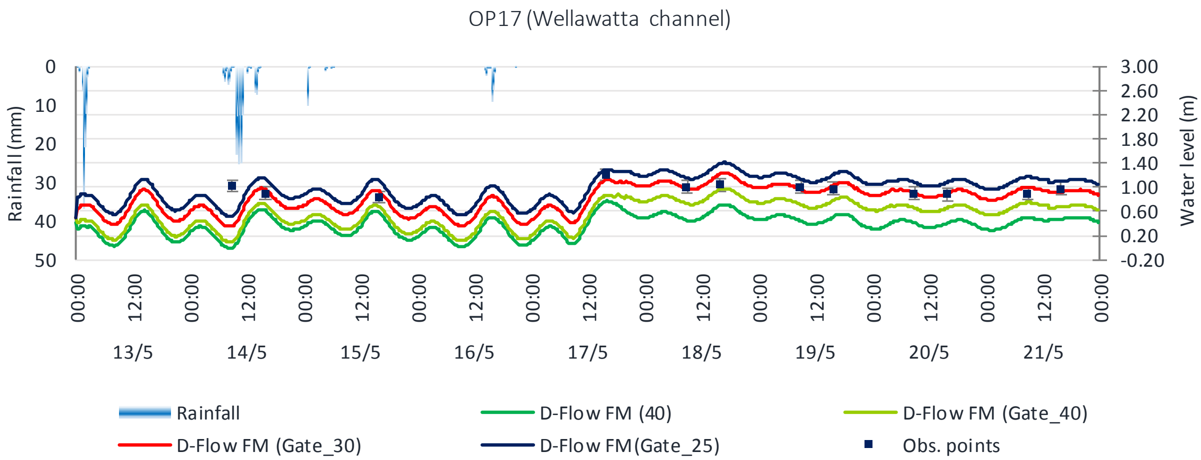

Figure 17. OP17: Gate incorporation (Gate_40) and alterations' combination (Gate_25 & Gate_30)

Dehiwala OL (OP16)

Focusing solely on MIKE FLOOD and D-Flow FM's performance during the 3 events selected and evaluating their overall behaviour of WLs noted in OP16, an additional aspect, namely the superior performance of D-Flow FM in OP16 was pointed out. As indicated in Figure 31, Figure 39 and Figure 52, D-Flow FM simulated WL time series in OP16 fitted most field observations, with deviations not exceeding 0.11m (AD with RD ≤ 25.5%) for all events selected. By solely considering the observations measured at this point and comparing them with respective ones recorded in OLs with similar topographic characteristics (i.e. OP17), mean deviations of 0.5m were calculated, with the WLs in OP16 being constantly lower. The dynamic environment observed close to OP16 due to the Indian ocean could comprise the reason interpreting these differentiations. Yet, the interesting aspect lay on D-Flow FM's ability to sufficiently reproduce this overall behaviour of WL oscillations in all 3 events, compared to MIKE FLOOD performance and despite implementing the same input data.

Considering the OP16 and Dehiwala outfall boundary locations in the catchment (Figure 2), a strong signal – stemming from the WL time series implemented as boundary conditions further downstream – was expected to have a great influence on the models' results. Such consideration was confirmed for D-Flow FM – as also stated previously – but not in the case of MIKE FLOOD. Given the OP16 position (very close to the boundary), MIKE FLOOD's performance could have only been explained providing that an additional boundary condition was implemented close enough to disturb these results. Undoubtedly, the NAM input constituted another boundary for the 1D MIKE system and thus, the RR component was anew suspected.

Acknowledging the topographic features' role in the models' runoff generation processes, the techniques with which the current DEM file was utilized by MIKE FLOOD and D-Flow FM was further investigated. As mentioned previously, MIKE FLOOD applied the NAM RR model to estimate rainfall and introduced it into the 1D MIKE system. For this purpose, Metro Colombo catchment was divided into sub catchments, each of which was further separated in a specific number of elevation zones. The average altitude used in these zones comprised an important parameter as many NAM model variables depended on it. Subsequently, the NAM model did not consider the initial DEM form to calculate the corresponding runoff but an approximation. On the other hand, D-Flow FM directly applied the DEM provided to estimate the runoff values ending up in its 1D network. Considering MIKE FLOOD's deviations in OP16, the RR component's impact on the overall behaviour of WLs as well as the importance of topography on the runoff generation processes, the DEM role in the WLs' determination was underlined, suggesting that erroneous elevation data could possibly explain the divergences observed.

5.4. Kimbulawala lake

As indicated in the subsection 4.1.3b, both D-Flow FM and MIKE FLOOD did not capture the observed behaviour of WLs at the OP15 (Figure 8) for 0516 event, demonstrating ADs of up to 1.2m between simulated and real observations.

To understand and further interpret the models' performance, a comprehensive inspection of Kimbulawala lake's position and conditions was conducted. Specifically, it is situated in the south of Parliament lake and their waters are openly connected, with the former feeding the latter lake. In 2013, two manually controlled structures – containing two gates each – and a spillway were placed upstream of Kimbulawala lake, in Kimbulawala road bridge (Figure 18 & Figure 23c). Considering that the Parliament lake's WLs did not exceed 1.1m, these structures remained open. Yet, once this WL threshold was surpassed, both structures were manually closed to protect the Parliament lake and surrounding regions from receiving more water and avoid potential inundation. Subsequently, under these conditions, the Kimbulawala lake's WLs were expected to rise significantly.

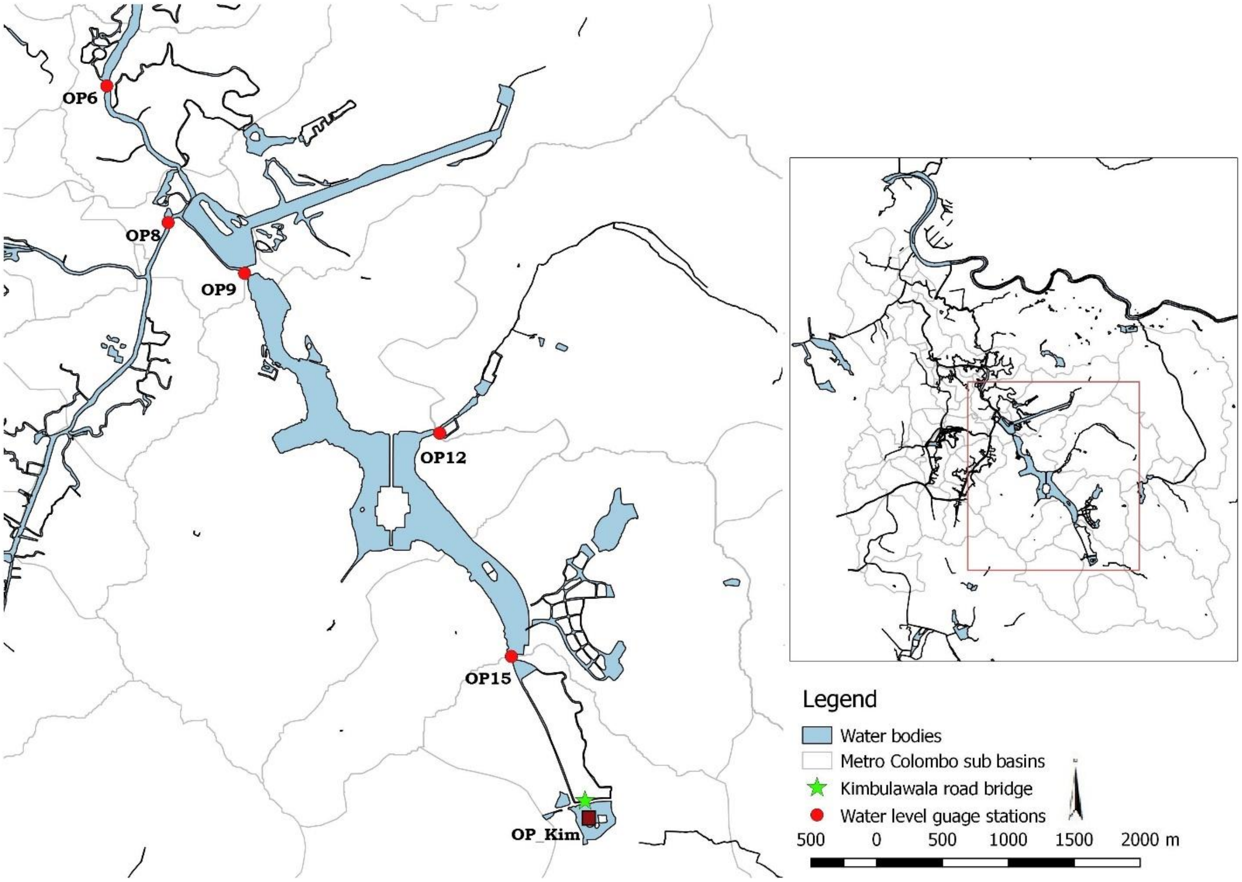

Figure 18. Overview of Parliament and Kimbulawala lakes

Taking the abovementioned description as well as the event itself into consideration, the field observations utilised for models' evaluation should have been measured south of the Kimbulawala road bridge for the high WLs to be justified. Under different circumstances, the observed WLs should have been equivalent to those measured in locations close by the Parliament lake (i.e. OP9 & OP12), due to the open water connection. Consequently, the OP15's position in both MIKE FLOOD and D-Flow FM models was suspected. By reviewing Figure 18, this concept was substantiated, as OP15 was found to be located inside the Parliament lake. Thus, the OP15 was spatially corrected (OP_Kim, Figure 18) and an additional simulation was conducted.

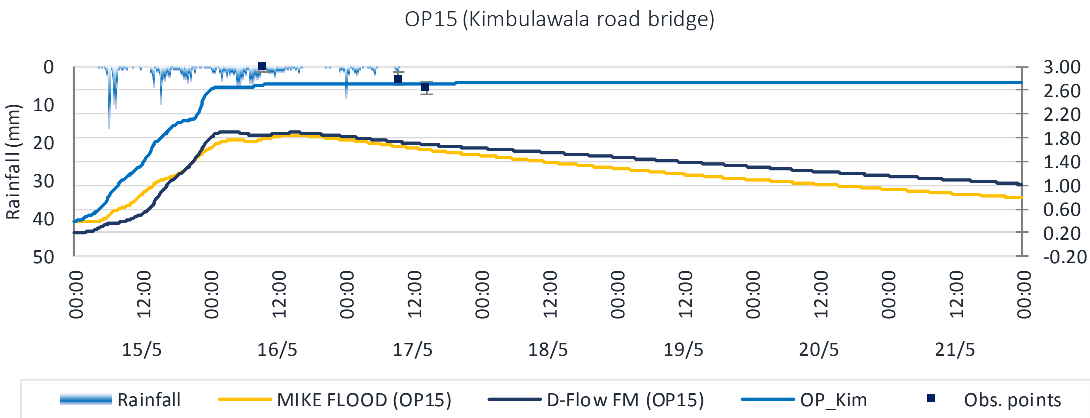

Figure 19. Simulated WLs in OP15 and spatially corrected OP_Kim against real observations (0516)

In Figure 19, previous models' performance in OP15 in conjunction with D-Flow FM simulation in OP_Kim (spatially corrected OP15) were plotted against the respective field measurements. As expected, prior to the event's occurrence, the WLs upstream of Kimbulawala road bridge were in accordance with the corresponding levels observed in the Parliament lake. At the rainfall event's outset, the system's WLs started increasing – with Kimbulawala lake receiving more water from the surrounding region, resulting in more abrupt WLs' rise. Once the Parliament lake's level exceeded 1.1m, the four gates located in Kimbulawala road bridge were manually closed and thus, the lakes were separated. As theoretically expected and previously described, under these conditions, Kimbulawala lake's level rose significantly, with its WLs estimated above 2.5m (real observations). As indicated in Figure 19, D-Flow FM succeeded in capturing the overall behaviour of water fluctuations noted in OP_Kim, with deviations ranging from 0.08m to 0.30m.

5.5. Differences in simulated inundation extents

In Chapter 4, MIKE FLOOD and D-Flow FM maps demonstrating the inundation extent for the 3 events selected were qualitatively described. Recurring but also case specific divergences in the models' performance were distinguished and further investigated in the following sub sections.

5.5.1. Models' hydrological processes & RR concepts

Due to D-Flow FM's beta testing phase, limitations with respect to the hydrological processes implemented were acknowledged. Specifically, water balance was incomplete, as evaporation, infiltration and interception were not included in the model's current version and their impact was reflected on the corresponding inundation extent maps. As indicated in Figure 9, D-Flow FM reproduction of inundation events demonstrated rainfall being captured in nearly the entire catchment's surface. Its performance deviated significantly from the respective MIKE FLOOD results, with inundated D-Flow FM regions simulated as completely dry in MIKE FLOOD. Yet, the water depth height in the majority of these locations did not exceed 0.02m, suggesting that the abovementioned hydrological processes could possibly aided in diminishing part of this water quantity. In addition, observation points located in inundated D-Flow FM but dry MIKE FLOOD catchment's regions would have contributed in investigating local depressions in D-Flow FM and quantitively determining the water reduction due to losses.

Despite the role of hydrological processes in the models' inundation extent mapping, the concept behind RR implementation comprised the principle interpreting the deviations in water depth and extent regarding ponding losses, illustrated in Figure 9. Specifically, MIKE FLOOD consisted of the 1D network – the input of which was the sub-catchments' lateral inflow generated and introduced by NAM RR model – and the 2D mesh. Due to its RR concept (described in Chapter 3), rainfall was implemented in NAM model, its calculated RR discharge was inserted into 1D MIKE system generating an increase in channels' WLs and only in cases where water surpassed the channels' walls, bank inundation started occurring. Subsequently, fluvial inundation (minor, mediocre or severe) was restricted around Kelani River and the catchment's channels. Thus, the abovementioned dry regions simulated in MIKE FLOOD maps did not necessarily represent the reality, as rainfall (responsible for pluvial inundation) was not applied there.

On the other hand, being a fully distributed model, D-Flow FM applied rainfall directly on the 2D mesh while the water behaviour and direction was fully driven by the catchment's topographic features. Subsequently, spatial rainfall was captured in the entire catchment's surface, generating local depression inundation in specific locations or ending up in Kelani River and region's channels. By taking these considerations into account, the D-Flow FM performance could be characterised as more realistic.

5.5.2. Double counting

As described in Chapter 3, in the current case study, major water bodies (i.e. lakes) were incorporated in the 1D network while 2D grid cells were excluded from these areas in both models to avoid double counting. On the other hand, such methodology was not applied in Metro Colombo channels due to the complex and time-consuming nature of the procedure. Consequently, double counting occurred in the entire 1D channels' network. Nevertheless, the relative area double counted was considered modest, as solely 20% of the current computational domain was covered by 1D channels, the average width of which was estimated at 10m or 1/3 of the grid cell. In addition, admitting a proper bathymetry in the 2D grid cells, inundation – and subsequently, double counting – only started once channels' WLs have surpassed street levels. Thus, water below these levels was not double counted. Subsequently, by taking the abovementioned arguments into consideration, the channels' double counting was accepted.

5.5.3. Selected example cases

As indicated in the section 4.2, flood data limitations did not allow conception of the events' magnitude and hampered the models' outcome analysis and assessment. Consequently, the current sub section was restricted in evaluating the performance of MIKE FLOOD against the respective one from D-Flow FM. Example cases were further investigated below.

Focusing solely on the sub-catchment located below Ambatale GS (GS2, Figure 20), distinct divergences between models' simulated water depth were noted. Specifically, MIKE FLOOD illustrated higher water depths, restricted around the channel whereas D-Flow FM depicted shallower inundation depth, distributed over the entire local region. Considering this sub-catchment's water sources – Kelani River discharge and rainfall – as well as the models' RR modules and respective impact on illustrating inundation, three models' aspects were suspected, namely i. distribution of water inside the catchment, ii. Kelani River's discharge into this side branch and iii. MIKE 11 NAM RR model. Thus, the models' water volumes were further estimated and compared.

Table 6. Inundation depth and extent in specific sub-catchments during 0516 event

Region	Volume - km^3 (MIKE FLOOD)	Volume - km^3 (D-Flow FM)	Area - km^2 (MIKE FLOOD)	Area - km^2 (D-Flow FM)	Max depth (MIKE FLOOD)	Max depth (D-Flow FM)
Ambatale	6.99	3.28	3.27	13.37	4.86	2.97
Kolonnawa catchment	15.29	3.30	9.61	13.94	3.84	2.05

Table 6 quantitatively demonstrated the differences in MIKE FLOOD and D-Flow FM simulated volumes, with the former being double in size. Subsequently, the hypothesis solely addressing distribution inside the local catchment as the principal reason for the observed differentiations was excluded. By comparing the WLs simulated in GS2 (Figure 42) during 0516 event, similar patterns were displayed, indicating that Kelani River was discharging equivalent water quantities at this point. In addition, the river junction leading to this sub-catchment's side branch was located right downstream of GS2, lacking any hydraulic structures that could hamper its flow (Figure 2). Therefore, both models' predicted discharges from Kelani River were expected and confirmed to be equivalent.

Taking the abovementioned considerations into account, MIKE 11 NAM RR model and its selected parameters were suspected.

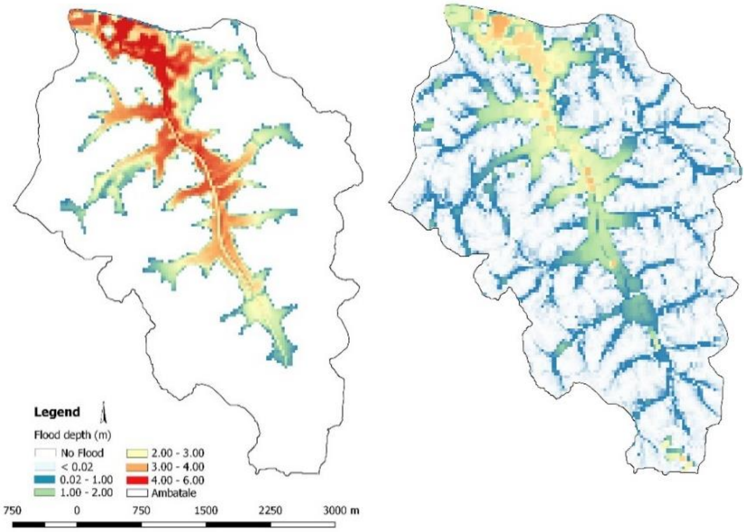

Figure 20. Comparison of MIKE FLOOD & D-Flow FM inundation maps (region nearby GS2, 0516)

Similar inundation patterns and water volumes were also observed in Kolonnawa catchment (Figure 21 & Table 6) during 0516 event. Analogous conclusions regarding their divergences' interpretation were derived.

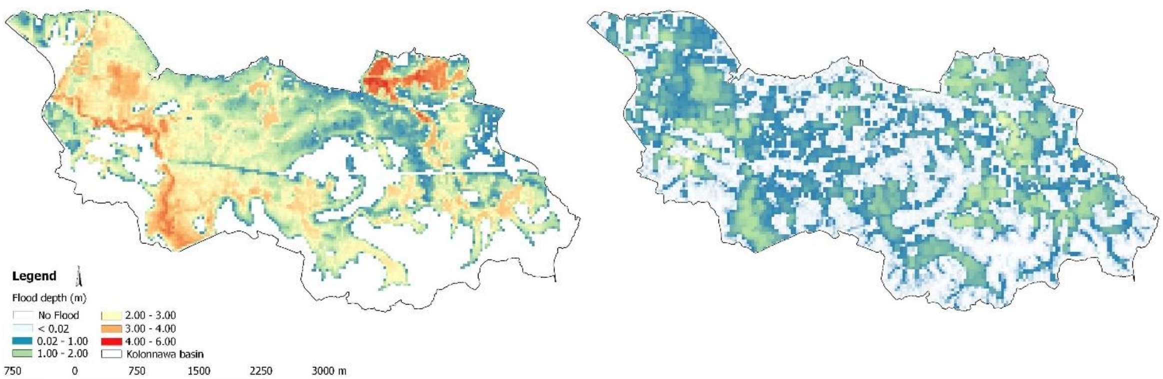

Figure 21. Comparison of MIKE FLOOD & D-Flow FM inundation maps (Kolonnawa catchment, 0516)

5.6. Models' computational time divergences

As described in sub section 4.3, despite MIKE FLOOD's greater number in both time steps and grid cells, its performance with respect to computational time was equivalent or superior in all three events, compared to D-Flow FM. Taking the models' schematisation and RR modules' differences into consideration, these discrepancies were further interpreted.

Addressing the former aspect, MIKE FLOOD implemented a modified DEM version – excluding regions above 3.5m+msl – as its RR principle was not dependent on the 2D model's elements. Subsequently, MIKE FLOOD's 2D mesh cells located in areas above 3.5m+msl were inactive. On the other hand, D-Flow FM RR concept was primarily based on accurate elevation, thus, the initial DEM was implemented and additional time was used for computations at those points.

As previously described, the models' distinct RR module's spatial discretisation resulted in dissimilar types of inundation, with MIKE FLOOD accounting solely for fluvial and D-Flow FM for a combination of fluvial and pluvial flooding. In the latter case, rainfall was implemented on the 2D mesh, meaning that the total cells' number contained water and were included in the computations. Subsequently, the model was significantly slowed down because all its grid cells became active.

In addition, taking the systems' processors into consideration, Table 5 demonstrated that MIKE FLOOD and D-Flow FM models run in computers with the same installed RAM, processing power and speed. Subsequently, deviations caused due to systems' characteristics were excluded.

6

Conclusions & Recommendations

The current thesis presented an evaluation of MIKE FLOOD and D-Flow FM models' performance in analysing urban fluvial and pluvial inundation. For this purpose, the real case study of Colombo Metropolitan region in Sri Lanka and three inundation events were selected. Principal models' differentiations were identified using reality as a reference and interpreted by specifying the dominant factors generating them. The outcome of this research is anticipated to aid modellers in choosing the most appropriate model principle based on the data availability, desired accuracy and computational time.

To the author's knowledge, the hydrodynamic models displayed were among the first attempts to simulate combined fluvial and pluvial inundation in terms of large spatial scale (c.100km^2) and with a relative fine resolution (30m mesh cell size). In addition, the present study comprised D-Flow FM's first implementation in urban inundation modelling.

The distinct nature of MIKE FLOOD and D-Flow FM hydrological and hydrodynamic concepts was reflected on divergences between the models and reality as well as models themselves. The preponderant factors explaining these discrepancies were concisely presented below.

- *Rainfall runoff concept and components.* Issues detected in both models' RR concept led to instantaneous response to rainfall as well as differences in the overall WL behaviour and simulated inundation. For MIKE FLOOD, this discrepancy stemmed from the overly short response time calculated by NAM RR model. For D-Flow FM, the problem laid on the non-application of loss processes – only routing was implemented.
- *Spatial discretisation of rainfall runoff module.* Considering MIKE FLOOD's NAM lumped and D-Flow FM's fully distributed RR modules, divergences in the simulated inundation maps were displayed. D-Flow FM accounted for a combined fluvial and pluvial inundation while MIKE FLOOD solely for fluvial flooding. Such discrepancies also influenced the computational time required. Addressing D-Flow FM, the direct rainfall application on the 2D mesh, resulted in a higher grid cell number active (flooded) and led to slower simulation times recorded, compared to MIKE FLOOD.
- *Input data.* Implementation of incorrect discharge and tidal time series as system boundaries generated remarkable divergences in the simulated water oscillations, inundation depth and extent during 0510 and 1110 events. Comprising an additional boundary condition, MIKE 11 NAM RR input significantly determined the inflow hydrographs applied and further influenced the simulated water behaviour.
- *D-Flow FM limitations.* The non-application of initial and infiltration losses in the current D-Flow FM version resulted in an incorrect water balance which influenced its overall performance. Hydraulic structures' restrictions also hampered its outcome, leading at temporary solutions' implementation to reproduce reality.

Considering its fully distributed RR module, D-Flow FM could be characterised as a more realistic approach, avoiding simplifications and spatial approximations implemented in lumped models. Yet, specifying and applying runoff volumes on the 2D elements of the overland surface required high data accuracy and resolution. Simulation times were also greater as the total number of mesh cells was considered in the computations.

Based on sub-catchment units, MIKE 11 NAM RR model applied a conceptual method to transform the runoff volumes and routing into inflow hydrographs and directly introduced them into the 1D MIKE system. In general terms, such methodology required less network and overland surface information for the RR module's specification. Lower computational times were also recorded, as the total number of MIKE FLOOD's mesh cells remained dry for the entire simulation – excluding specific parts being wet due to fluvial inundation.

In conclusion, despite their discrepancies and shortcomings, both MIKE FLOOD and D-Flow FM captured the overall water oscillations observed in Metro Colombo catchment during the three selected events. Simulated inundation maps' evaluation was hindered due to the lack of real observations. Thus, the importance of field measurements' availability and quality was underlined, as these comprise the cornerstone of hydrological and hydrodynamic modelling, on which flood risk management decisions and strategies are based. Taking advantage of the models' capabilities and potentials as well as the increase in data availability and resolution, future research should be oriented towards:

- Finer DEM and mesh resolutions testing in highly urbanised environments
- Unstructured and flexible mesh testing by applying local refinements on the catchment's distinct features (i.e. marshy wetlands)
- Realistic representation of catchment's features (i.e. replace lakes' 1D representation with 2D)

Nevertheless, the above described approaches should constantly be in balance with the respective models' computational time and data requirements.

References

Abbott, M. B., Bathurst, J. C., Cunge, J. A., O'Connell, P. E., & Rasmussen, J. (1986b). An introduction to the European Hydrological System - Système Hydrologique Européen (SHE), 2: Structure of a physically-based, distributed modelling system. *Journal of hydrology, 87*(1-2), pp. 61-77.

Abbott, M., & Ionescu, F. (1967). On the numerical computation of nearly-horizontal flows. *Journal of Hydraulic Research, 5*, pp. 97-117.

Abbott, M., Bathurst, J., Cunge, J., O'Connell, P., & Rasmussen, J. (1986a). An introduction to the European Hydrological System - Système Hydrologique Européen (SHE): 1. History and Philosophy of a physically-based, distributed modelling system. *Journal of Hydrology, 87*(1-2), pp. 45-59.

Allitt, R., Blanksby, J., Djordjević , S., Maksimović , C., & Stewart, D. (2009). *Investigations into 1D-1D and 1D-2D Urban Flood Modelling - UKWIR project.* Blackpool, UK: WaPUG Autumn Conference 2009.

Almeida, G., Bates, P., Freer, J., & Souvignet, M. (2012). Improving the stability of a simple formulation of the shallow water equations for 2-D flood modeling. *Water Resources Research, 48*(5).

Arnold, J. G., Srinavasan, R., Muttiah, R. S., & Williams, J. R. (1998). Large area hydrologic modeling and assessment: Part 1. Model development. *Journal of American Water Resources Association, 34*(1), pp. 73-89.

Aronica, G., & Lanza, L. (2005). Drainage efficiency in urban areas: a case study. *Hydrological processes, 19*(5), pp. 1105-1119.

Bach, P., Rauch, W., Mikkelsen, P., McCarthy, D., & Deletic, A. (2014). A critical review of integrated urban water modelling–Urban drainage and beyond. *Environmental modelling & software, 54*, pp. 88-107.

Bates, P., Horritt, M., & Fewtrell, T. (2010). A simple inertial formulation of the shallow water equations for efficient two-dimensional flood inundation modelling. *Journal of Hydrology, 387*(1-2), pp. 33-45.

Bathurst, J., Wicks, J., & O'Connell, P. (1995). The SHE/ SHESED basin scale water flow and sediment transport modelling system. *Computer Models of Watershed Hydrology*, pp. 563-594.

Bellos, V., & Tsakiris, G. (2015). Comparing various methods of building representation for 2D flood modelling in built-up areas. *Water Resources Management, 29*(2), pp. 379-397.

Bergström, S. (1976). *Development and application of a conceptual runoff model for Scandinavian catchments.* SMHI Norrköping, Report No. RH07.

Beven, K. (2011). *Rainfall-runoff modelling: the primer.* John Wiley & Sons.

Beven, K. J., & Kirkby, M. J. (1979). A physically based, variable contributing area model of basin hydrology/ Un modèle à base physique de zone d'appel variable de l'hydrologie du bassin versant. *Hydrological Sciences Journal, 24*(1), pp. 43-69.

Beven, K., & Kirkby, M. (1979). A physicallybased, variable contributing area model of basin hydrology. *Hydrological Sciences Bulletin, 24*(1), pp. 43-69.

Brown, R., Keath, N., & Wong, T. (2009). Urban water management in cities: historical, current and future regimes. *Water science and technology, 59*(5), pp. 847-855.

Burnash, R., Ferral, R., & McGuire, R. (1973). *A generalised streamflow simulation system: Conceptual modelling for digital computers.* US Dept of Commerce, National Weather Service and State of California, Dept of Water resources.

Burt, T., & Weerasinghe, K. (2014). Rainfall distributions in Sri Lanka in time and space: An analysis based in daily rainfall data. *Climate, 4*, pp. 242-263.

Casulli, V., & Stelling, G. (2013). A semi-implicit numerical model for urban drainage systems. *International Journal for Numerical Methods in Fluids, 73*(16), pp. 600-614.

Chang, T.-J., Wang, C.-H., & Chen, A. (2015). A novel approach to model dynamic flow interactions between storm sewer system and overland surface for different land covers in urban areas. *Journal of Hydrology, 524*, pp. 662-679.

Chen, A. S., Djordjević, S., Leandro, J., & Savić, D. A. (2010). An analysis of the combined consequences of pluvial and fluvial flooding. *Water Science and Technology, 62*(7), pp. 1491-1498.

Chen, A., Djordjević, S., Leandro, J., & Savić, D. (2007). The urban inundation model with bidirectional flow interaction between 2D overland surface and 1D sewer networks. Lyon, France: NOVATECH 2007.

Cook, A., & Merwade, V. (2009). Effect of topographic data, geometric configuration and modeling approach on flood inundation mapping. *Journal of Hydrology, 1*, pp. 131-142.

COWI A/S; Lanka Hydraulics Institute. (2013). *Report on the Upgrading and Application of the Hydraulic Model.* World Bank.

Crawford, N. H., & Linsley, R. (1966). *Digital simulation in hydrology: Stanford Watershed Model IV.* Stanford: Dept of Civil Engineering, University of California, Technical Report No. 39.

DeFries, R., & Eshleman, N. (2004). Land-use change and hydrologic processes: a major focus of the future. *Hydrological Processes, 18*(11), pp. 2183-2186.

Deltares. (2017). *D-Flow Flexible Mesh: User and Reference Manuals.*

Deltares. (2017, 02 27). *SOBEK Suite.* Retrieved from Deltares: https://www.deltares.nl/en/software/sobek/

Deltares; ADPC; CECB. (2016). *Consultancy Services for conducting a detailed flood risk assessment for Colombo Metropolitan Region.*

Depietri, Y., Renaud, F., & Kallis, G. (2011). Heat waves and floods in urban areas: a policy-oriented review of ecosystem services. *Sustainability science, 7*(1), pp. 95-107.

DHI. (2010). MIKE 11, MIKE 21 and MIKE FLOOD User and Reference Manuals.

Djordjević, S., Prodanović, D., & Maksimović, C. (1999). An approach to simulation of dual drainage. *Water Science Technology, 39*(9), pp. 95-103.

Djordjević, S., Prodanović, D., & Walters, G. (2004). Simulation of transcritical flow in pipe/channel networks. *Simulation of transcritical flow in pipe/channel networks, 130*(12), pp. 1167–1178.

Dooge, J. (1973). Linear theory of hydrologic systems (No. 1468). *Agricultural Research Service, US Department of Agriculture.*

Downer, C., & Ogden, F. (2004). GSSHA: Model to simulate diverse stream flow producing processes. *ASCE Journal of Hydrologic Engineering, 9*(3), pp. 161-174.

Downer, C., Ogden, F., Niedzialek, J., & Liu, S. (2006). Gridded Surface/Subsurface Hydrologic Analysis (GSSHA) Model: A model for simulating diverse streamflow producing processes. *Taylor and Francis Group, CRC Press*, pp. 131-159.

Eagleson, P., Mejia-R, R., & March, F. (1966). Computation of optimum realizable unit hydrographs. *Water Resources Research, 2*(4), pp. 755-764.

Ellis, E., Kaplan, J., Fuller, D., Vavrus, S., Goldewijk, K., & Verburg, P. (2013). Used planet: A global history. *Proceedings of the National Academy of Sciences, 110*(20), pp. 7978-7985.

Fewtrell, T., Duncan, A., Sampson, C., Neal, J., & Bates, P. (2011). Benchmarking urban flood models of varying complexity and scale using high resolution terrestrial LiDAR data. *Physics and Chemistry of the Earth, Parts A/B/C, 36*(7), pp. 281-291.

Fletcher, T., Andrieu, H., & Hamel, P. (2013). Understanding, management and modelling of urban hydrology and its consequences for receiving waters: a state of the art. *Advances in Water Resources, 51*, pp. 261-279.

Freeze, R., & Harlan, R. (1969). Blueprint for a physically-based, digitally-simulated hydrologic response model. *Journal of Hydrology, 9*(3), pp. 237-258.

Gallegos, H. A., Schubert, J. E., & Sanders, B. F. (2009). Two-dimensional, high-resolution modeling of urban dam-break flooding: A case study of Baldwin Hills, California. *Advances in water resources, 8*, pp. 1323-1335.

Ghimire, B., Chen, A., Guidolin, M., Keedwell, E., Djordjević, S., & Savić, D. (2013). Formulation of a fast 2D urban pluvial flood model using a cellular automata approach. *Journal of Hydroinformatics*, pp. 676-686.

Gibson, M., Savic, D., Djordjević, S., Chen, A., Fraser, S., & Watson, T. (2016). Accuracy and computational efficiency of 2D urban surface flood modelling based on cellular automata. *Procedia Engineering, 154*, pp. 801-810.

Guha-Sapir, D., & Wahlstrom, M. (2015). *The human cost of weather related disasters 1995-2015.* CRED; UNISDR. Retrieved from http://www.unisdr.org/files/46796_cop21weatherdisastersreport2015.pdf

Hsu, M., Chen, S., & Chang, T. (2002). Dynamic inundation simulation of storm water interaction between sewer system and overland flows. *Journal of the Chinese Institute of Engineers, 25*(2), pp. 171-177.

Huber, W., Dickinson, R., Barnwell Jr, T., & Branch, A. (1988). *Storm Water Management Model: User's Manual Version 4.0* . United States: Environmental Protection Agency.

Hunter, N., Bates, P., Horritt, M., De Roo, P., & Werner, M. (2005). Utility of different data types for calibrating flood inundation models within the GLUE framework. *Hydrology and Earth System Sciences, 9*(4), pp. 412-430.

Hunter, N., Bates, P., Neelz, S., Pender, G., Villanueva, I., Wright, N., . . . Mason, D. (2008). Benchmarking 2D hydraulic models for urban flooding. *Proceedings of the Institution of Civil Engineers: Water Management, 161*(1), pp. 13-30.

Innovyze. (2013). *InfoWorks ICM.* Monrovia, CA, USA: Innovyze.

IPCC. (2012). *Managing the Risks of Extreme Events and Disasters to Advance Climate Adaptation.* Cambridge, UK and New York, NY, USA: Cambridge University Press.

Jha, A., Bloch, R., & Lamond, J. (2012). *Cities and Flooding: A Guide to Integrated Urban Flood Risk Management for the 21st Century.* World Bank. © World Bank.

Jonkman, S. (2014). Loss of Life Due to Floods: General Overview. In J. J. Bierens, *Drowning* (pp. 957-965). Berlin: Springer Berlin Heidelberg.

Kim, B., Sanders, B., Famiglietti, J., & Guinot, V. (2015). Urban flood modeling with porous shallow-water equations: A case study of model errors in the presence of anisotropic porosity. *Journal of Hydrology, 523*, pp. 680-692.

Kirkby, M. (1976). *Hydrograph modelling strategies.* Leeds: University of Leeds, Dept. of Geography.

Koks, E., Jongman, B., Husby, T., & Botzen, W. (2015). Combining hazard, exposure and social vulnerability to provide lessons for flood risk management. *Environmental Science & Policy, 47*, pp. 42-45.

Kuichling, E. (1889). The relation between the rainfall and the discharge of sewers in populous districts. *Transactions of the American Society of Civil Engineers, 20*(1), pp. 1-56.

Kuiry, S., Sen, D., & Bates, P. (2010). A coupled 1D-quasi 2D flood inundation model with unstructured grids. *Journal of Hydraulic Engineering, 136*(8), pp. 493-506.

Leandro, J., Chen, A. S., Djordjević, S., & Savić, D. A. (2009). Comparison of 1D/1D and 1D/2D coupled (sewer/surface) hydraulic models for urban flood simulation. *Journal of hydraulic engineering, 135*(6), pp. 495-504.

Leandro, J., Djordjević, S., Chen, A., & Savic, D. (2007). *The use of multiple-linking-element for connecting surface and subsurfsce networks.* IAHR, Venice, Italy: Proc., 32nd Congress of IAHR - Harmonizing the Demands of Art and Nature in Hydraulics.

Maksimović, C., Prodanović, D., Boonya-Aroonnet, S., Leitao, J., Djordjević, S., & Allitt, R. (2009). Overland flow and pathway analysis for modelling of urban pluvial flooding. *Journal of Hydraulic Research, 47*(4), pp. 512-523.

Marambe, B., Silva, P., Weerahewa, J., Pushpakumara, G., Punyawardena, R., & Pallawala, R. (2014). Enabling policies for agricultural adaptations to climate change in Sri Lanka. In L. W. (ed.), *Handbook of Climate Change Adaptation.* Berlin Heidelberg: Springer-Verlag.

Mark, O., Weesakul, S., Apirumanekul, C., Aroonnet, S., & Djordjević, S. (2004). Potential and limitations of 1D modelling of urban flooding. *Journal of Hydrology, 299*(3-4), pp. 284-299.

Martins, R., Leandro, J., & Djordjević, S. (2015). A well balanced Roe scheme for the local inertial equations with an unstructured mesh. *Advances in Water Resources*, pp. 351-363.

Martins, R., Leandro, J., & Djordjević, S. (2015). A well balanced Roe scheme for the local inertial equations with an unstructured mesh. *Advances in Water Resources*, pp. 351-363.

Mechler, R., & Bouwer, L. M. (2014). Understanding trends and projections of disaster losses and climate change: is vulnerability the missing link? *Climatic Change, 133*(1), pp. 1-13.

Mirei, S., & Juichiro, A. (2003). Numerical and experimental study on two-dimensional flood flows with and without structures. *Journal of Hydraulic Engineering, 129*(10), pp. 817-821.

Moore, R., & Clarke, R. (1981). A distribution function approach to rainfall-runoff modelling. *Water Resources Research, 17*(5), pp. 1367-1382.

Mulvaney, T. (1851). On the use of self-registering rain and flood gauges in making observations of the relations of rain fall and flood discharges in a given catchment. *Transactions of the Institution of Civil Engineers of Ireland, 4*(2), pp. 18-31.

Natale, L., & Todini, E. (1977). *A constrainted parameter estimation technique for linear models in hydrology.* New York: Ciridni, T.A. et al. (Eds), Wiley.

Néelz, S., & Pender, G. (2013). *Benchmarking the latest generation of 2D hydraulic modelling packages.* Horison House, Deanery Road, Bristol, BS1 9AH: Environment Agency.

Ogden, F. L., Raj Pradhan, N. R., Downer, C. W., & Zahner, J. A. (2011). Relative importance of impervious area, drainage density, width function, and subsurface storm drainage on flood runoff from an urbanized catchment. *Water Resources Research, 47*(12).

Pina, R., Ochoa-Rodriguez, S., Simões, N., Mijic, A., Marques, A., & Maksimović, Č. (2016). Semi-vs. fully-distributed urban stormwater models: model set up and comparison with two real case studies. *Water, 8*(2), p. 58.

Popescu, I. (2014). *Computational Hydraulics.* IWA Publishing.

Price, R. (2011). *Urban hydroinformatics: data, models, and decision support for integrated urban water management.* IWA publishing.

Protection, C. (2007). Directive 2007/60/EC of the European Parliament and of the Council of 23 October 2007 on the assessment and management of flood risks.

Rossman, L. (2010). *Storm Water Management Model: User's Manual Version 5.0*. United States: Environmental Protection Agency.

Salvadore, E., Bronders, J., & Batelaan, O. (2015). Hydrological modelling of urbanized catchments: A review and future directions. *Journal of Hydroloy, 529*, pp. 62-81.

Sanders, B., Schubert, J., & Gallegos, H. (2008). Integral formulation of shallow-water equations with anisotropic porosity for urban flood modeling. *Journal of Hydrology, 1*, pp. 19-38.

Schmitt, T., Thomas, M., & Ettrich, N. (2004). Analysis and modeling of flooding in urban drainage systems. *Journal of Hydrology, 299*(3), pp. 300-311.

Seyoum, S., Vojinovic, Z., Price, R., & Weesakul, S. (2012). Coupled 1D and noninertia 2D flood inundation model for simulation of urban flooding. *Journal of hydraulic engineering, 138*(1), pp. 23-34.

Software, DHI. (2014). *MIKE-URBAN - Collection System.* Hørsholm, Denmark.

Son, A.-L., Kim, B., & Han, K.-Y. (2016). A simple and robust method for simultaneous consideration of overland and underground space in urban flood modelling. *Water, 11*, pp. 494-506.

Stelling, G. (2012). Quadtree flood simulations with sub-grid digital elevation models. *Proceedings of the Institution of Civil Engineers, 165*(10), pp. 567-580.

Todini, E., & Wallis, J. (1978). A real-time rainfall-runoff model for an on-line flood warning system. *Application of Kalman filter to hydrology, hydraulics and water resources, edited by: Chaolin, C.*, pp. 355-368.

Turner, A., Colby, J., Csontos, R., & Batten, M. (2013). Flood modeling using a synthesis of multi-platform LiDAR data. *Water, 5*(4), pp. 1533-1560.

UNFPA. (2016, October 3). *Urbanization.* Retrieved January 27, 2017, from United Nations Population Fund: http://www.unfpa.org/urbanization

UN-Habitat. (2012a). *State of the World's Cities 2012/2013: Prosperity of Cities.* Nairobi: United Nations Human Settlements Programme.

UN-Habitat. (2016). *Urbanization and development: Emerging Futures, World Cities Report 2016.* Nairobi: United Nations Human Settlements Programme.

United Nations. (2014). *World Urbanization Prospects: The 2014 Revision, Highlights (ST/ESA/SER.A/352).* Department of Economic and Social Affairs, Population Division.

United Nations. (2016). *The World's Cities in 2016 - Data Booklet (ST/ESA/SER.A/392).* Department of Economic and Social Affairs, Population Division.

van Dijk, E., van der Meulen, J., Kluck, J., & Straatman, J. (2014). Comparing modelling techniques for analyzing urban pluvial flooding. *Water science and technology, 69*(2), pp. 305-311.

Visser, H., Petersen, A. C., & Ligtvoet, W. (2014). On the relation between weather-related disaster impacts, vulnerability and climate change. *Climatic Change, 125*(3-4), pp. 461-477.

Vojinovic, Z., & Tutulic, D. (2009). On the use of 1D and coupled 1D-2D modelling approaches for assessment of flood damage in urban areas. *Urban Water Journal, 6*, pp. 183-199.

Vojinovic, Z., Seyoum, S., Mwalwaka, J., & Price, R. (2011). Effects of model schematisation, geometry and parameter values on urban flood modelling. *Water Science and Technology, 63*(3), pp. 462-467.

Wood, E. F., & O'Connell, P. E. (1985). *Real-time forecasting.* New York: Hydrological Forecasting, John Wiley and Sons.

World Bank. (2017, March 10). *Metro Colombo Urban Development Project.* Retrieved from http://projects.worldbank.org/P122735/metro-colombo-urban-development-project?lang=en

World Bank; CIAT. (2015). *Climate-smart agriculture in Sri Lanka. CSA country profile for Africa, Asia, and Latin America and the Caribbean series.* Washington D.C: The World Bank Group.

XP Software. (2013). *XP-SWMM Stormwater and Wastewater Management Model: Getting Started Manual.* Portland, OR, USA.

Zehe, E., Becker, R., Bárdossy, A., & Plate, E. (2005). Uncertainty of simulated catchment scale runoff response in the presence of threshold processes: Role of initial soil moisture and preciitation. *Journal of Hydrology, 315*(1), pp. 183-202.

Zehe, E., Blume, T., & Blöschl, G. (2010). The principle of 'maximum energy dissipation': A novel thermodynamic perspective on rapid water flow in connected soil structures. *Philosophical Transactions of the Royal Society of London B, 365*(1545), pp. 1377-1386.

Zhong, Z. (1998). General hydrodynamic model for sewer/channel network systems. *Journal of Hydraulic Engineering, 123*(3), pp. 307-315.

Appendixes

► *In the current section, additional information regarding urban inundation modelling and Metro Colombo case is given aiming at providing a comprehensive view of the study conducted.* ◄

Appendix A

A.1. Brief historical overview

Water management transition scheme in urban environments is clearly reflected in urban water system modelling emergence and evolution (Brown et al., 2009; Bach et al., 2014). Specifically, in the early 1900s, clean water supply and sanitation comprised urban population's fundamental objectives. Admitting the necessity to investigate the components, processes and interactions related to rainfall-runoff, urban drainage and sewer systems resulted in the first respective scientific publications as well as the emergence of prime rainfall-runoff modelling concepts (Mulvaney, 1851; Kuichling, 1889; Dooge, 1973). In the 1950s, the introduction of system engineering approaches for complicated dynamic schemes' analysis and advances in the models' estimation phase techniques strongly stimulated the entire modelling progress, leading to more realistic estimations (Eagleson et al., 1966; Natale & Todini, 1977).

Originated in the 1960s, lumped conceptual models aimed at illustrating the physical interpretation of the system processes in a catchment scale by means of linked conceptual elements, each of which displayed a distinct subsystem. Representing a relatively simple approach, lumped modelling could provide an initial assessment of the catchment response and be particularly useful in cases where no spatial data were available. In addition, the introduction of widely available digital computers aided in overcoming computational modelling constraints and resulted in several rainfall-runoff models. Examples include Stanford Model IV (Crawford & Linsley, 1966), Sacramento (Burnash et al., 1973) and HBV model (Bergström, 1976), to name but a few.

In the meantime, population growth and urbanisation rates started influencing urban environments' structure significantly, resulting in spatial restructuring of land use patterns. In addition to spatial complexity, flood and pollution risks augmented the pressure on addressing safety issues and further motivated advanced modelling techniques (Bach et al., 2014; Salvadore et al., 2015). Real-time forecasting and integrated urban drainage models gained notable interest and were developed principally based on existing modelling techniques' advancements (Todini & Wallis, 1978; Wood & O'Connell, 1985). Yet, deviating from the traditional individual process descriptions and introducing the concept of interacting surface-subsurface flow processes as an alternative way of modelling rainfall-runoff constituted a significant step forward and still forms the basis for current advanced distributed models (Freeze & Harlan, 1969; Beven, 2011). However, due to the limited knowledge and comprehension of physically-based distributed models (i.e. limited knowledge of input requirements), the numerous requirements for parameter specification in conjunction with important computational constraints, their capabilities were solely acknowledged and implemented the last three decades (Beven, 2011; Pina et al., 2016). Examples include the Systéme Hydrologique Européen (SHE) model (Abbott et al., 1986a & b; Bathurst, Wicks, & O'Connell, 1995), SHE's advanced versions - MIKE SHE and SHETRAN- which include sediment, water quality and 3D subsurface components, GSSHA (Downer & Ogden, 2004; Downer et al., 2006) and CATFLOW model (Zehe et al., 2005; 2010).

Based on a similar but less detailed principle, simplified distributed rainfall-runoff models were also introduced, representing the catchment's spatial variability with respect to runoff generation by applying different types of distribution function components (Beven, 2011). Three predominant types of this approach could be distinguished, including distribution functions based on statistics, hydrological similarity (Kirkby, 1976) and hydrological response units (HRUs). According to Beven (2011), models of the latter type are alternatively called semi-distributed models (Beven, 2011). Typical examples of the concept's initial implementation include TOPMODEL topography-based model (Beven & Kirkby, 1979), PMD (Moore & Clarke, 1981) and USDA SWAT model (Arnold et. al, 1998).

Over the last three decades, remarkable technological advancements, including exponential growth in computer power, advances in numerical methods for partial differential equations' (PDEs') solution, programming techniques, freeware tools and digital databases in conjunction with an increase in data availability and quality strongly stimulated rainfall-runoff modelling, allowing for higher spatiotemporal resolution, scale expansion and more robust solutions (Price, 2011; Stelling, 2012; Fletcher et al., 2013; Ghimire, et al., 2013; Casulli & Stelling, 2013; Salvadore et al., 2015). Such improvements along with the contemporary societies' necessities for more detailed and accurate rainfall-runoff modelling re-established and reinforced the concept of distributed models (Fletcher et al., 2013; Pina et al., 2016).

Hence, as breakthroughs in science and technology constantly reinforce computers' capacity and efficiency, restrictions in physically-based distributed modelling will gradually be minimized allowing for more detailed, qualitative and sophisticated methodologies and outcomes. From one point of view, such developments can certainly be considered as the prevailing state-of-the-art in rainfall-runoff modelling. On the other hand, models' complexity entails a greater number of parameters' involvement escalating the calibration difficulties and subsequently, the predictions' uncertainty. In addition, taking the models' evolution into consideration, it is clear that as their complexity increased through generations, so did their requirements for data quality and quantity. Therefore, as long as strong limitations in data availability persist, researchers should primarily determine their study interest and purpose before selecting their modelling concept and methodology.

Appendix B

B.1. Details of Metro Colombo OPs and hydraulic structures

Overview of Colombo Metropolitan region

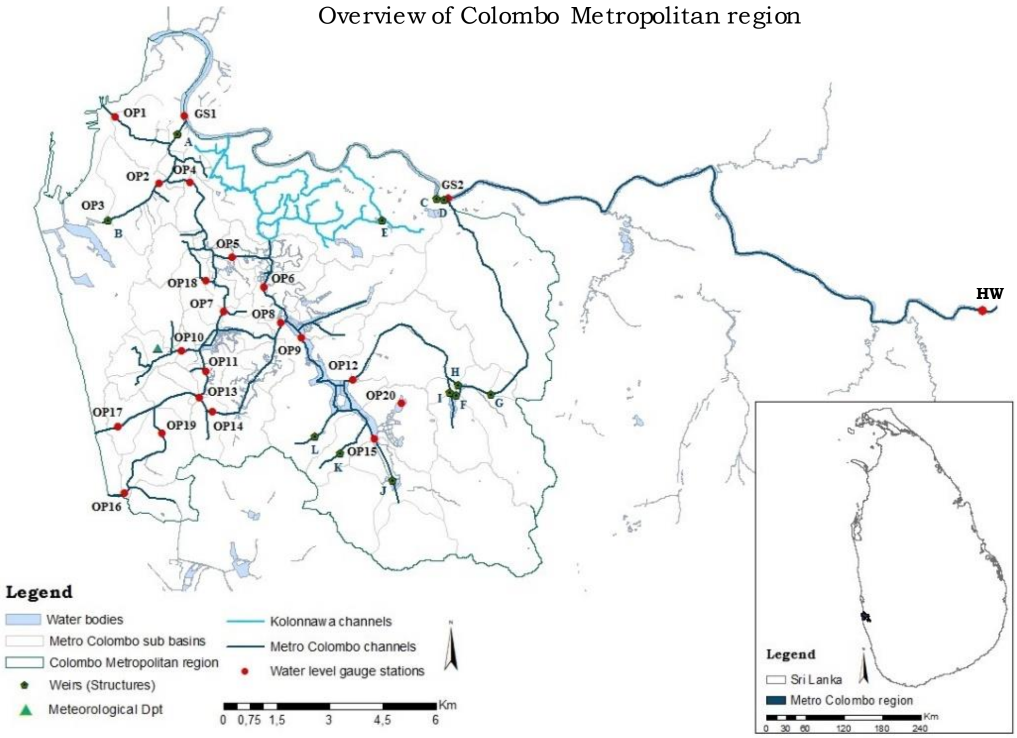

Table 7. Overview of hydraulic structures

No.	Location	Coordinates		Dimensions	
		X	Y	Crest level (m+msl)	Crest width (m)
A	North Lock, St. Sebastian north canal	400917.9415	495042.2687	-1.30	4.90
B	South Lock, St. Sebastian south canal	398956.0909	492609.9892	1.84	4.00
C	SBW, Ambatale, Kelani River	408214.5077	493245.6998	0.00	100.00
D	KCB, Ambatale Kelani River	408561.5650	493207.8913	0.50	100.00
E	Road Overtop Connection, Kolonnawa region	406683.9643	492571.9821	2.88	49.28
F	Offtake street, Talangama lake	408796.7798	487660.0000	6.64	15.20
G	Talangama lake	409786,4175	487680.3829	5.00	12.00
H	Averihena bund spillway, Talangama lake	408849.0473	487946,7067	6.20	7.50
I	Original Spillway, Talangama lake	408615.6362	487743.0914	7.10	4.25
J	Kimbulawala lake	406990.3973	485246,4904	2.40	200.00
K	Amaragoda drop, Madiwela East, Parliament lake	405505.8586	486016.8940	4.04	50.00

L	Parliament lake	404803.9032	486491,9516	2.39	150.00

Table 8. Overview of water level gauging stations and observed water levels during the historical inundation events

ID	Gauging site				No. of observations		
	Name	D-Flow FM Coordinates X	Y	MIKE Chainage [a]	0510	1110	0516
OP1	Mutwal tunnel	339130.2809	495522.4751	103.00	-	-	-
OP2	St. Sebastian north canal	400909.7188	495017.0000	1422.52	-	-	4
OP3	St. Sebastian south canal (Babapulle bridge)	400395.6000	493618.9000	1707.89	-	-	1
OP4	Dematagoda canal	401260.2000	493666.8000	2754.15	-	-	3
OP5	Kolonnawa canal (Yakbadda bridge)	402454.8123	491541.7555	3321.24	-	-	1
OP6	Kolonnawa canal (Mandinnagoda bridge)	403344.1952	490703.8852	1408.92	-	-	-
OP7	Heen Ela - Mahawatta connection	402215.0000	490005.5000	49.99	16	8	2
OP8	Kotte north canal (bridge)	403820.7000	489681.4000	80.11	-	-	-
OP9	Parliament lake (Kotte road bridge)	404412.6000	489275.5000	2998.38	-	-	2
OP10	Torrington canal (Railway bridge)	401023.3206	488890.2260	1057.45	15	8	-
OP11	Heen Ela (Kirimandala Mawatha bridge)	401696.5000	488300.0000	1959.17	15	4	3
OP12	Parliament lake (Jana Kala Kendraya bridge)	405869.1000	488085.2000	1131.40	-	-	2
OP13	Kirulapana canal (Open university bridge)	401521.1000	487576.8000	1345.29	15	-	-
OP14	Kirulapana canal (Nawala road bridge)	401904.3000	487169.8000	625.74	15	-	-
OP15	Parliament lake (Kimbulawala road bridge)	406465.4000	486416.3000	1847	-	-	3
OP16	Dehiwala canal (Galle road bridge)	399404.8000	484881.1000	3309.66	15	6	3
OP17	Wellawatta canal (Galle road bridge)	399218.3000	486752.9000	1116.83	12	8	4
OP18	Serpentine canal	401706.5000	490875.3000	1459	-	-	-
OP19	Dehiwala canal (High level road bridge)	400451.3000	486576.8000	795.48	15	-	-
OP20	Rampalwatta lake				-	-	1
GS1	Nagalagama Street	401106.8000	495536.7000	3805.09	Hourly measurements		

[a] Distance calculated from specific reference points in the model (i.e. branch's starting point).

GS2	Ambatale	408562.7000	493204.6000	14813	Hourly measurements

B.2. Field visit pictures

In the current sub section, pictures showing the measurement techniques and devices used in Metro Colombo catchment are presented[18]. They were taken during a field visit conducted in August 21st, 2016.

Figure 22. Staff gauges in Nagalagama Street – GS1 (a), Ambatale – GS2 (b) and multiple channels' OLs within Metro Colombo catchment (c, d, e, f & g).

[18] The pictures presented were provided by Deltares.

Figure 23. Pluviograph (a) and black bucket (b) for measuring rainfall, control structure in Kimbulawala lake (e) and study site's locations including the area downstream of Wellawatta OP (c) and Colombo wetland (e)

B.3. MIKE 11 NAM RR model

As part of the "Metro Colombo Urban Development" project (World Bank, 2017), an existing MIKE 11 NAM RR model built and applied for Metro Colombo catchment was further updated[19]. This module was used to represent Metro Colombo catchment which generated later inflows to the fluvial network of the current study. NAM model consisted of model parameters, initial conditions and meteorological data.

Elevation input

Metro Colombo catchment was divided into 51 sub-catchments – created based on contour maps corresponding to the DEM provided by SLLRDC. Each of these sub-catchments was thus, characterised by specific elevation zones, the average altitude of which was estimated to determine NAM model variables (i.e. sub-catchment average precipitation).

Modelling components

To reproduce the hydrological cycle's land phase, NAM simulations were carried out by constantly accounting for the water content in various interrelated storages representing different catchment's physical elements (surface storage, lower/root zone storage and groundwater storage) (DHI, 2010). These storages were described in the hydrological model using distinct parameters, the most important of which included U_{max} (surface storage), L_{max} (root zone storage), CQOF (overland flow), CKIF (interflow), CK1,2 (overland flow routing), TG (groundwater recharge) and CK_{BF} (baseflow). The resulting runoff was split into overland flow, interflow and baseflow components.

In the current project, the abovementioned parameters were further corrected principally due to land use changes[20]. Specifically, U_{max} values were significantly decreased (below the typical values – possibly due to extensive urbanisation and imperviousness percentage increase) in most of the sub-catchments while L_{max} values were increased (Table 9). CQOF values showed also an increasing trend – possibly due to the increase in impervious surfaces. The amount of interflow (CKIF) remained constant as it was not influenced by urbanisation changes, yet, both runoff time and overland flow (CK1,2) were increased, as shown in the table below (Table 9). In addition, even though root zone threshold value for groundwater recharge (TG) and time constant for routing baseflow (CKBF) constituted fundamental groundwater parameters in NAM model, they were not expected to be significantly influenced by urbanisation trends and subsequently, their values were equal to zero.

[19] An updated NAM hydrological model for Metro Colombo catchment was provided by SLLRDC. The work was carried out by COWI (COWI, 2013).

[20] In Metro Colombo catchment, such alterations predominantly described rural/ semi-urban to urban changes.

Table 9. Previously implemented (COWI) and updated NAM parameters

A/A	Catchment Overview			Surface & Rootzone parameters										
	Code	Area (1)	Area (2)	Umax (3)	Umax (4)	Lmax (5)	Lmax (6)	CQOF (7)	CQOF (8)	CKIF	CK1,2 (9)	CK1,2 (10)	TOF	TIF
1	C_03	5.571	5.318	6.00	2.86	63.45	36.4	0.64	0.67	48	8.86	3.38	0	0
2	C_04	5.591	5.065	6.00	5.53	63.46	70.20	0.67	0.63	48	8.90	8.13	0	0
3	C_05	6.679	7.511	6.00	5.68	63.45	72.00	0.71	0.66	48	9.59	7.46	0	0
4	C_06	1.476	1.233	6.00	5.89	63.46	74.80	0.63	0.66	48	3.54	6.56	0	0
5	C_07	2.177	2.108	6.00	5.41	63.50	68.80	0.64	0.84	500	5.10	6.25	0	0
6	C_08	0.297	0.822	6.00	4.18	51.08	42.70	0.79	0.96	500	1.85	4.28	0	0
7	C_09A	1.243	1.496	6.00	5.85	56.25	65.80	0.67	0.72	500	2.97	4.59	0	0
8	C_10	1.216	0.915	5.00	4.74	51.08	58.00	0.74	0.78	500	4.38	4.92	0	0
9	C_11	0.967	1.249	5.00	5.31	63.46	80.80	0.67	0.63	500	3.47	6.77	0	0
10	C_12	0.844	0.844	5.00	5.37	47.77	61.50	0.65	0.61	500	4.04	9.75	0	0
11	C_13	0.461	0.634	5.00	4.73	47.77	54.30	0.79	0.83	500	2.46	6.09	0	0
12	C_14	0.282	0.351	4.57	3.14	48.49	40.00	0.85	1.00	500	2.46	4.34	0	0
13	C_15	0.318	0.312	6.44	5.01	47.77	44.60	0.71	0.87	500	2.46	5.79	0	0
14	C_16	0.347	0.631	6.44	5.92	47.77	52.70	0.56	0.60	500	2.46	7.06	0	0
15	C_17	0.586	0.558	6.44	7.06	60.14	79.10	0.56	0.50	500	4.21	8.53	0	0
16	C_18	0.330	0.25	6.66	5.33	47.77	45.90	0.79	0.94	500	2.46	6.00	0	0
17	C_19	0.925	1.286	6.44	3.76	60.14	42.10	0.67	0.94	500	4.45	3.97	0	0
18	C_21	0.999	1.17	4.05	3.59	41.86	44.50	0.77	0.86	500	4.79	7.73	0	0
19	C_22	3.170	3.334	4.12	3.90	41.64	47.30	0.75	0.79	500	9.91	6.90	0	0
20	C_23	1.186	1.777	4.33	4.09	44.98	51.00	0.71	0.75	500	5.68	6.58	0	0
21	C_24	2.088	1.695	4.33	3.46	49.10	47.10	0.79	0.94	500	10.01	10.3	0	0
22	C_25	0.740	0.767	4.80	4.01	41.23	41.23	0.74	0.86	500	3.54	7.18	0	0
23	C_26	1.604	2.135	5.43	4.47	49.18	48.60	0.74	0.87	500	7.68	13.7	0	0
24	C_28	2.236	2.002	5.60	5.17	53.19	58.90	0.68	0.73	500	7.00	4.11	0	0
25	C_29	2.614	3.781	4.39	3.96	49.05	53.10	0.72	0.78	500	8.17	2.52	0	0
26	C_30	0.310	0.655	3.70	3.15	35.74	36.50	0.80	0.92	500	2.46	3.16	0	0
27	C_31	0.486	0.5	3.66	3.10	22.93	23.30	0.76	0.88	500	2.46	2.52	0	0
28	C_32	0.345	0.501	4.37	3.89	30.06	32.10	0.74	0.82	500	2.46	3.16	0	0
29	C_33	2.299	2.288	4.76	4.56	35.83	41.20	0.74	0.77	500	7.18	7.57	0	0
30	MALABE	12.750	13.371	9.45	8.19	55.00	71.50	0.57	0.64	500	10.50	7.11	0	0
31	C_27A	1.000	1.441	5.60	5.02	47.77	51.40	0.77	0.85	500	4.79	10.20	0	0
32	C_27B	1.200	1.316	5.60	5.02	47.77	51.40	0.77	0.85	500	5.74	7.49	0	0
33	C_29C	0.300	0.353	5.19	4.69	49.13	53.20	0.79	0.86	500	2.46	4.35	0	0
34	C_25A	0.928	0.928	5.73	4.79	52.81	52.90	0.74	0.86	500	4.79	6.97	0	0
35	C_25B	0.720	0.568	5.73	4.79	52.81	52.90	0.74	0.86	500	3.45	5.29	0	0
36	C_19A	0.067	0.067	4.25	4.25	38.10	38.10	0.79	0.79	500	2.01	2.01	0	0
37	C_28A	0.250	0.072	5.23	4.83	35.74	39.60	0.75	0.81	500	2.46	2.74	0	0
38	C_09C	2.800	0.869	6.00	5.85	63.46	74.20	0.67	0.68	48	5.09	5.20	0	0
39	C_09D	1.500	1.471	6.00	5.85	63.45	74.20	0.67	0.68	48	2.47	4.10	0	0
40	C_09B	0.500	0.661	6.00	5.85	63.46	74.20	0.67	0.68	48	2.46	4.29	0	0
41	C_09D2	0.300	1.790	6.00	5.85	63.46	74.20	0.67	0.68	48	1.65	9.34	0	0
42	C_02A	2.600	2.555	6.00	3.44	63.46	43.60	0.61	0.64	48	8.11	7.82	0	0
43	C_02B	5.756	6.808	6.00	3.44	63.46	43.60	0.61	0.62	48	10.79	6.46	0	0
44	C_02C	5.400	5.052	6.00	3.44	63.46	43.60	0.61	0.66	48	10.12	12.5	0	0
45	C_02D	1.600	0.416	6.00	3.44	63.46	43.60	0.61	0.79	48	7.66	2.08	0	0
46	C_02E	0.200	0.404	6.00	3.44	63.46	43.60	0.61	0.62	48	2.46	4.17	0	0
47	C_01A	7.470	6.494	6.00	5.63	70.50	79.30	0.58	0.62	48	13.75	14.6	0	0
48	C_01B	3.630	3.059	6.00	5.63	70.50	79.30	0.58	0.83	48	11.11	5.23	0	0
49	C_01C	3.410	3.189	6.00	5.63	70.50	79.30	0.58	0.88	48	11.09	4.44	0	0
50	C_01D	1.440	2.892	6.00	5.63	70.50	79.30	0.58	0.63	48	3.08	4.76	0	0
51	C_20	0.584	0.584	5.73	5.73	63.40	63.40	0.74	0.74	500	2.85	2.85	0	0

(1), (2) Area (km^2), (3), (4) Umax, (5), (6) Lmax, (7), (8) CQOF, (9), (10) CK1,2 presented in COWI report (COWI, 2013) & current MIKE 11 NAM, respectively.

Appendix C

C.1. Simulation of WLs during 0510, 1110 & 0516 events

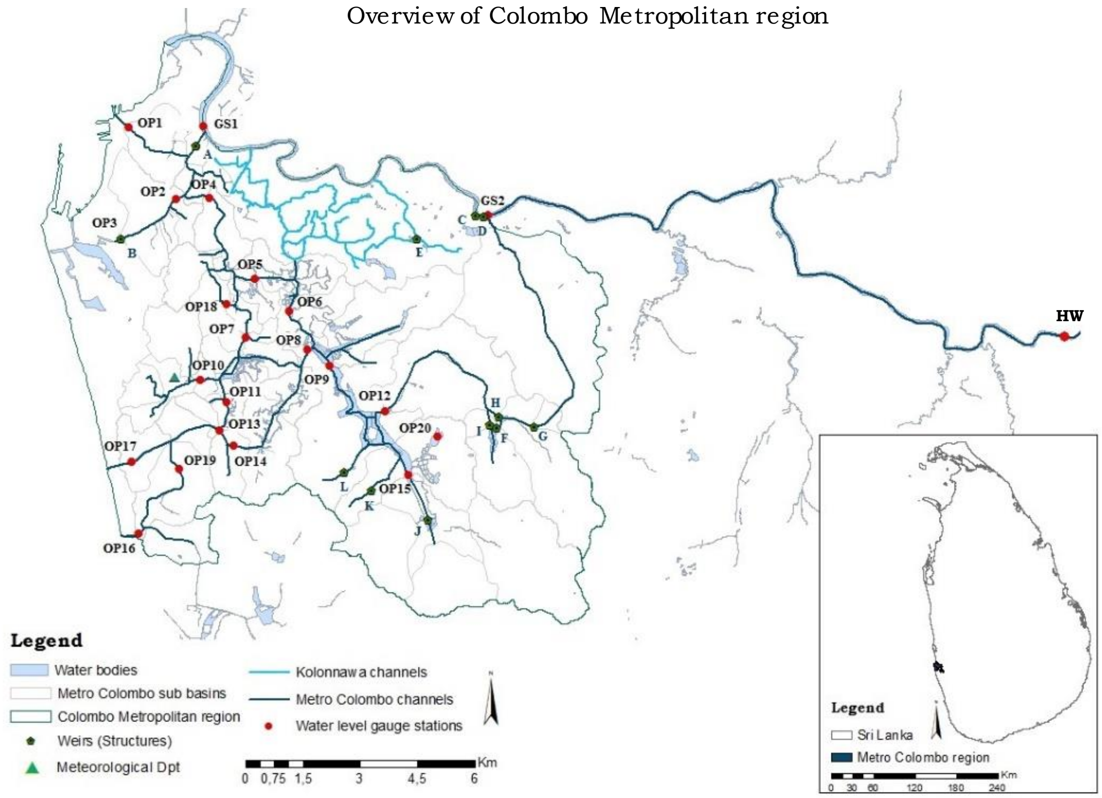

May 2010 (0510)

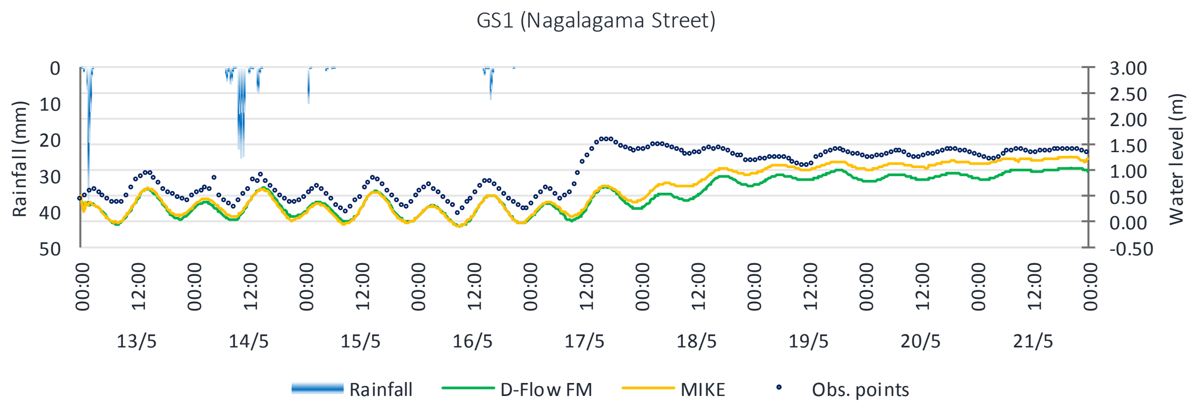

Figure 24. Simulated WL fluctuations against field observations in GS1 (0510)

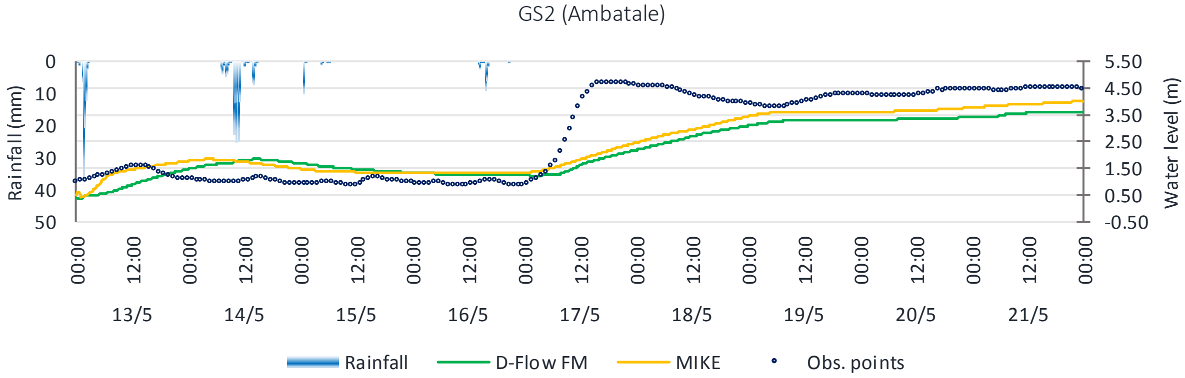

Figure 25. Simulated WL fluctuations against field observations in GS2 (0510)

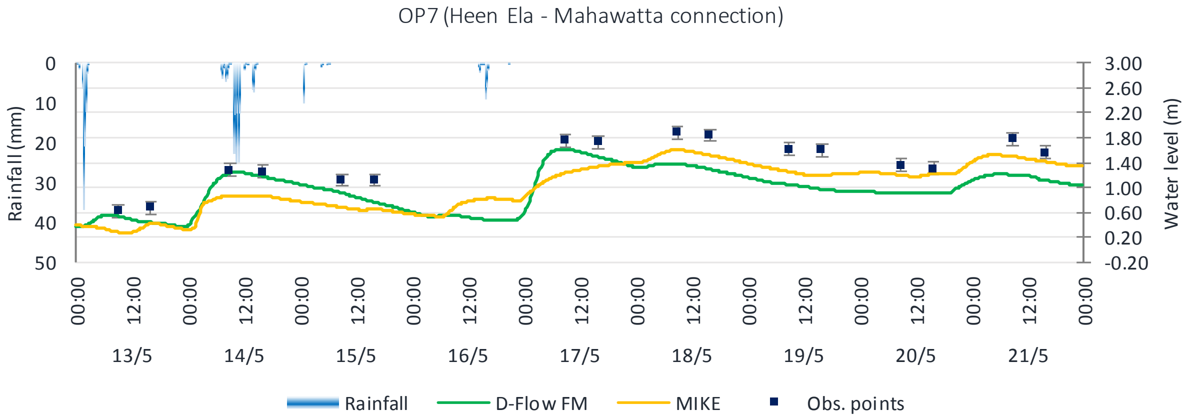

Figure 26. Simulated WL fluctuations against field observations in OP7 (0510)

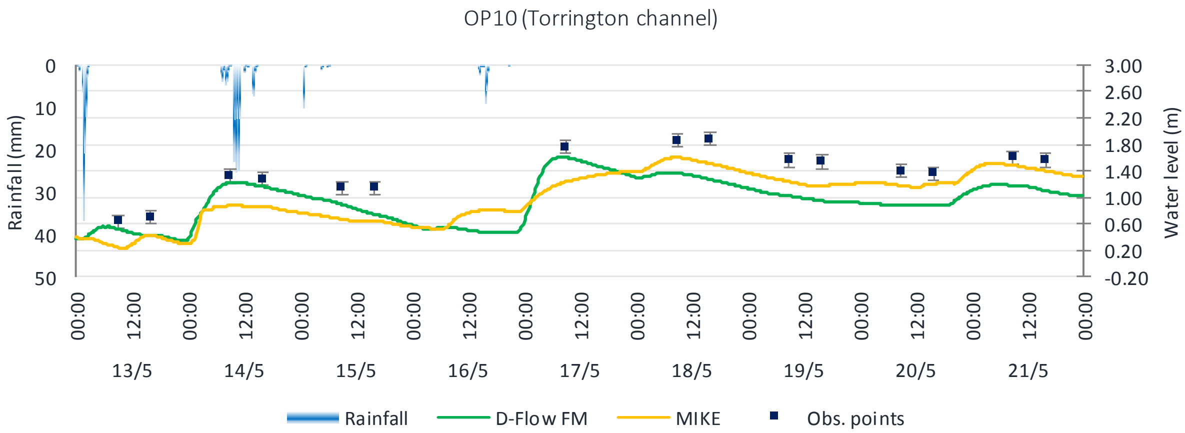

Figure 27. Simulated WL fluctuations against field observations in OP10 (0510)

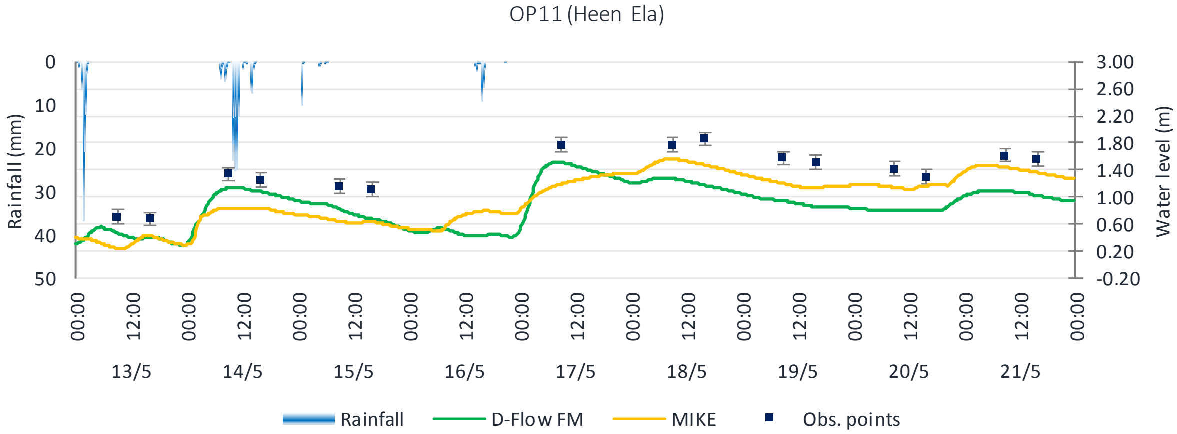

Figure 28. Simulated WL fluctuations against field observations in OP11 (0510)

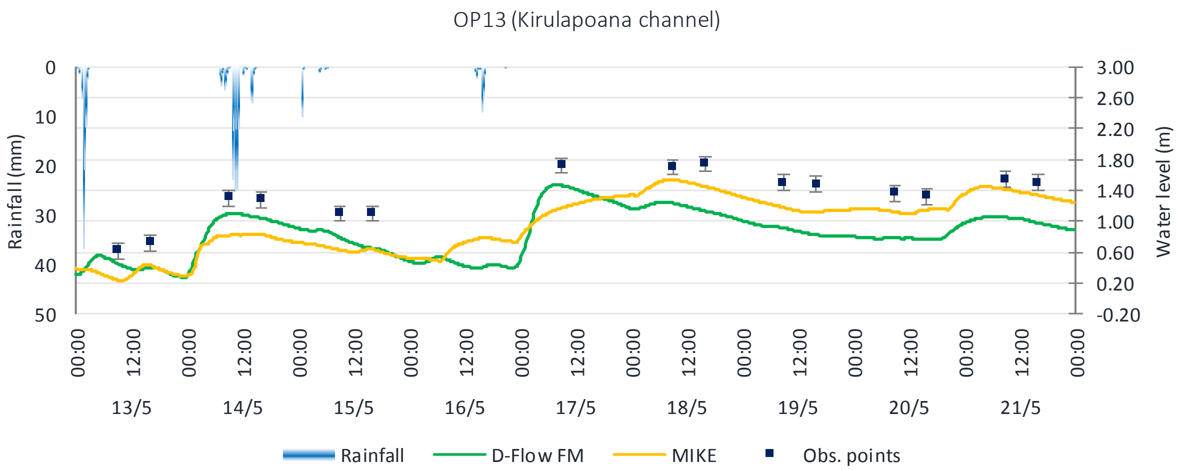

Figure 29. Simulated WL fluctuations against field observations in OP13 (0510)

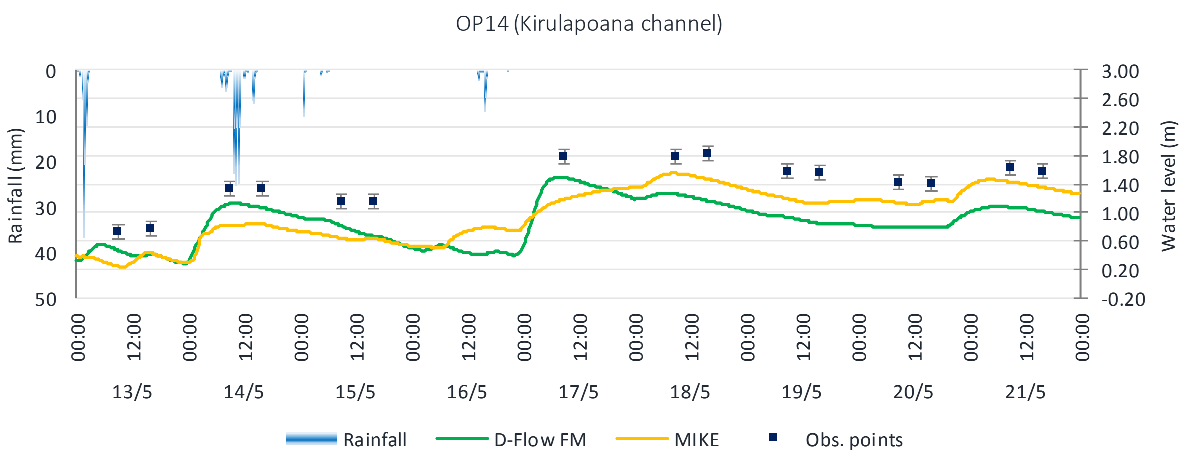

Figure 30. Simulated WL fluctuations against field observations in OP14 (0510)

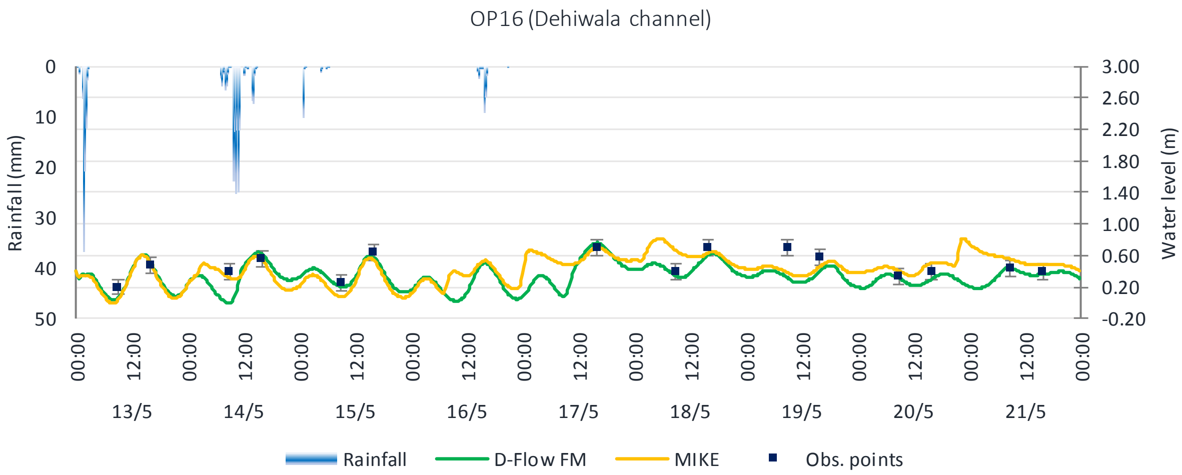

Figure 31. Simulated WL fluctuations against field observations in OP16 (0510)

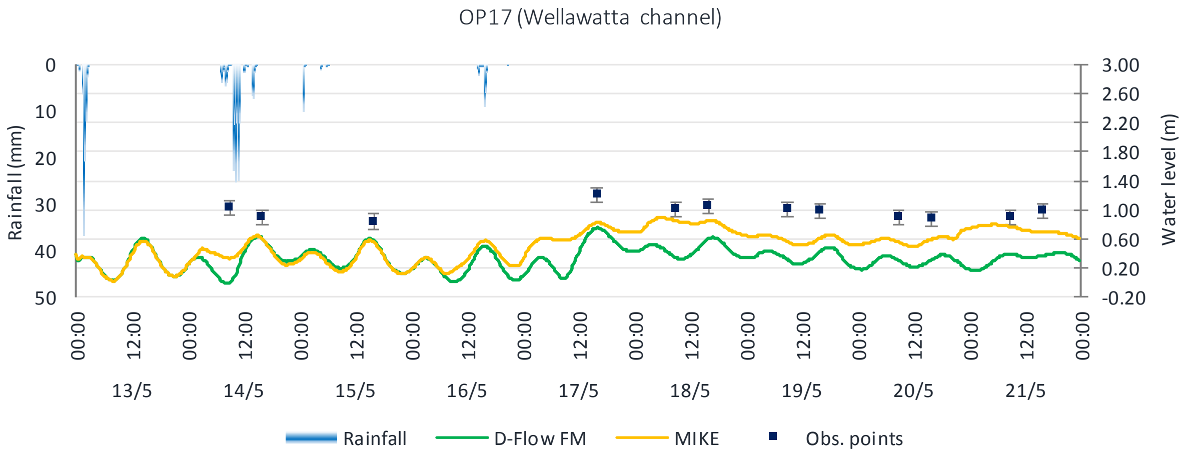

Figure 32. Simulated WL fluctuations against field observations in OP17 (0510)

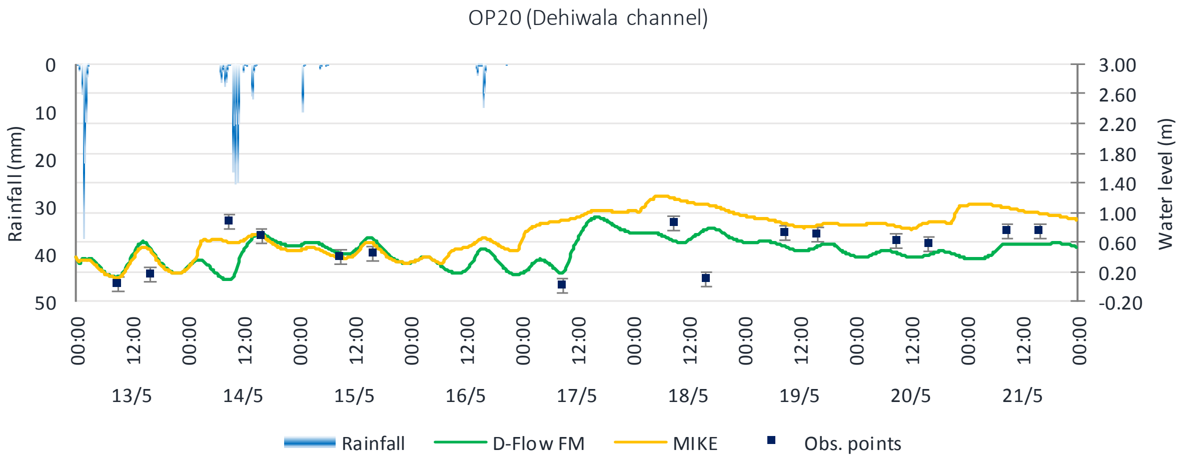

Figure 33. Simulated WL fluctuations against field observations in OP20 (0510)

November 2010 (1110)

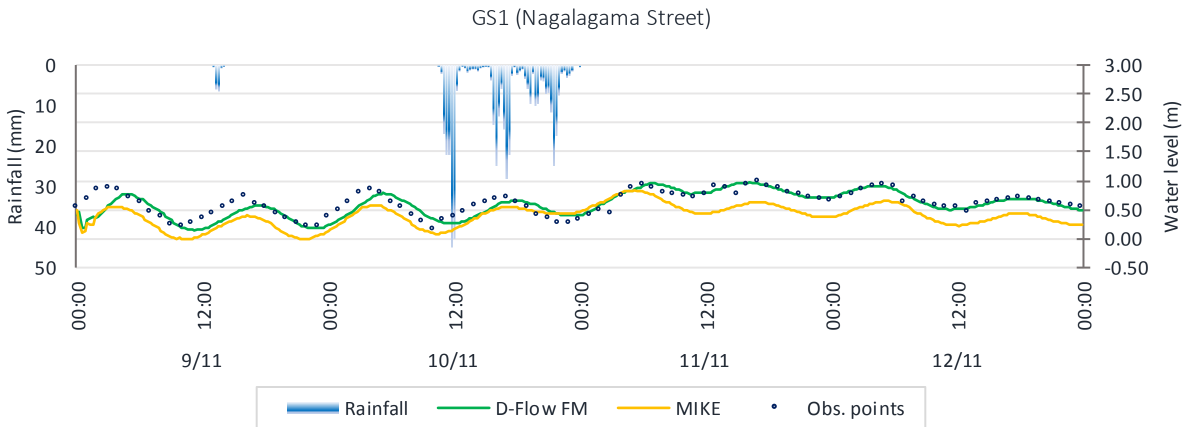

Figure 34. Simulated WL fluctuations against field observations in GS1 (1110)

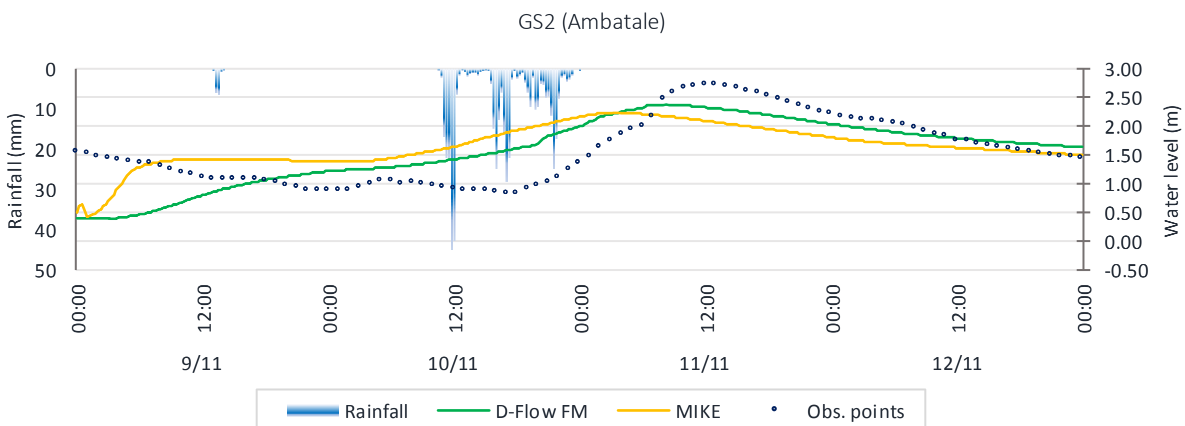

Figure 35. Simulated WL fluctuations against field observations in GS2 (1110)

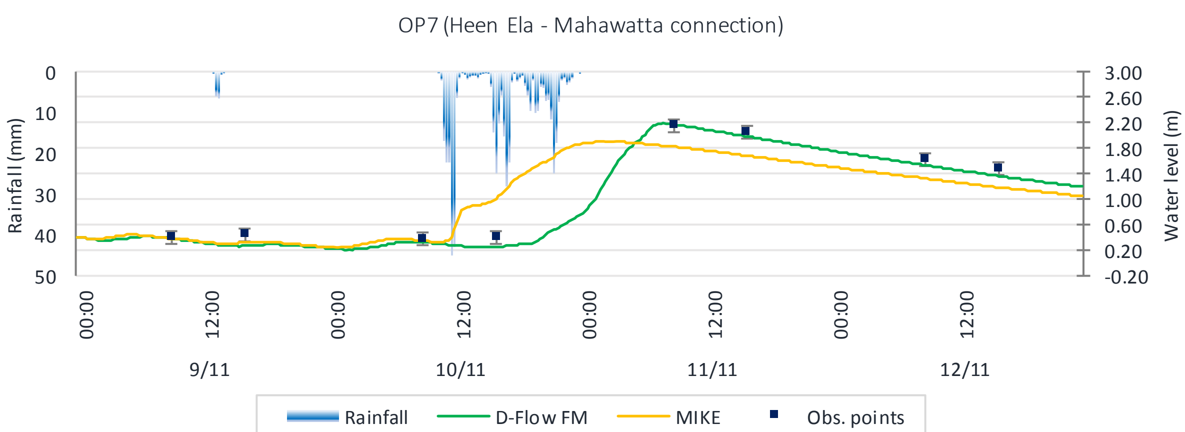

Figure 36. Simulated WL fluctuations against field observations in OP7 (1110)

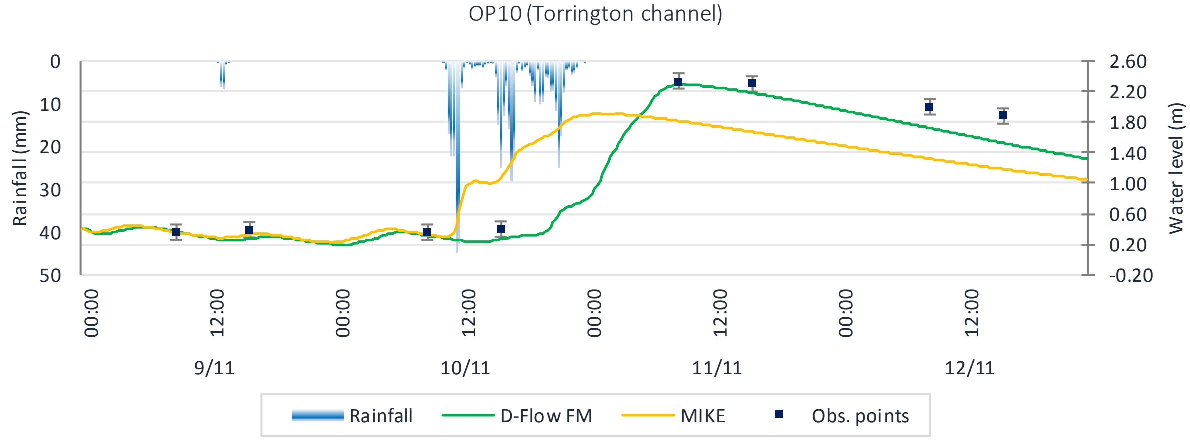

Figure 37. Simulated WL fluctuations against field observations in OP10 (1110)

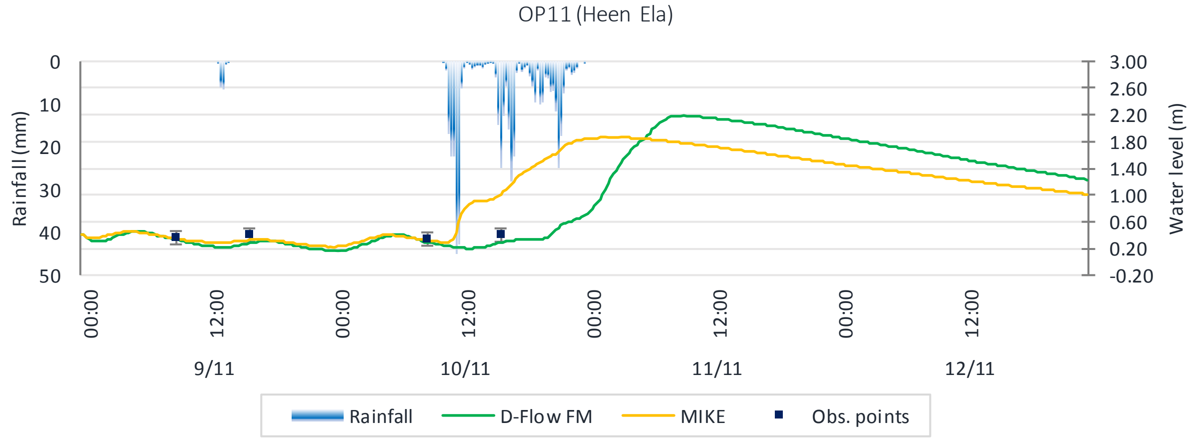

Figure 38. Simulated WL fluctuations against field observations in OP11 (1110)

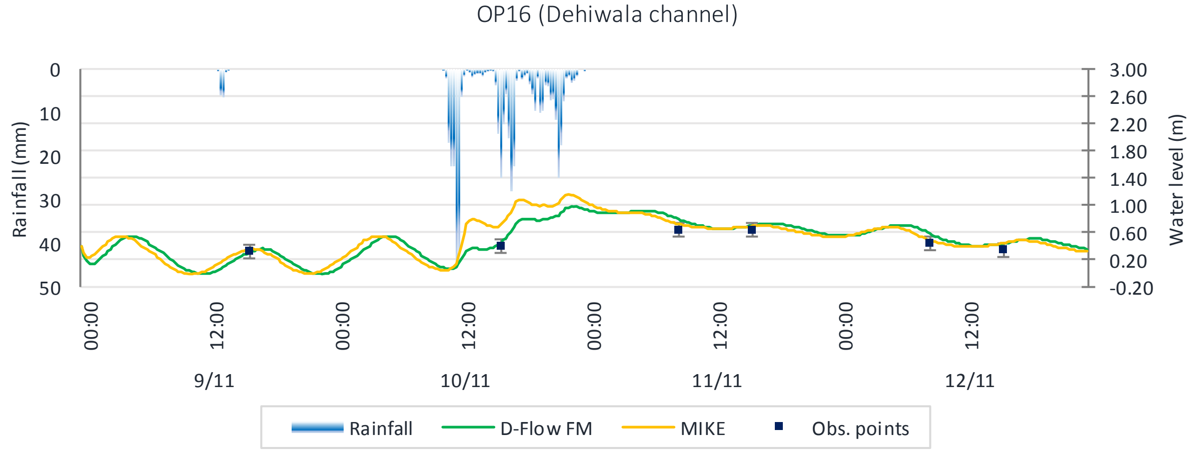

Figure 39. Simulated WL fluctuations against field observations in OP16 (1110)

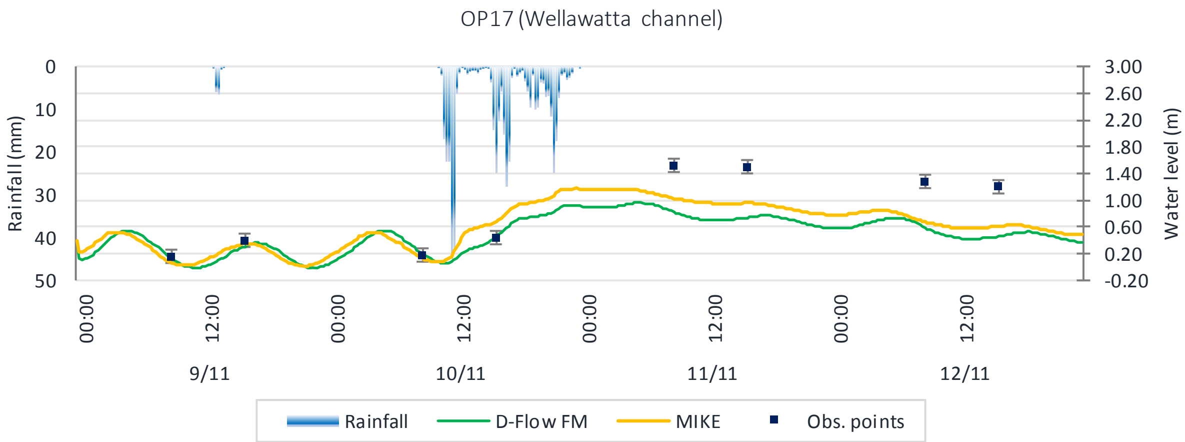

Figure 40. Simulated WL fluctuations against field observations in OP17 (1110)

May 2016 (0516)

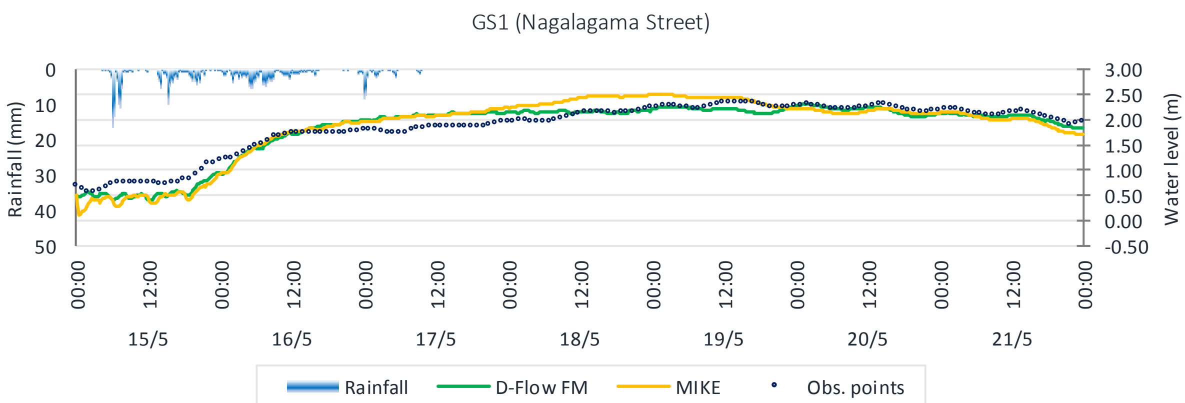

Figure 41. Simulated WL fluctuations against field observations in GS1 (0516)

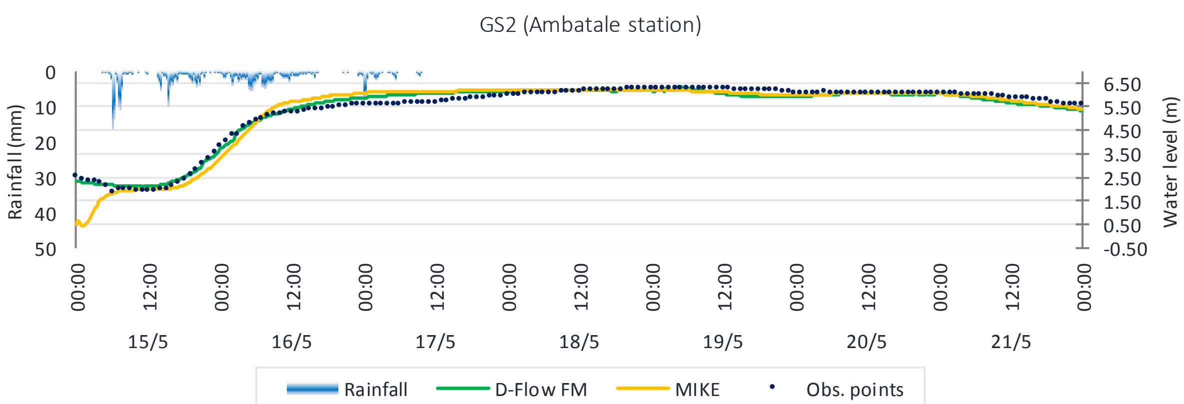

Figure 42. Simulated WL fluctuations against field observations in GS2 (0516)

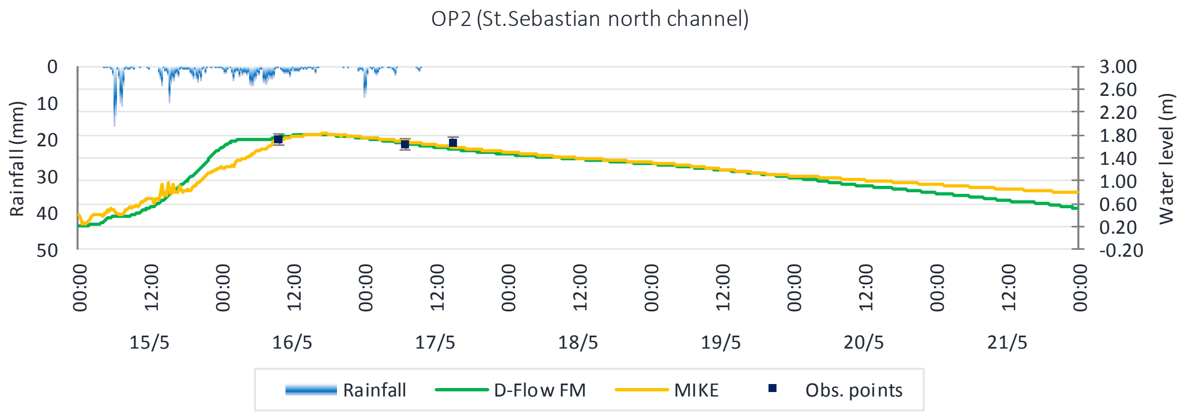

Figure 43. Simulated WL fluctuations against field observations in OP2 (0516)

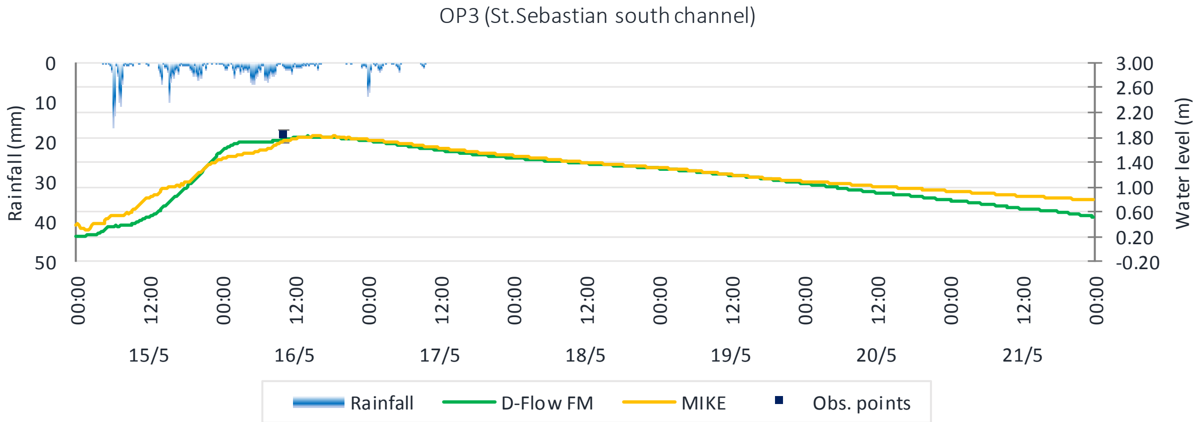

Figure 44. Simulated WL fluctuations against field observations in OP3 (0516)

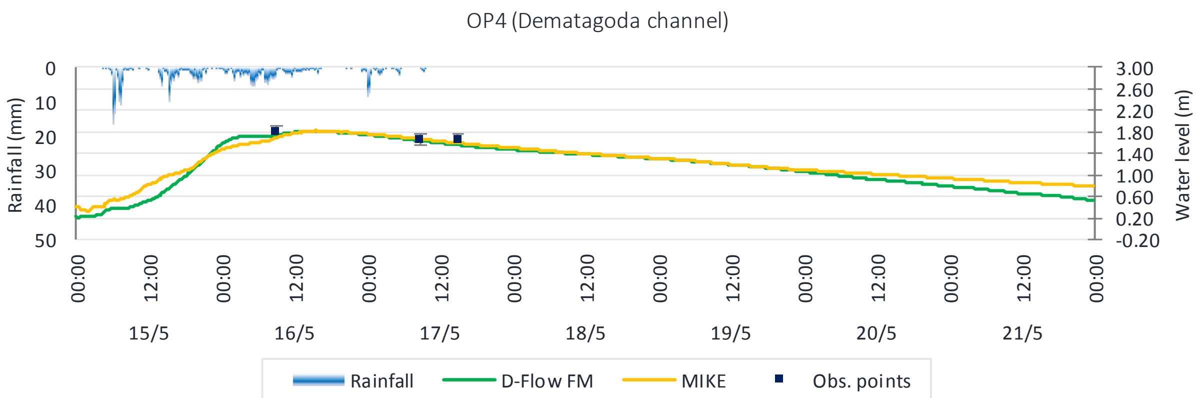

Figure 45. Simulated WL fluctuations against field observations in OP4 (0516)

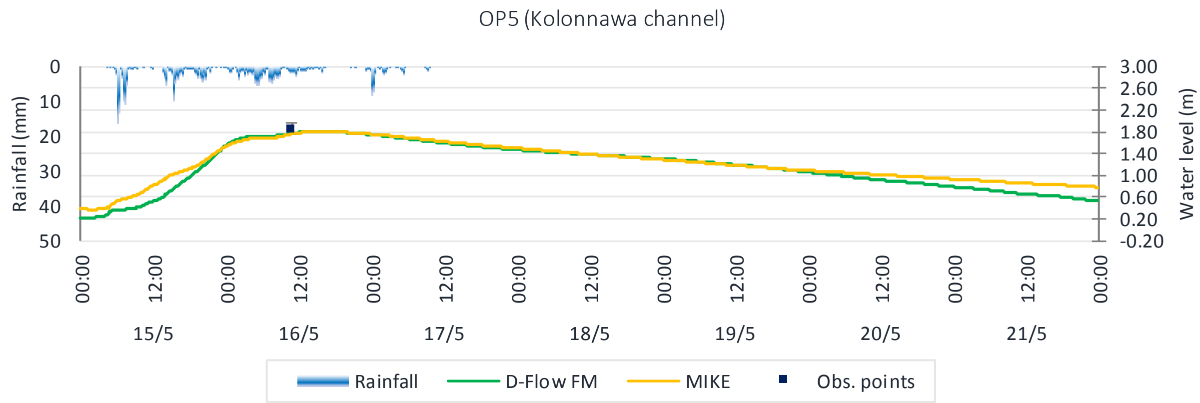

Figure 46. Simulated WL fluctuations against field observations in OP5 (0516)

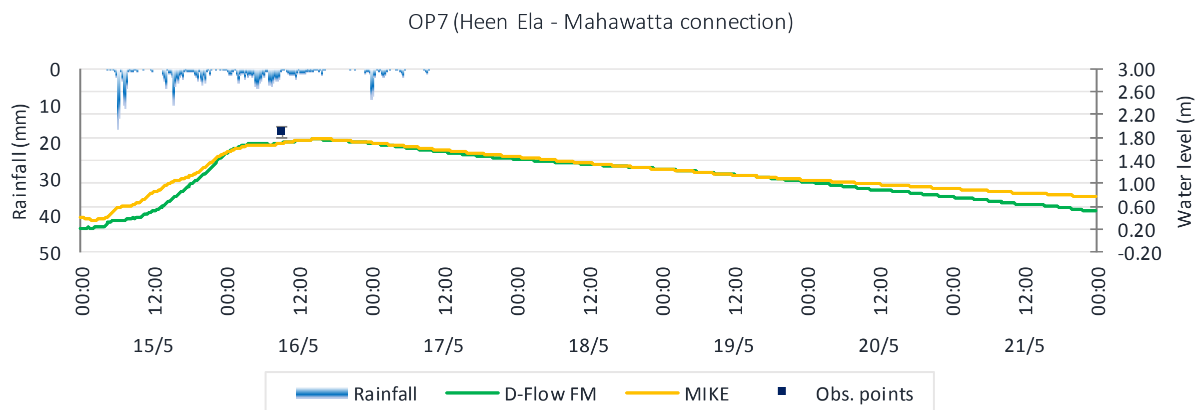

Figure 47. Simulated WL fluctuations against field observations in OP7 (0516)

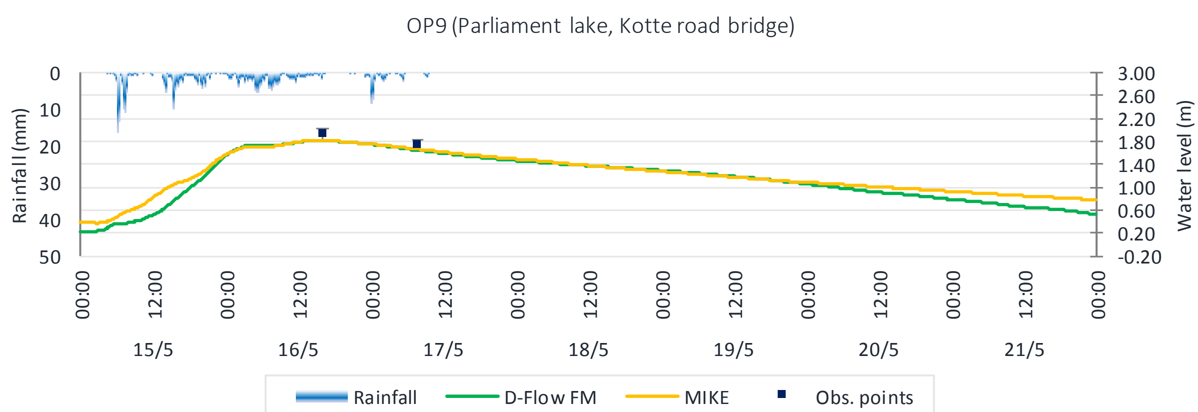

Figure 48. Simulated WL fluctuations against field observations in OP9 (0516)

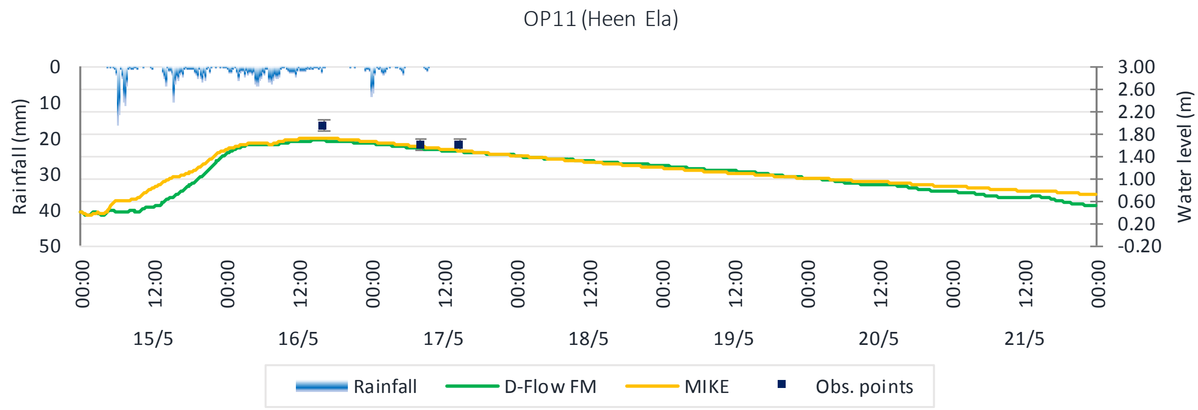

Figure 49. Simulated WL fluctuations against field observations in OP11 (0516)

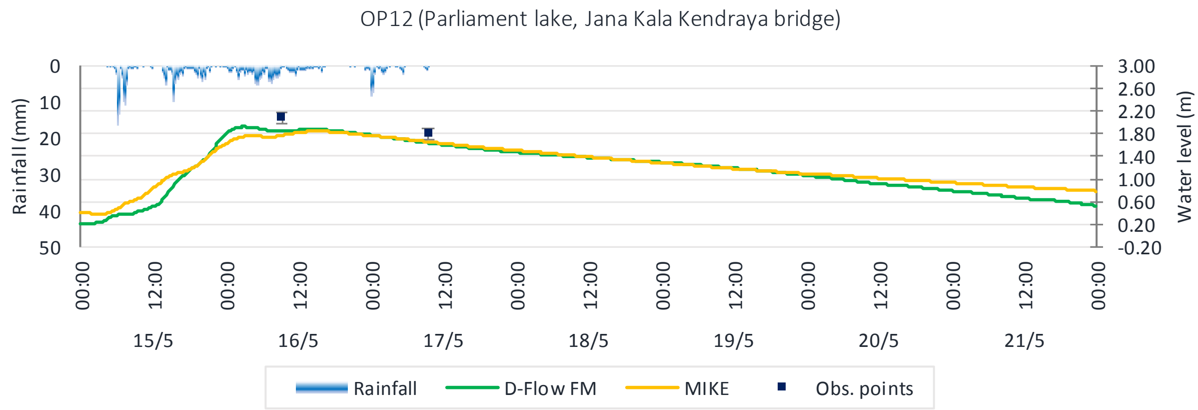

Figure 50. Simulated WL fluctuations against field observations in OP12 (0516)

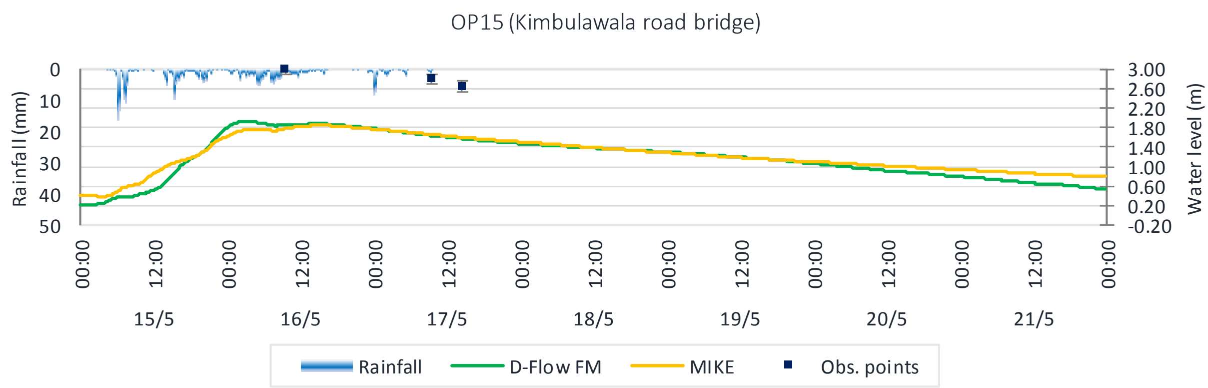

Figure 51. Simulated WL fluctuations against field observations in OP15 (0516)

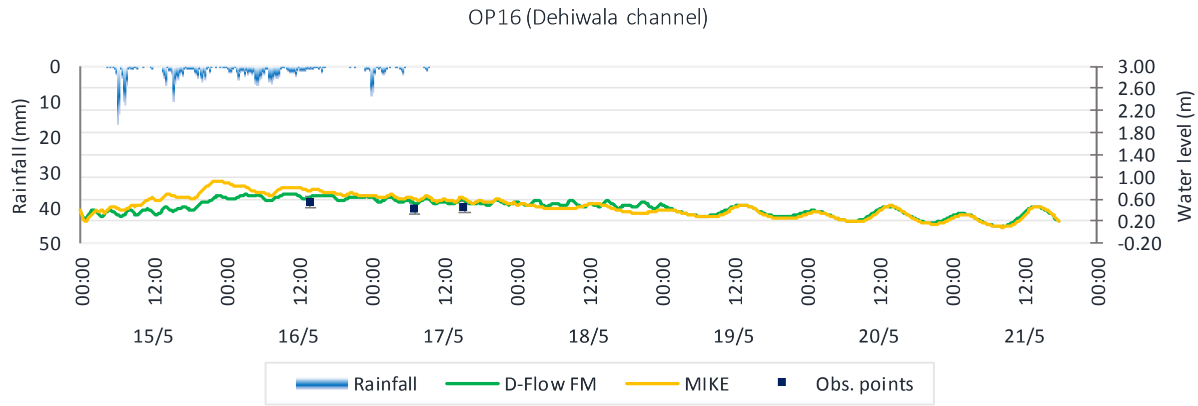

Figure 52. Simulated WL fluctuations against field observations in OP16 (0516)

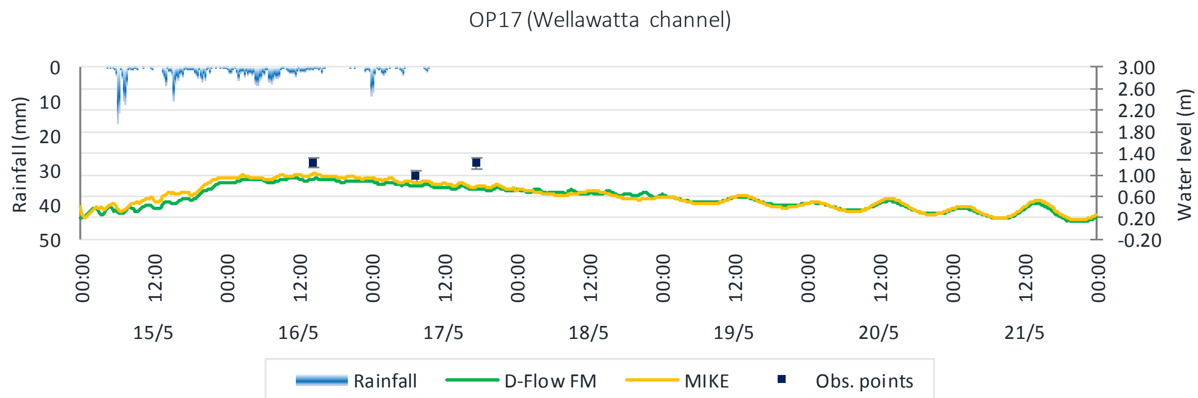

Figure 53. Simulated WL fluctuations against field observations in OP17 (0516)

C.2. ADs & RDs at point observations

In the current sub section, the ADs and RDs of MIKE FLOOD and D-Flow FM simulated values with real observations were presented. Their categorisation was event based. Each graph represented an observation location (i.e. OP7) and included all field measurements conducted at this point during the specific event. MIKE FLOOD (orange) and D-Flow FM (green) AD/RDs were presented in separate columns. ADs were illustrated with vivid colours in meters (left column) and RDs with pale colours in percentages (right column).

May 2010 (0510)

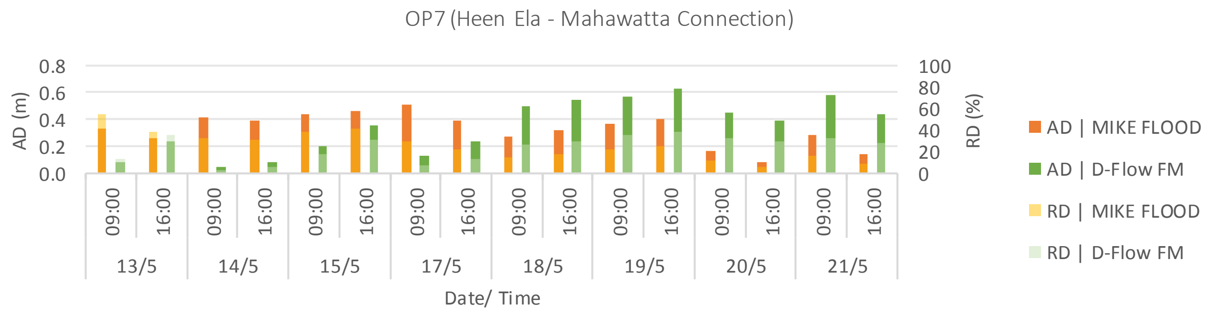

Figure 54. ADs & RDs of models' simulated values with real observations in OP7 (0510)

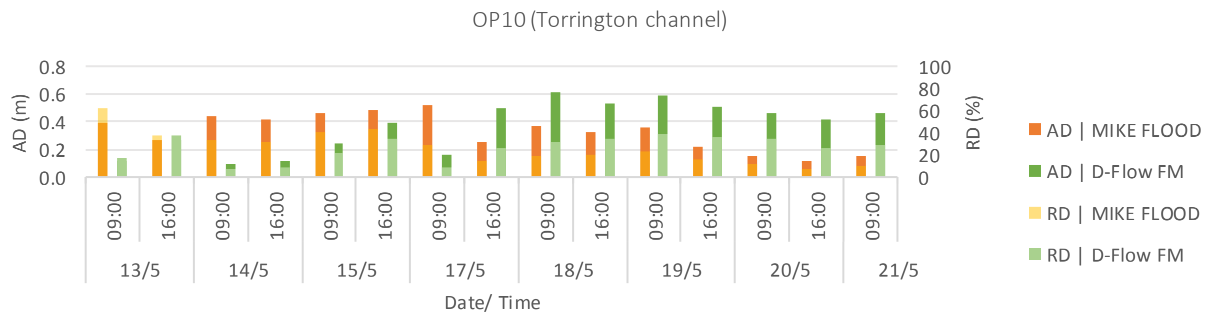

Figure 55. ADs & RDs of models' simulated values with real observations in OP10 (0510)

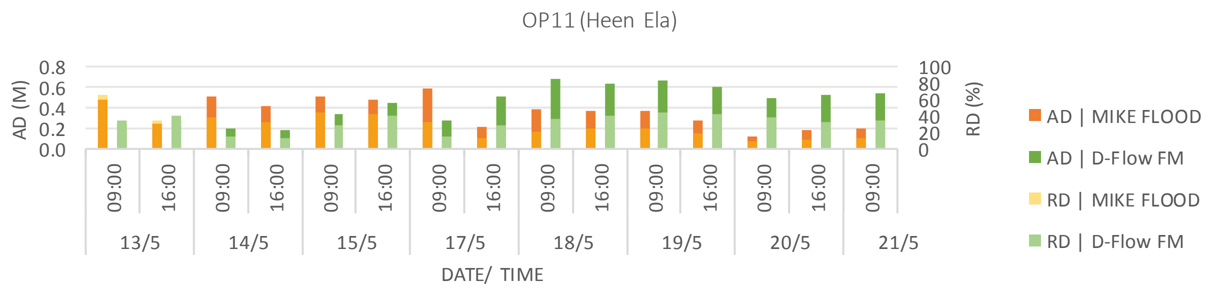

Figure 56. ADs & RDs of models' simulated values with real observations in OP11 (0510)

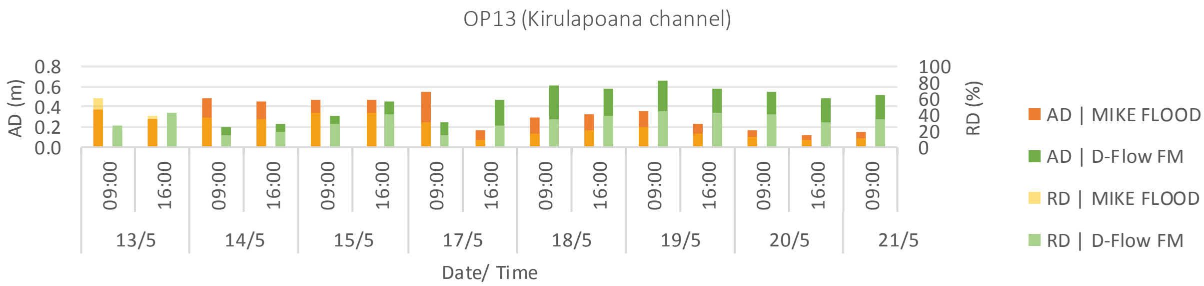

Figure 57. ADs & RDs of models' simulated values with real observations in OP13 (0510)

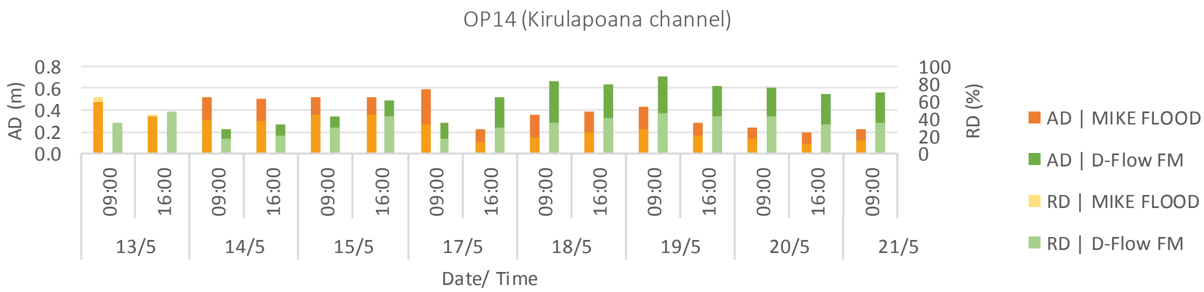

Figure 58. ADs & RDs of models' simulated values with real observations in OP14 (0510)

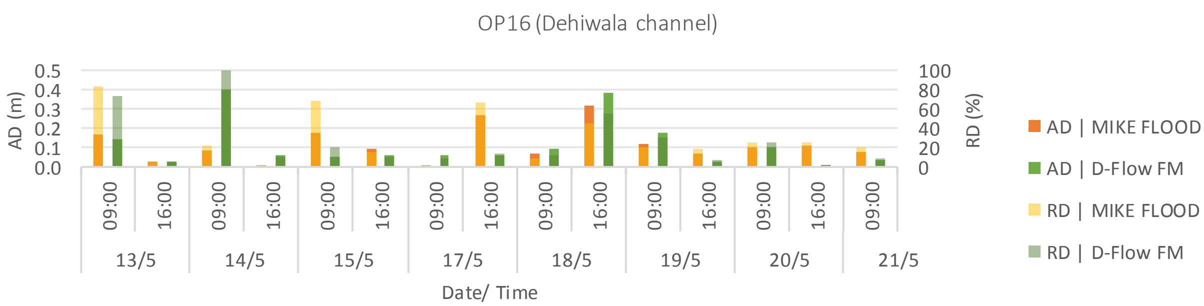

Figure 59. ADs & RDs of models' simulated values with real observations in OP16 (0510)

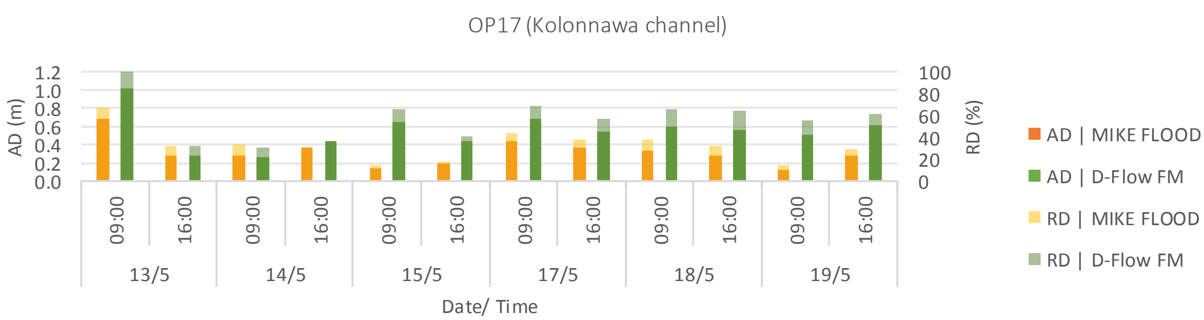

Figure 60. ADs & RDs of models' simulated values with real observations in OP17 (0510)

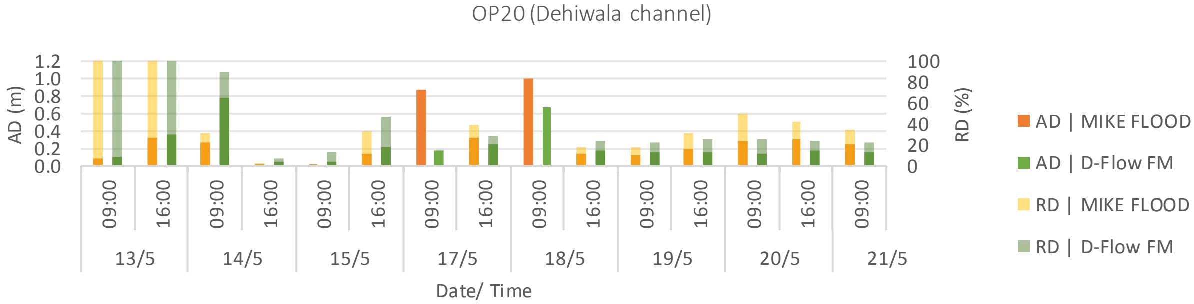

Figure 61. ADs & RDs of models' simulated values with real observations in OP20 (0510)

November 2010 (1110)

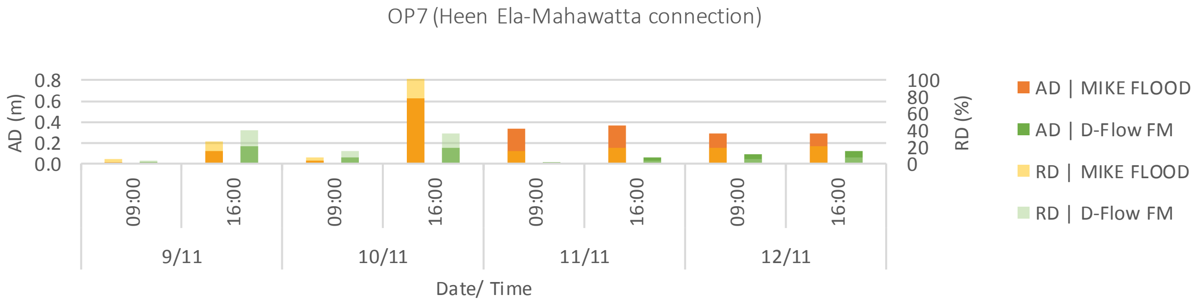

Figure 62. ADs & RDs of models' simulated values with real observations in OP7 (1110)

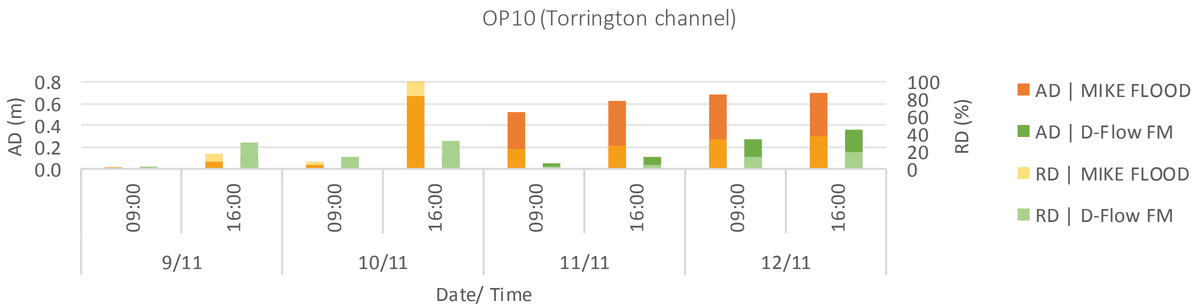

Figure 63. ADs & RDs of models' simulated values with real observations in OP10 (1110)

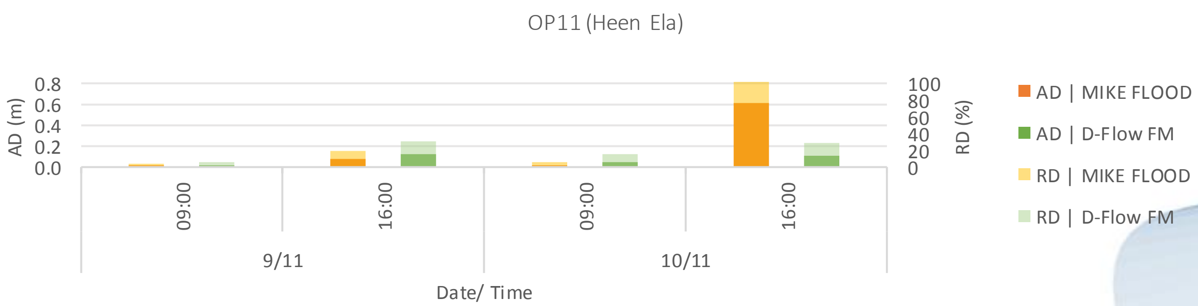

Figure 64. ADs & RDs of models' simulated values with real observations in OP11 (1110)

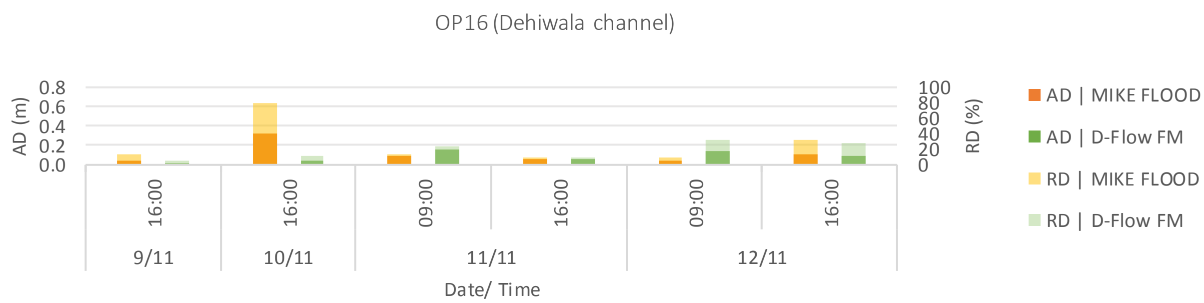

Figure 65. ADs & RDs of models' simulated values with real observations in OP16 (1110)

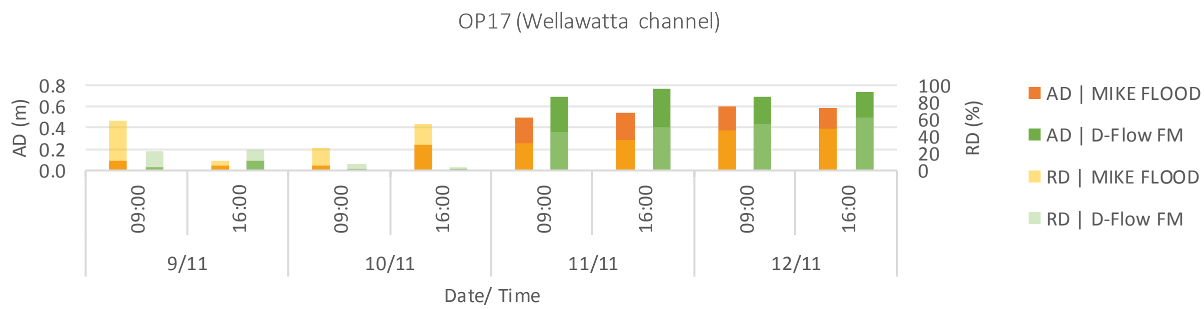

Figure 66. ADs & RDs of models' simulated values with real observations in OP17 (1110)

May 2016 (0516)

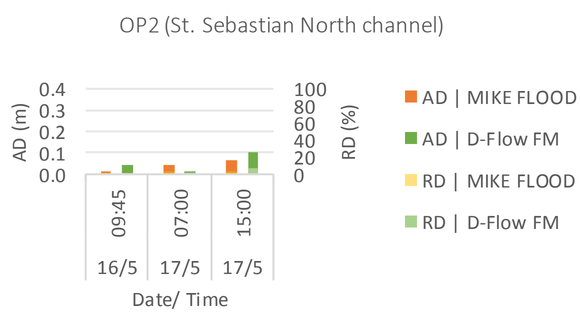

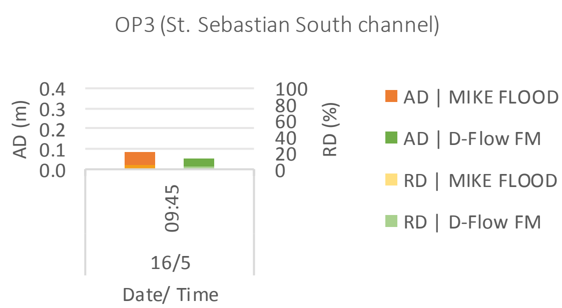

Figure 67. ADs & RDs of models' simulated values with real observations in OP2 & OP3 (0516)

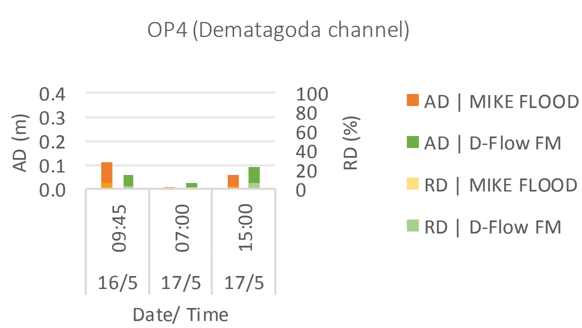

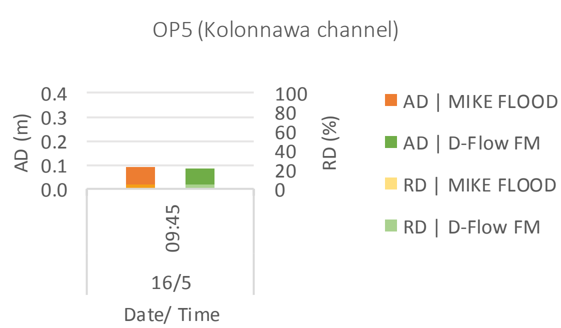

Figure 68. ADs & RDs of models' simulated values with real observations in OP4 & OP5 (0516)

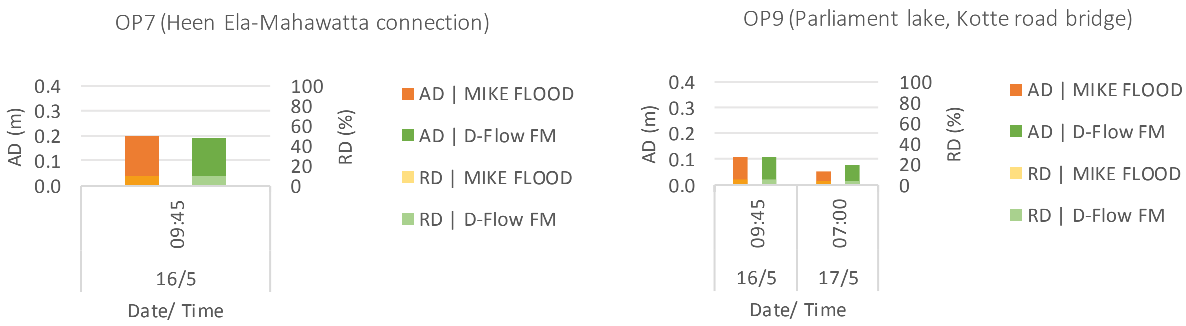

Figure 69. ADs & RDs of models' simulated values with real observations in OP7 & OP9 (0516)

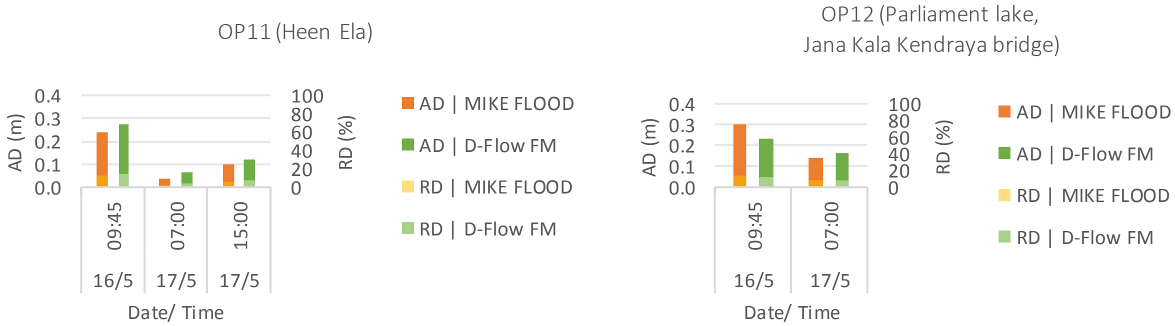

Figure 70. ADs & RDs of models' simulated values with real observations in OP11 & OP12 (0516)

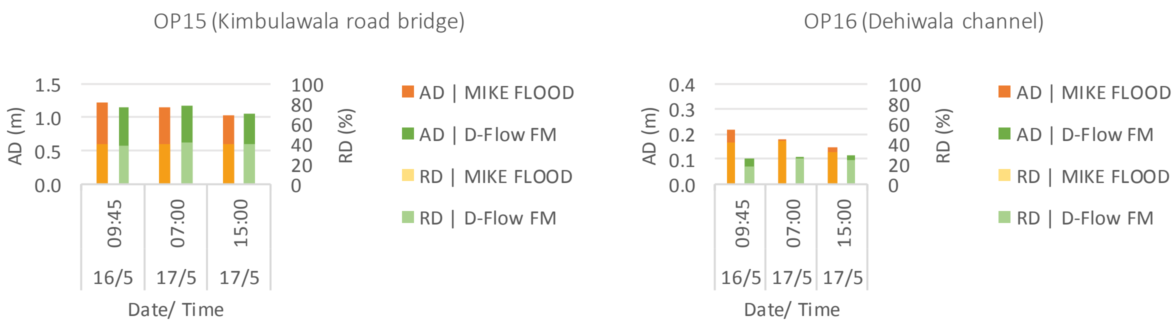

Figure 71. ADs & RDs of models' simulated values with real observations in OP15 & OP16 (0516)

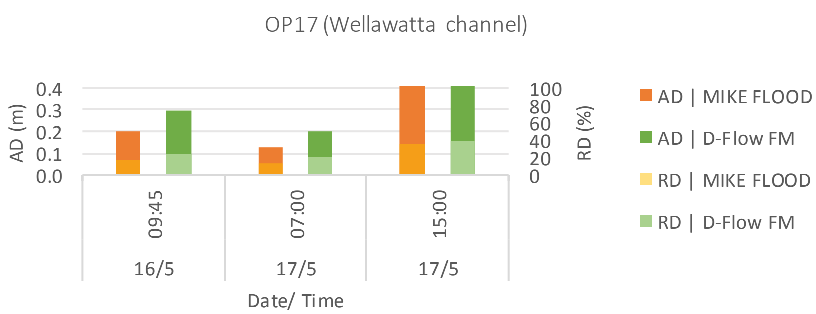

Figure 72. ADs & RDs of models' simulated values with real observations in OP17 (0516)